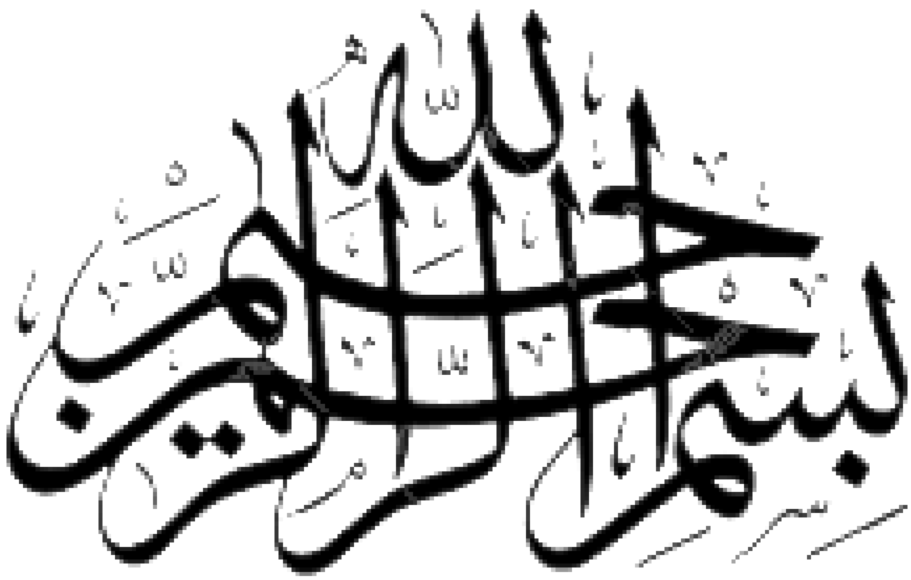
بسم الله الرحمن الرحيم

Nonlinear Mathematical Models with Chemical Reaction

By

Sadia Rashid

Department of Mathematics
Quaid-I-Azam University
Islamabad, Pakistan

2020

Nonlinear Mathematical Models with Chemical Reaction

By

Sadia Rashid

Supervised by

Prof. Dr. Muhammad Ayub

Department of Mathematics
Quaid-I-Azam University
Islamabad, Pakistan

2020

Nonlinear Mathematical Models with Chemical Reaction

A DISSERTATION SUBMITTED IN THE PARTIAL FULFILLMENT OF THE REQUIREMENT FOR THE DIGREE OF

DOCTOR OF PHILOSOPHY

IN

MATHEMATICS

Supervised by

Prof. Dr. Muhammad Ayub

Department of Mathematics
Quaid-I-Azam University
Islamabad, Pakistan

2020

Author's Declaration

I,**Sadia Rashid,**hereby state that my PhD thesis titled **Nonlinear Mathematical Models With Chemical Reaction**is my own work and has not been submitted previously by me for taking any degree from the Quaid-I-Azam University Islamabad, Pakistan or anywhere else in the country/world.

At any time if my statement is found to be incorrect even after my graduate the university has the right to withdraw my PhD degree.

Name of Student: **Sadia Rashid**

Date: **13-Nov-2020**

Plagiarism Undertaking

I solemnly declare that research work presented in the thesis titled "**Nonlinear Mathematical Models With Chemical Reaction**" is solely my research work with no significant contribution from any other person. Small contribution/help wherever taken has been duly acknowledged and that complete thesis has been written by me.

I understand the zero tolerance policy of the HEC and **Quaid-i-Azam University** towards plagiarism. Therefore, I as an Author of the above titled thesis declare that no portion of my thesis has been plagiarized and any material used as reference is properly referred/cited.

I undertake that if I am found guilty of any formal plagiarism in the above titled thesis even afterward of PhD degree, the University reserves the rights to withdraw/revoke my PhD degree and that HEC and the University has the right to publish my name on the HEC/University Website on which names of students are placed who submitted plagiarized thesis.

Student/Author Signature

Name: **Sadia Rashid**

Certificate of Approval

This is to certify that the research work presented in this thesis entitled **Nonlinear Mathematical Models With Chemical Reaction**was conducted by **Ms. Sadia Rashid** under the kind supervision of **Prof. Dr. Muhammad Ayub**. No part of this thesis has been submitted anywhere else for any other degree. This thesis is submitted to the Department of Mathematics, Quaid-i-Azam University, Islamabad in partial fulfillment of the requirements for the degree of Doctor of Philosophy in field of Mathematics from Department of Mathematics, Quaid-i-Azam University Islamabad, Pakistan.

Student Name: **Sadia Rashid** Signature:________

External committee:

a) **External Examiner 1**: Signature:________
Name: **Prof. Dr. Muhammad Mushtaq**
Designation: Professor
Office Address: Department of Mathematics, COMSATS University, Park Road Chak Shahzad, Islamabad.

b) **External Examiner 2**: Signature:________
Name: **Dr.Rahmat Ellahi**
Designation: Associate Professor
Office Address: Department of Mathematics & Statistics, Faculty of Basics Applied Sciences International Islamic University, Islamabad.

c) **Internal Examiner:** Signature:________
Name: **Prof. Dr. Muhammad Ayub**
Designation: Professor
Office Address: Department of Mathematics, QAU Islamabad.

Supervisor Name: Signature:________
Prof. Dr. Muhammad Ayub

Name of Dean/ HOD Signature:________

Prof. Dr. Sohail Nadeem

Nonlinear Mathematical Models With Chemical Reaction

By

Sadia Rashid

CERTIFICATE

A THESIS SUBMITTED IN THE PARTIAL FULFILLMENT OF THE REQUIREMENTS FOR THE DEGREE OF THE

DOCTOR OFPHILOSOPHY IN MATHEMATICS

We accept this thesis as conforming to the required standard

1. ______________________
Prof. Dr. Sohail Nadeem
(Chairman)

2. ______________________
Prof. Dr.Muhammad Ayub
(Supervisor)

3. ______________________
Prof. Dr. Muhammad Mushtaq
(External Examiner)

4. ______________________
Dr.Rahmat Ellahi
(External Examiner)

Department of Mathematics, COMSATS University, Park Road Chak Shahzad, Islamabad.

Department of Mathematics & Statistics International Islamic University, Sector H-10 Islamabad.

Department of Mathematics
Quaid-I-Azam University
Islamabad, Pakistan
2020

DEDICATED TO MY PARENTS,

MY DAUGHTER & MY HUSBAND

Acknowledgments

In the name of Allah, the Most Merciful and the Most Compassionate, all praise to be Allah, the Lord of the worlds and prayers to Muhammad PBUH and his progeny. His servants and messenger. I am completely sure that this thesis would have never turned into reality without his guidance. I express sincere gratitude to my university for giving me an opportunity to complete this thesis. Foremost I am obliged to my supervisor Professor Muhammad Dr. Ayub. His unwavering enthusiasm for Mathematics kept me constantly engaged at every step along immense knowledge and patience led to the completing of this PhD thesis. I am grateful to my respected teachers Dr. Tasawar Hayat, Dr. Sohail Nadeem, Dr. Masood Khan, Dr. Malik Muhammad Yousaf and Dr. Muhammad Aslam for their valuable suggestions in all aspects.

This acknowledgment will surely remain incomplete if I wouldn’t express my deep indebtedness and cordial thanks to the people who mean world to me, my family. I enact my heartfelt thanks and respect, which springs from my soul to my parents, whose prayers are accompaniment in the journey of my life. Each and every credit goes to them for making me what I am today. I am in great debt to acknowledge the heartstrings and prayers of my caring sisters, brother and and husband whose value to me only grow with age. I acknowledge my husband, who is my champion and who motivated me farther than I thought I could. He always supported and motivated me for the successful completion of my PhD thesis. I don’t imagine a life without their love and blessings. Thank you all for having faith in me.

My appreciation also extends to my laboratory colleagues especially Dr. Muhammad Ijaz Khan and Dr. Sumaira Qayyum. Their mentoring and encouragement have been valuable.

My heartfelt thanks to Dr. Tanzila Hayat, Dr. Maryum Subhani, Dr. Humaira Sardar, Dr. Nuzhat Irshad, Ms Madiha bibi, Ms Madiha Rashid, Ms Samiya for always being there and bearing with me the good and bad times during my wonderful days of PhD. I also thanks to all those people who directly or indirectly helped me during my PhD journey.

The contributions vary but the appreciation is still large thus I leave it in the hands of Allah to repay the debt to all those beautiful people. May Allah make all our intentions sincere for His pleasure alone (Aameen).

Nov. 13, 2020
Sadia Rashid

Preface

It is commonly known as the many materials like melts, muds, emulsions, tomato paste, shampoos, soaps, molten plastics, condensed milk, apple sauces, sugar solution, food stuffs, polymeric liquids etc do not hold the Newtonian's law of viscosity and therefore known as the non-Newtonian fluids. The non-Newtonian fluids are charactertized as three types namely, differential, rate and integral types. It is noted that the differential type fluids have been examined much in the literature compared with the rate type fluids. The rate type fluid models exhibit the characteristics of relaxation and retardation times which cannot be handled through differential type fluids. However these fluids are unable to predict shear thinning/thickening and normal stress effects. There are many chemical reacting system classification subject to species chemical reaction with bounded activation energy. Activation energy is an essential part in chemical reaction. Such models arise in geo-thermal, chemical engineering, mechanics of water and oil storage processes. The communication between mass transfer and chemical reaction are typically exceptionally compound and can identified in the creation and utilization of reactant classes for different duties both inside fluid and mass transmission. With these motivations in mind, the present thesis is organized as follows.

Having all the above aspects in mind, in this thesis, we visualized the aspects of various type nonlinear fluids under different conditions and laws. The Fourier's and Fick's laws and their advanced forms are used for better modeling of heat and mass transport processes. The structure of this thesis is governed as follows.

Literature review regarding previous published attempts, description of solution procedure and relations for conservation of mass, linear momentum and energy are given in chapter one.

Chapter two addresses three-dimensional nanomaterial flow of Maxwell material over a stretchable moving sheet. The flow in rotating frame is generated by linear stretched sheet.

Furthermore, nanofluid mechanism is addressed subject to thermophoresis and Brownian diffusions. Chemical reaction at a stretchable surface is accounted via modified Arrhenius energy. Boundary layer approximation is utilized. Suitable variables lead to strong nonlinear ODEs. Numerical approach is implemented for solution development. The velocity components, temperature and mass concentration are scrutinized. Computational iterations for mass and heat transfer rates are discussed through tabulated forms. The observations of this chapter have been published in **Applied Nanoscience March (2019), DOI: 10.1007/S13204-019-00998-3 .**

Purpose of Chapters three is to examine Darcy- Forchheimer in a rotating frame. Flow due to stretched sheet fills the porous space. Binary chemical reaction is entertained. Resulting system is numarically solved. The plots are arranged for rotational parameter, porosity parameter, coefficients of inertia, Prandtl number and Schmidt number. It is revealed that rotation on Velocity has opposite effects when compared with temperature and concentration distribution. Skin friction coefficient and local Nusselt and Sherwood numbers are numarically discussed. Motion of the fluid reduces for higher porosity parameter and inertia coefficient. The findings of this chapter have been published in **International Journal of Method for Heat and Fluid Flow, Vol.29 No.3, pp 935-948.https://doi.org/10.1108/HFF-06-2018-0292.**

Chpter four is prepared to examine outcome of activation energy in rotating flow of an Oldroyd-B nano liquid.. Flow is generated due to stretched surface. Binary chemical reaction is studied. Brownian and thermophoresis effects are considered. The system of nonlinear ordinary differential equations are derived. Convergent series solutions are obtained by homotopy analysis method. The resulting expressions for velocities, temperature and concentration are computed for different embedded parameters. It is found that velocities have decreasing effect when rotation parameter is enhanced. Brownian and thermophoresis are increasing functions of temperature and concentration. The physical quantities are sketched and discussed numerically. Concentration and temperature fields show decreasing behavior via Brownian and thermophoresis parameters This material is published in **International Journal of Method for Heat and Fluid Flow, July (2019), DOI.org/10.1108/HFF-12-2018-0755.**

Chapter five explores 3D incompressible steady MHD flow of Oldroyd-B material in a rotating frame. The flow is caused through linearly stretched sheet. Applied magnetic field is accounted. Cubic autocatalytic chemical reaction is considered at the surface. Convective conditions at the boundary are considered for heat transport. Flow problem is modeled with the help of boundary layer approximations. Homotopy method is utilized for the series solutions. Impacts of Materials of these three chapters have been Accepted in **Indian Journal of Physics**

Main aim of chapter six is to to study the three-dimensional rotating mixed convective flow of nanomaterial. Chemical reaction associated with Arrhenius energy is also accounted. Flow is created through exponential stretchable sheet. Slip mechanisms to nanomaterial like Brownian and thermophoresis diffusions are considered. Moreover, heat transfer analysis is developed in existence of heat source/sink and radiative flux. Similarity transformations are implemented to develop the system of nonlinear ordinary ones. Numerical approach (Built-in-Shooting) has been utilized to handle the governing mathematical system. Graphically impacts of pertinent parameters on the velocity, mass concentration and temperature are deliberated. Local Nusselt number and Sherwood number are examined and analyzed. It is noticed that temperature field enhances versus radiation and heat source/sink parameter while it decays through higher Prandtl number. The outcomes of this chapter are published in **Applied Nanoscience, March (2019), DOI: https//doi.org/10.1007/s1320**

Chapter seven highlights to investigate three-dimensional steady rotating flow of rate type fluid (Maxwell fluid) over an exponential stretching surface. The Maxwell fluid saturates the porous space via Darcy-Forchheimer relation. Flow caused by the exponential stretchable surface of sheet. Chemical reaction along with Arrhenius energy is considered at the surface. Energy expression is modeled subject to heat source/sink and radiation flux. Appropriate transformations leads to ordinary ones. Homotopy method is implemented for the series solutions. Pertinent parameters are discussed graphically. Special consideration is given to the engineering quantities like Sherwood and Nusselt numbers and discussed numerically through tabular form. Temperature distribution enhances versus higher radiation and heat source/sink parameter while decays for larger Prandtl number. Furthermore velocity shows decreasing trend through larger porosity and Deborah number. The obtained results are published in **Applied Nanoscience, March (2019), DOI:10.1007/s13204-019-01008-2**

This chapter eight is prepared to explores the three-dimensional steady incompressible flow of Oldroyd-B fluid subject to stretchable surface. The flow of material induced through stretchable surface with Darcy-Forchheimer medium. Homogeneous-heterogeneous reactions are considered. Convective boundary conditions and heat source/sink effects are considered for the heat transport. Boundary layer concept is used in the development of flow problem. Series solutions are obtained of the nonlinear system through homotopy technique. Physical significance of pertinent parameters are discussed and plotted graphically. Heat transfer rate is discussed numerically. The outcomes of this chapter are published in **Applied Nanoscience, April (2019) , DOI:10.1007/s13204-019-01037-x.**

Nomenclature

$\mathbf{V}'$	velocity field
$\mathbf{S}^*$	extra stress tensor
$\boldsymbol{\tau}$	Cauchy stress tensor
$\mathbf{I}$	Identity tensor
Ω	angular speed,
k_r	reaction rate
U_0	reference velocity
$\mathbf{b}$	body force per unit mass
q	heat flux
q_r	radiative heat flux
$\mathbf{j}^*$	mass flux
ρ_f	density of liquid
p	pressure gradient
$\mathbf{A}_1$	first Rivlin-Ericksen tensor
$\boldsymbol{\nabla}$	vector differential operator
τ	heat capacity ratio
$(\rho c)_p$	effective heat capacity of nanoparticles
$(\rho c)_f$	heat capacity of fluid
D_B	Brownian motion coefficient
D_T	thermophoresis diffusion coefficient
λ_1^*, λ_2^*	fluid relaxation and retardation time
a	stretching rate
$\mathbf{T}.\mathbf{L}$	viscous dissipation

c_p	specific heat at constant pressure
h_f	heat transfer coefficient
$\frac{D}{Dt}$	covariant derivative
u, v, w	velocity components
x, y, z	space coordinates
L	characteristics length
μ	dynamic viscosity
D	mass diffusivity
a_0	positive constant
ν	kinematic viscosity
$u_w(x)$	stretching velocity
k_2	heterogeneous strength
T^*	transpose
T	fluid temperature
T_w	wall temperature
T_f	hot fluid temperature
T_∞	ambient fluid temperature
M	magnetic field
C	fluid concentration
C_w	wall concentration
C_∞	ambient fluid concentration
k_1	homogeneous strength
E_a	activation energy

$\mathbf{\nabla C}$	concentration gradient
k	fluid thermal conductivity
α_m	thermal diffusivity
λ	rotation parameter
κ	Boltmann constant
β_1, β_2	Deborah numbers for relaxation and retardation times
δ	temperature difference
a	stretching rate
β	porosity parameter
F_r	inertia coefficient
E_1	activation energy
Pr	Prandtl number
σ	chemical reaction rate
β_0^*	thermal expansion coefficient
β_0	solutal expansion coefficient
R	tharmal radiation
c_f	specific heat
h_f	heat transfer coefficient
a_0	positive constant
g_e	acceleration gravity
B_0	magnetic field strength

σ^{**}	electrical conductivity
σ^{*}	stefan-Boltzmann constant
Q_0	heat source/sink coefficient
h_s	heat transfer coefficient
g	gravitational acceleration
E	activation energy parameter
n	fitted rate constant
λ_1	mixed convection parameter
N	buoyancy ratio parameter
Gr	Grashof number
A	emperature exponent parameter
S	heat source/sink variable
m	mean absorption coefficient
B	concentration exponent
$S\,(>0)$	heat generation parameter
$S\,(<0)$	heat absorption parameter
N_b	Brownian motion parameter
N_t	thermophoresis parameter
K	permeability of porous medium
R	thermal radiation parameter

γ	Biot number
Sc	Schmidt number
C_f	surface drag force
Sc	Schmidt number
Nu_x	local Nusselt number
C_b	drag coefficient
F	non-uniform inertia coefficient
$\boldsymbol{\tau}^{ij}$	components of Cauchy stress tensor
$\mathbf{S}^{*ij}$	components of Extra stress tensor
$\mathbf{A}^{ij}$	components of first Rivlin-Ericksen tensor

Sh_x	local Sherwood number
τ_w	surface shear stress
q_w^*	surface heat flux wall
j_w^*	surface mass flux wall
Re_x	local Reynolds number
$\mathcal{N}_f$	nonlinear operator
u	unknown dependent function
q	embedding variable
$\hbar$	auxiliary variable
$\mathcal{L}^*$	linear operator
$f_0(\eta), g_0(\eta), \theta_0(\eta), \phi_0(\eta)$	initial guesses
$f_{m^*}(\eta), g_{m^*}(\eta), \theta_{m^*}(\eta), \phi_{m^*}(\eta)$	general solutions
$f_{m^*}^*(\eta),\ g_{m^*}^*(\eta), \theta_{m^*}^*(\eta), \phi_{m^*}^*(\eta)$	special solutions
A_{*i}	arbitrary constants
η	independent variable
ψ	stream function
$f'(\eta)$	velocity field
$\theta(\eta)$	thermal field
$\phi(\eta)$	concentration field
$g(\eta)$	micro-rotation velocity field

Contents

Chapter 1

Review and some fundamental laws

1.1 Introduction

Review of previous related studies related to boundary layer flow, mixed convection, nanomaterial, heat and mass transfer analysis with chemical reaction, thermal conductivity are incorporated here. Mathematical formulation for viscous, Oldroyd-B fluid, maxwell fluid are discussed for better understanding of upcoming chapters. The solution techniques like Homotopy analysis method (HAM), Optimal homotopy analysis method ($OHAM$) are briefly explained in present chapter.

1.2 Background

Recently nanomaterial in context of their enhanced thermal characteristics has become much consideration of the investigators. Nanoparticles comprise base liquid with nanometer sized particles, such as oxides, metals, carbides or carbon nanotubes. Nanomaterials have advantage to improve their thermal conductivity and the convective heat transport coefficient when compare with the base liquid. There are altered consumptions of nanomaterials in heat exchanger, centrifugal and axial blades compressor, gas turbines blades, microelectronic board's circuit and numerous organic application. Thus Choi. [1] analyzed the impacts of nanomaterials in base liquids which upgraded the thermal conductivity of base liquid. A numerical model of nanoliquid which demonstrates the thermophoresis and Brownian development is examined by

Buongiorno. [2] Frequent investigators have been considered various nanomaterial by taking into single and two-phase models of nanoliquid. Hayat et al. [3] examined peristaltic flow of viscoelastic nanomaterials subject to Hall and ion impacts. Hayat et al. [4] also evaluated silver and copper water nanofluid flow with subject to radiation. The under discussion subject matter has become a burning issue of many researchers besides they are engaged for investigation of nanomaterials under different aspects **(see Refs.[5 − 22])**. Momentum and heat transport in boundary layer flow subject to stretched sheet from both theoretical and practical perspectives have been discussed by numerous researchers and engineers. It is because of their broader applications like food production, polymer technology, advanced energy conversion system and engineering and spinning of fiber in heat transfer at high temperature. Radiative heat transport play very imperative role in these field. Thermal radiation impacts are important when comparison between the surface and the ambient temperature is enhanced. Viscoelastic material flow effects with thermal radiation and mixed convection subject to porous wedge is inspected by Rashidi et al. [23]. [24]. Mukhopadhyay presented thermal radiation with suction/blowing effects on flow due to exponentially stretching. Radiative flux impacts in viscous material over a stretchable surface is scrutinized by Hayat and Sajid. [25]. MHD viscoelastic boundary layer stretchable flow versus thermal radiation and non-uniform heat source/sink are presented by Nandeppanavar et al. [26]. Bhattacharyya et al. [27] have examined radiative flux behavior in micropolar liquid subject to porous shrinking surface. Second law analysis for variable viscosity on a vertical plate with radiative flux is scrutinized by Makinde et al. [28] Some meaningful consideration with numerous flow assumptions are presented $[29 - 44]$.

Materials which have nonlinear deformation upon the applications of shear stress are termed as non-Newtonian. Non-Newtonian material (fluid) plays an important role in various parts of mechanical engineering, textile industries and branches of applied science. There are numerous applications of such materials for instance, honey, tomato, toothpaste, mud, shampoo, paints and so many others. Not only single relation is required to examine the different characteristics of non- Newtonian material. There are numerous non-Newtonian materials models like Jeffrey model, Eyring model, Prandtl Eyring model, Casson model, second grade, Sisko model, Oldroyd-B model, Carreaue model and so on. Here we have considered Oldroyd-B model which is a rate material that exhibits properties of retardation and relaxation times. Zhang et al. [45]

discussed heat transport characteristics in Oldroyd-B nanoliquid flow related time dependent thin film stretchable sheet. Shivakumara et al. [46] scrutinized thermal convective instability in flow of Oldroyd-B nanoliquid fluid subject to porous medium. Forced convective nanomaterial flow of Oldroyd-B fluid between two isothermal stretchable disks with magnetic field is examined by Hashmi et al. [47]. Zhang et al. [48] explored thin film flow of Oldroyd-B nanoliquid with Cattaneo-Christov double diffusion. They also considered chemical reaction and dissipation effects. Shehzad et al. [49] scrutinized 3D-forced convective Oldroyd-B fluid flow with thermophoresis and Brownian diffusions. Kumar et al. [50] discussed the nanomaterial flow of Oldroyd-B fluid subject to radiative flux and dissipation. Electrical conducting nanomaterial flow of non-Newtonian liquid subject to porous stretchable sheet is discussed by Das et al. [51]. Gireesha et al. [52] discussed heat and mass transport in nanoliquid flow of Oldroyd-B material with heat source/sink by a stretchable surface. Khan and Mahmood [53] discussed combined effects of heat source/sink and thermophoretic diffusion effects on nanoliquid flow of non-Newtonian fluid inside stretchable disks. Flow of Oldroyd-B nanomaterial with heat source/sink and radiative flux is explored by Waqas et al. [54]. Refs. [$55-86$] represent various fluid models subject to different flow assumptions.

There are many chemically reacting system classifications subject to species chemical reaction with limited activation energy. The communication among mass transfer and chemical reaction are typically exceptionally compound and can be detected in the creation and consumption of reactant classes for various situations both inside liquid and mass transmission. Activation energy is very important factor in chemical species. It is least obligatory energy which is used to start chemical reaction. Activation energy concept is often applicable in these areas such as geothermal, chemical engineering, oil and water emulsions, geothermal reservoirs. Firstly Bestman [87] discussed the chemical reaction and activation energy with boundary layer flow. He applied perturbation technique to investigate the role of activation energy. Makinde et al. [88] reported impacts of mixed convection in unsteady flow with suction/injection, thermal radiation and Arrhenius reaction. Maleque [89] reported exothermic/endothermic reaction in mixed convection flow. Awad et al. [90] explored Arrhenius activation energy with rotating fluid flow. Radiation effect in Casson-fluid flow with activation energy is examined by Sheikh et al [91]. Khan et al. [92] discussed effect of activation energy impacts on entropy generation with radiation motion of nanomaterial. Rotating Maxwell fluid flow subject to with activation energy is explored by Mustafa et al [93]. Khan et al. [94] elucidated the Cross nanofluid flow with activation energy. Buoyancy effects on MHD nanofluid flow with chemical reaction activation energy is addressed by Hayat et al [95]. Latest attempts regarding activation energy can be seen through studies $[96-99]$.

The homogeneity and heterogeneity are two chemical conceptions that we designate related to the uniformity of a subject. The term homogeneous denotes to "same" and heterogeneous refers to "different". The chemical processes that occur in a single phase (liquid, gaseous or solid) are homogeneous reaction. There are two broad classes of reactions namely homogeneous and heterogeneous based on the physical state of present substances. The most important of homogenous processes are the reactions inside gasses (for example, the combination of common household gas and oxygen to yield a flame) and the processes between fluids or substances melted in liquids (for instance, the reactions or processes between aqueous solutions of bases and acids). From the theoretical point of view, homogeneous processes are the simpler of two categories of processes because the chemical changes that take place are exclusively dependent on the nature of interactions of reacting substances. In this considered flow analysis, we have implemented the cubic autocatalytic chemical reaction at the surface. Mass diffusions are assumed equal to examine the attributes of mass concentration. Refs. $[100-109]$.

1.3 Basic laws

1.3.1 Conservation law of mass

According to conservation law of mass, the mass cannot be created and it cannot be destroyed. In mathematical expression it can be written as

$$\frac{\partial \rho}{\partial t} + \mathbf{\nabla}.\left(\rho \mathbf{V}^{'}\right) = 0. \tag{1.1}$$

Mass conservation's law for incompressible fluid takes the form

$$\mathbf{\nabla}.\mathbf{V}^{'} = 0. \tag{1.2}$$

In Cartesian coordinates

$$\frac{\partial u}{\partial x}+\frac{\partial v}{\partial y}+\frac{\partial w}{\partial z}=0. \tag{1.3}$$

1.3.2 Conservation law of linear momentum

This law states that total linear momentum of the system is conserved. It is derived from Newton's second law and mathematically can be represented as follows:

$$\rho\frac{d\mathbf{V}'}{dt}=\boldsymbol{\nabla}.\boldsymbol{\tau}^{*}+\rho\mathbf{b}^{*}. \tag{1.4}$$

Cauchy stress tensor is defined by

$$\boldsymbol{\tau}^{*}=-p\mathbf{I}^{*}+\mathbf{S}^{*}. \tag{1.5}$$

In Cartesian coordinates and using velocity field $\mathbf{V}'=[u(x,y,z),v(x,y,z),w(x,y,z)]$.

1.3.3 Conservation law of energy

The law of conservation of energy reveals that the total energy of the system remains constant. It is derived from the first law of thermodynamics. In mathematical form we can express it in the following way:

$$\rho c_p\frac{dT}{dt}=\boldsymbol{\tau}^{*}.\mathbf{L}^{*}-\operatorname{div}\mathbf{q}^{*}-\operatorname{div}\mathbf{q}^{*}r. \tag{1.6}$$

The term on the L.H.S of Eq. (1.6) denotes internal energy, first term on R.H.S denotes viscous dissipation while the second and third terms represent thermal and radiative heat fluxes respectively.

1.3.4 Equation of mass transport

The total concentration of the system under observation remains constant according to the Equation of mass transport. Mathematically we have

$$\frac{dC}{dt}=-\boldsymbol{\nabla}.\mathbf{j}^{*}. \tag{1.7}$$

From Fick's first law we have

$$\mathbf{j}^{*}= -D\boldsymbol{\nabla}C. \tag{1.8}$$

Thus equation of mass transport becomes

$$\frac{dC}{dt} = D\boldsymbol{\nabla}^{2}C. \tag{1.9}$$

1.4 Non-Newtonian Liquids

1.4.1 Viscous fluid

Those fluids which obey the Newton's law of viscosity. Extra stress tensor for the Newtonian fluid is as follows:

$$\mathbf{S}^{*}=\mu\mathbf{A}_{1}. \tag{1.10}$$

Mathematically first Rivlin-Ericksen is

$$\mathbf{A}_{1} = \operatorname{grad}\mathbf{V}^{'} + \left(\operatorname{grad}\mathbf{V}^{'}\right)^{T^{*}}. \tag{1.11}$$

1.4.2 Maxwell fluid

It is the non-Newtonian fluid model and the simplest subclass of rate type fluids which elaborates the features of linear viscoelastic fluids having only relaxation time. Extra stress tensor for a Maxwell fluid is presented by

$$\mathbf{S}^{*} + \lambda_{1}^{*}\left(\frac{d\mathbf{S}^{*}}{dt} - \mathbf{L}\mathbf{S}^{*} - \mathbf{S}^{*}\mathbf{L}^{t}\right)] = \mu\mathbf{A}_{1}. \tag{1.12}$$

1.4.3 Oldroyd- B liquid

Here one considers

$$\boldsymbol{\tau}^{*} = -p\mathbf{I}^{*}+\mathbf{S}^{*}, \tag{1.13}$$

an extra stress tensor is defined by

$$\mathbf{S}^{*} + \lambda_{1}^{*}\left(\frac{d\mathbf{S}^{*}}{dt} - \mathbf{L}\mathbf{S}^{*} - \mathbf{S}^{*}\mathbf{L}^{t}\right)] = \mu\left[\mathbf{A}_{1} + \lambda_{2}^{*}\left(\frac{d\mathbf{A}_{1}}{dt} - \mathbf{L}\mathbf{S}^{*} - \mathbf{S}^{*}\mathbf{L}^{t}\right)\right]. \tag{1.14}$$

1.5 Solution methodologies

1.5.1 Homotopy analysis method(HAM)

The idea of homotopy was firstly given by Liao [110] in 1992. This method deals highly nonlinear problems. The detail procedure of this method is applied in chapters 4, 5, 7 and 8.

1.5.2 Optimal homotopy analysis method$(OHAM)$

The concept of minimization is used for average square residual errors.

$$\varepsilon_{m^*}^{g} = \frac{1}{k^*+1}\sum_{j=0}^{k^*}\left[\mathcal{N}_f\left(\sum_{i=0}^{m^*} f\left(\eta\right), \sum_{i=0}^{m^*} g\left(\eta\right)\right)_{\eta=j\delta^*\eta}\right]^2, \tag{1.15}$$

$$\varepsilon_{m^*}^{\theta} = \frac{1}{k^*+1}\sum_{j=0}^{k^*}\left[\mathcal{N}_\theta\left(\sum_{i=0}^{m^*} \theta\left(\eta\right), \sum_{i=0}^{m^*} f\left(\eta\right), \sum_{i=0}^{m^*} \phi\left(\eta\right)\right)_{\eta=j\delta^*\eta}\right]^2, \tag{1.16}$$

$$\varepsilon_{m^*}^{\phi} = \frac{1}{k^*+1}\sum_{j=0}^{k^*}\left[\mathcal{N}_\phi\left(\sum_{i=0}^{m^*} \phi\left(\eta\right), \sum_{i=0}^{m^*} \theta\left(\eta\right), \sum_{i=0}^{m^*} f\left(\eta\right),\right)_{\eta=j\delta^*\eta}\right]^2. \tag{1.17}$$

Total squared residual error is expressed as:

$$\varepsilon_{m}^{t} = \varepsilon_{m^*}^{f} + \varepsilon_{m^*}^{g} + \varepsilon_{m^*}^{\theta} + \varepsilon_{m^*}^{\phi}. \tag{1.18}$$

Chapter 2

Numerical treatment for rotating nanofluid flow with chemical reaction and activation energy

Many analysts and researchers claim that nanomaterials can be employed to improve the thermal performance of base material. Heat transport over stretchable surface has been examined by numerous engineers due to their vast applications. We consider three-dimensional nanomaterial flow of Maxwell material over a stretchable moving sheet. The flow in rotating frame is generated by linear stretched sheet. Chemical reaction at a stretchable surface is accounted via modified Arrhenius energy. Boundary layer approximation is utilized. Suitable variables lead to strong nonlinear ODEs. Numerical approach is implemented for solution development. Computational iterations for mass and heat transfer rates are discussed through tabulated forms.

.

2.1 Formulation

Here $3D$ Maxwell nanomaterial flow over a rotating frame is considered. The flow in rotating frame is generated by linear stretched sheet. Schematic flow analysis is presented in Fig. 2.1

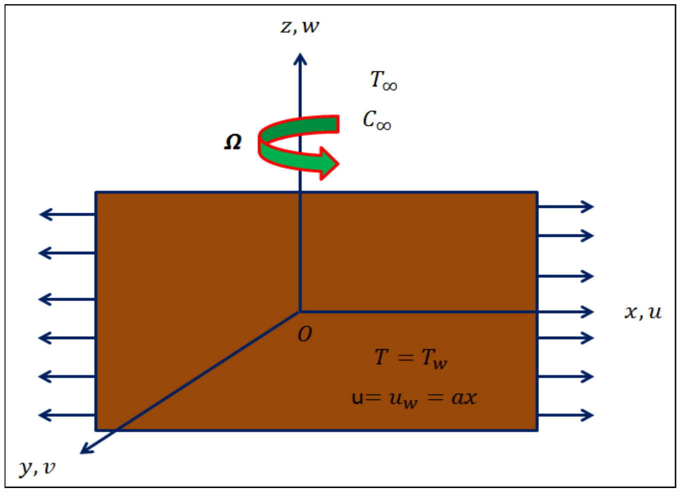

Fig. 2.1. Schematic flow analysis

$$\frac{\partial u}{\partial x}+\frac{\partial v}{\partial y}+\frac{\partial w}{\partial z}=0, \tag{2.1}$$

$$\left.\begin{array}{c} u\frac{\partial u}{\partial x}+v\frac{\partial u}{\partial y}+w\frac{\partial u}{\partial z}-2\Omega v=\nu\frac{\partial^2 u}{\partial z^2} \\ -\lambda_1^*\left(\begin{array}{c} u^2\frac{\partial^2 u}{\partial x^2}+v^2\frac{\partial^2 u}{\partial y^2}+w^2\frac{\partial^2 u}{\partial z^2}+2uv\frac{\partial^2 u}{\partial x\partial y} \\ +2vw\frac{\partial^2 u}{\partial y\partial z}+2uw\frac{\partial^2 u}{\partial x\partial z} \\ -2\Omega\left(u\frac{\partial v}{\partial x}+v\frac{\partial v}{\partial y}+w\frac{\partial v}{\partial z}\right)+2\Omega\left(v\frac{\partial u}{\partial x}-u\frac{\partial u}{\partial y}\right) \end{array}\right) \end{array}\right\} \tag{2.2}$$

$$\left.\begin{array}{c} u\frac{\partial v}{\partial x}+v\frac{\partial v}{\partial y}+w\frac{\partial v}{\partial z}+2\Omega u=\nu\frac{\partial^2 v}{\partial z^2} \\ -\lambda_1^*\left(\begin{array}{c} w^2\frac{\partial^2 v}{\partial z^2}+v^2\frac{\partial^2 v}{\partial y^2}+u^2\frac{\partial^2 v}{\partial x^2}+2uv\frac{\partial^2 v}{\partial xy} \\ +2vw\frac{\partial^2 v}{\partial xz}+2uw\frac{\partial^2 v}{\partial x\partial z} \\ +2\Omega\left(u\frac{\partial u}{\partial x}+v\frac{\partial u}{\partial y}+w\frac{\partial u}{\partial z}\right)+2\Omega\left(v\frac{\partial v}{\partial x}-u\frac{\partial v}{\partial y}\right) \end{array}\right) \end{array}\right\} \tag{2.3}$$

$$u\frac{\partial T}{\partial x}+v\frac{\partial T}{\partial y}+w\frac{\partial T}{\partial z}=\alpha_m\frac{\partial^2 T}{\partial z^2}+\frac{(\rho c)_p}{(\rho c)_f}\left(D_B\left(\frac{\partial T}{\partial z}\frac{\partial C}{\partial z}\right)+\frac{D_T}{T_\infty}\left(\frac{\partial T}{\partial z}\right)^2\right), \tag{2.4}$$

$$u\frac{\partial C}{\partial x}+v\frac{\partial C}{\partial y}+w\frac{\partial C}{\partial z}=D_B\left(\frac{\partial^2 C}{\partial z^2}\right)-\kappa_r^2\left(\frac{T}{T_\infty}\right)^n e^{-\frac{Ea}{KT}}\left(C-C_\infty\right)+\frac{D_T}{T_\infty}\left(\frac{\partial^2 T}{\partial z^2}\right), \tag{2.5}$$

with

$$\left.\begin{array}{c} u=u_w\left(x\right)=ax, \quad v=0, \quad w=0, \quad T=T_w, \quad C=C_w \quad \text{.as} \quad z=0, \\ u\longrightarrow 0, \quad v\longrightarrow 0, \quad T\longrightarrow T_\infty, \quad C\longrightarrow C_\infty \quad \text{as} \quad z\longrightarrow\infty. \end{array}\right\} \tag{2.6}$$

Considering

$$\left.\begin{array}{c} \eta=\sqrt{\frac{a}{v}}z, \quad u=axf'(\eta), \quad v=axg(\eta), \quad w=-\left(av\right)^{\frac{1}{2}}f(\eta), \\ \theta(\eta)=\frac{T-T_\infty}{T_w-T_\infty}, \quad \phi(\eta)=\frac{C-C_\infty}{C_w-C_\infty}. \end{array}\right\} \tag{2.7}$$

One has

$$f'''+ff''-f'^2+2\lambda\left(g-\beta_1 fg'\right)+\beta_1\left(2ff'f''-f^2f'''\right)=0, \tag{2.8}$$

$$g''+fg'-f'g-2\lambda\left(f'+\beta\left(f'^2-ff''+g^2\right)\right)+\beta_1\left(2ff'g'-f^2g''\right)=0, \tag{2.9}$$

$$\theta''+\Pr\left(f\theta'+Nb\theta'\phi'+Nt\theta'^2\right)=0, \tag{2.10}$$

$$\phi''+Scf\phi'+\frac{Nt}{Nb}\theta''-Sc\sigma\left[1+\delta\sigma\right]^n\exp\left[-\frac{E_1}{1+\delta\sigma}\right]\phi=0, \tag{2.11}$$

$$\left.\begin{array}{c} f\left(0\right)=g\left(0\right)=0,\ f'\left(0\right),=1, \quad \theta\left(0\right)=\phi\left(0\right)=1, \\ f'\left(\infty\right)\longrightarrow 0,\ g\left(\infty\right)\longrightarrow 0,\ \theta\left(\infty\right)\longrightarrow 0,\ \phi\left(\infty\right)\longrightarrow 0, \end{array}\right\} \tag{2.12}$$

dimensionless parameters are define as

$$\left.\begin{array}{c} \lambda=\frac{\Omega}{a},\ \beta_1=\lambda_1^*a,\ Pr=\frac{v}{\alpha_m}, \\ Nb=\frac{(\rho c)_p D_b(C_w-C_\infty)}{(\rho c)_f\nu},\ Nt=\frac{(\rho c)_p D_T(T_w-T_\infty)}{(\rho c)_f vT_\infty}, \\ Sc=\frac{\nu}{D_B},\ E_1=\frac{E_a}{\kappa T_\infty},\ \delta=\frac{Tw-T_\infty}{T_\infty},\ \sigma=\frac{k_r^2}{a},\ \mathrm{Re}_x=\frac{ax^2}{\nu} \end{array}\right\}. \tag{2.13}$$

The physical quantities are given by

$$\left.\begin{array}{c} Nu_x=\frac{xq_w}{k(Tw-T_\infty)}, \\ Sh_x=\frac{xj_w}{D(C_w-C_\infty)}, \end{array}\right\} \tag{2.14}$$

with

$$\left.\begin{array}{c} q_w^*=-k\frac{\partial T}{\partial z}\mid_{z=o}, \\ j_w^*=-D\frac{\partial C}{\partial z}\mid_{z=o}, \end{array}\right\} \tag{2.15}$$

finally we have

$$\left.\begin{aligned} Nu_x \operatorname{Re}_x^{-0.5} &= -\theta'(0), \\ Sh_x \operatorname{Re}_x^{-0.5} &= -\phi'(0). \end{aligned}\right\} \tag{2.16}$$

2.2 Analysis

This section is organized for the physical interpretation of non-dimensional velocities $f'(\eta)$ and $g(\eta)$ and concentration $\phi(\eta)$ and temperature $\theta(\eta)$. Fig 2.2 shows that how β_1 affects the velocity $f'(\eta)$. It is noticed that rising values of β_1 show decreasing behavior of velocity $f'(\eta)$ and related layer thickness. Fig. 2.3 illustrates λ outcome on $f'(\eta)$. Greater estimations of λ lead to lower velocity $f'(\eta)$. Also layer thickness for λ is also reduced. Fig. 2.4 display variation of β_1 on velocity distribution $g(\eta)$. Behavior of $g(\eta)$ indicated that flow is negative in y direction. It is seen that magnitude of $g(\eta)$ enhances near the surface. Fig. 2.5 explains the behavior of λ on velocity $g(\eta)$. Here we noticed that magnitude of $g(\eta)$ enhances for higher λ. It is due to the reason that rotational frequency rises for larger (λ). Fig. 2.6 displays influence of β_1 on $\theta(\eta)$. Here we observed $\theta(\eta)$ and layer thickness is enhanced for higher β_1. Fig. 2.7 shows that larger rotation parameter λ yield strong temperature field. Fig. 2.8 describes how Nt affects the $\theta(\eta)$. Influence of Nb on $\theta(\eta)$ is presented in Fig. 2.9. Here both thermophoresis and Brownian motion have increasing behavior. Fig. 2.10 displays Pr effects on $\theta(\eta)$. Higher Pr produces weaker thermal diffusivity which give degeneration in $\theta(\eta)$. Fig.2.11 indicated effect of β_1 on ϕ. We can see here that ϕ is an increasing function of β_1. Fig. 2.12 depicts Nt effects on concentration $\phi(\eta)$. Both ϕ and layer thickness are increased for larger Nt. Influence Nb of on concentration is shown in Fig. 2.13. Here behavior of mass concentration is reverse to that of Nt. Fig. 2.14 represents concentration field effects via activation energy E_1. Thickness of concentrated layer is more by increasing E_1. Effect of Sc on $\phi(\eta)$ is displayed in Fig. 2.15. We can see that $\phi(\eta)$ has decreasing trend via larger Sc. Note that when Sc gradually increases, then Brownian dispersion coefficient diminishes and thus concentration is weaker. Fig. 2.16. depicts to portrayed the impacts of σ reaction rate constant on nanoparticle concentration $\phi(\eta)$. As expected the concentration is decreased when $\sigma > 0$. Effect of δ on $\phi(\eta)$ is shown Fig. 2.17. Obviously $\phi(\eta)$ and δ have inverse relation. It indicates that difference between ambient and wall temperature is higher when mass layer thickness is enhanced.

Tables 2.1 is sketched for the computational iterations of Nusselt number subject to λ, β_1, Pr, Nt and Nb. We have seen that Nusselt number has lower impact for rising (λ, β_1) while, reverse behavior is observed for (Pr). Table 2.2 is plotted for computational iterations of Sherwood number via Sc, E_1, δ and σ. We analyzed that Sherwood number has small and higher estimations for rising (δ, σ) and (Sc, E_1) respectively.

Table. 2.1: Numerical iterations for local Nusselt number

λ	β	Pr	Nt	Nb	$-\theta'(0)$
0.3	0.2	1.0	0.1	0.3	0.456627
0.5					0.417498
0.3					0.292401
1.0	1.5	1.0	0.1	0.3	0.421987
	2.0				0.367132
	4.0				0.105183
0.3	0.5	1.5	0.1	0.3	0.421987
		2.0			0..624356
		3.0			0.748203
0.3	0.2	1.0	0.2	0.3	0.440829
			0.5		0.397037
			0.7		0.37063
0.3	0.2	1.0	0.2	0.1	0.495429
				0.3	0.440829
				0.5	0.390917

Table. 2.2: Numerical iterations for local Sherwood number

Sc	δ	E_1	σ	$-\phi'(0)$
1.0	0.3	1.0	1.0	0.710795
3.0				1.37655
5.0				1.84207
1.0	0.1	1.0	1.0	0.714662
	0.3			0.494606
	0.5			0.49365
1.0	0.2	2.0	1.5	0.492867
		4.0		0.565425
		6.0		0.60443
0.2	0.3	1.0	1.5	0.720555
			2.0	0.717143
			2.5	0.716795

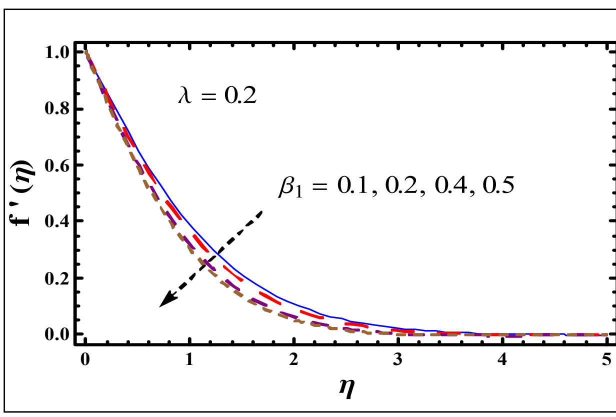

Fig. 2.2. β_1 against $f'(\eta)$.

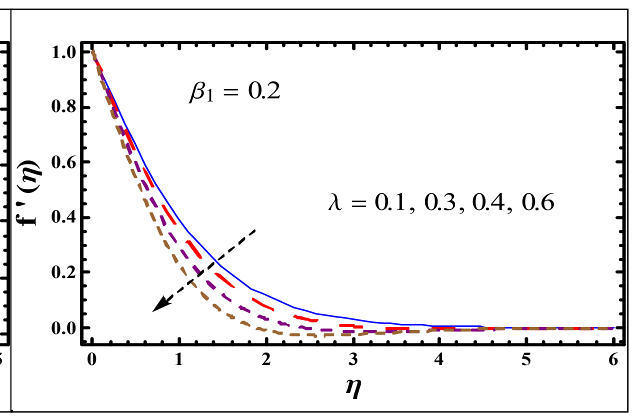

Fig. 2.3. λ against $f'(\eta)$.

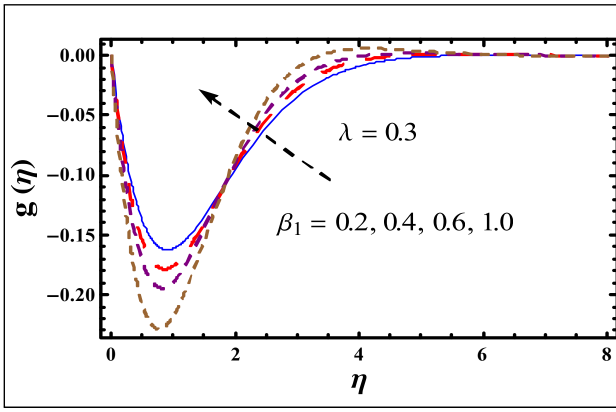

Fig. 2.4. β_1 against $g(\eta)$.

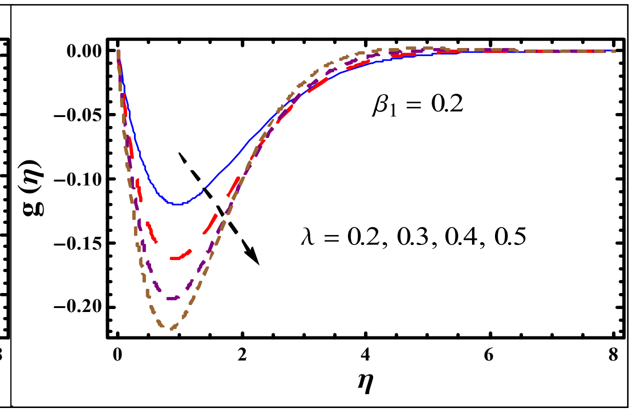

Fig. 2.5. λ against $g(\eta)$.

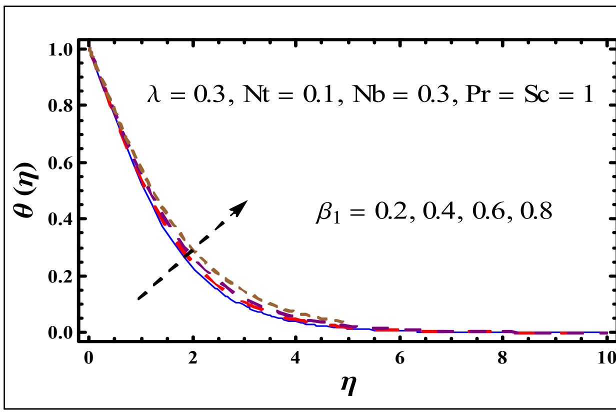

Fig. 2.6. $\beta_1$against $\theta(\eta)$.

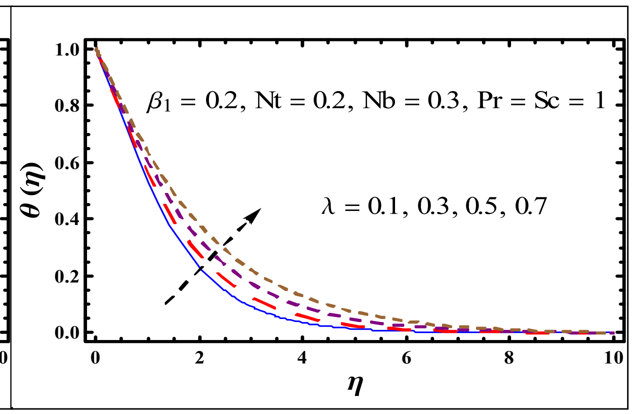

Fig. 2.7. λ against $\theta(\eta)$.

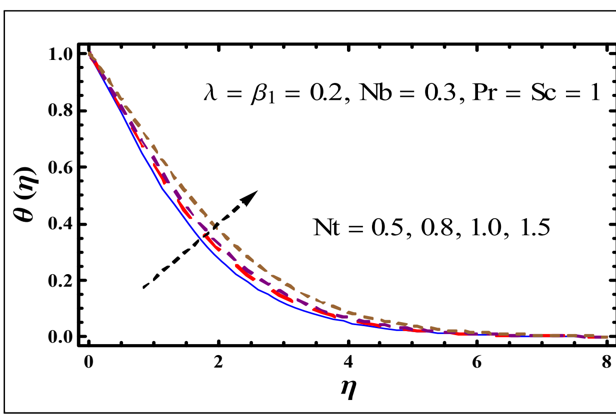

Fig. 2.8. Nt against $\theta(\eta)$.

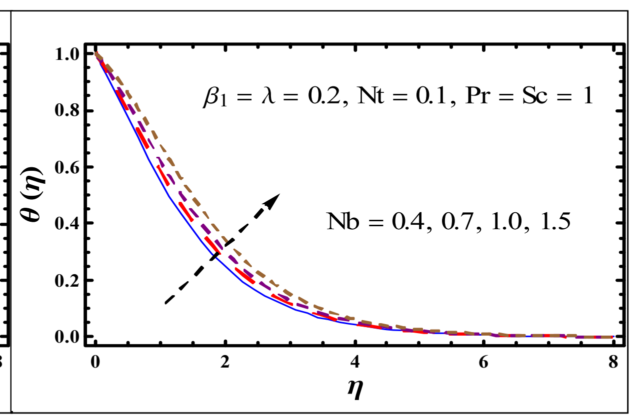

Fig. 2.9. Nb against $\theta(\eta)$.

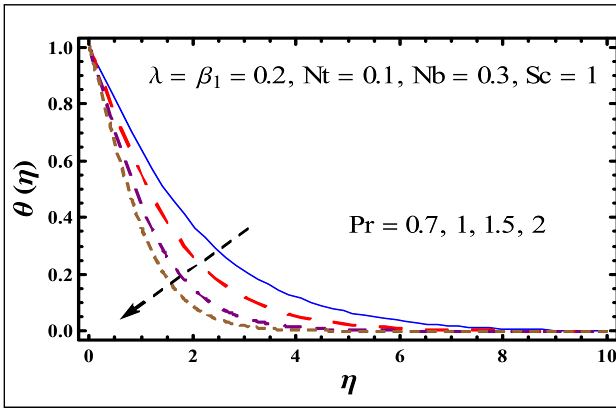

Fig. 2.10. Pr against $\theta(\eta)$.

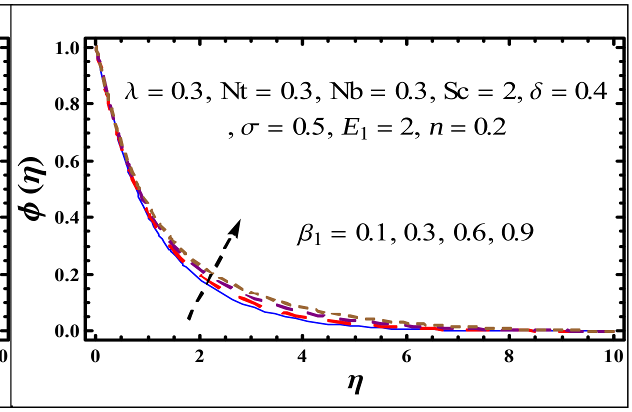

Fig. 2.11. β_1 against $\phi(\eta)$.

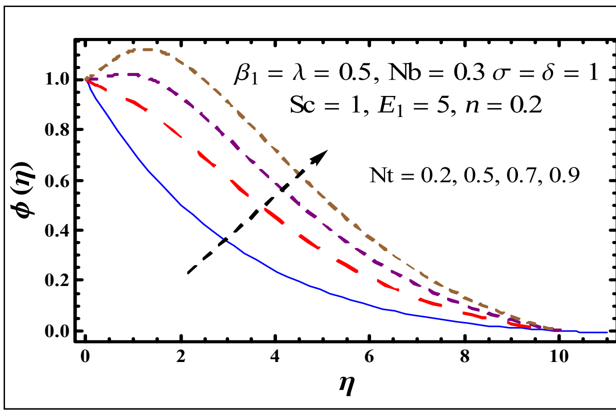

Fig. 2.12. Nt against $\phi(\eta)$.

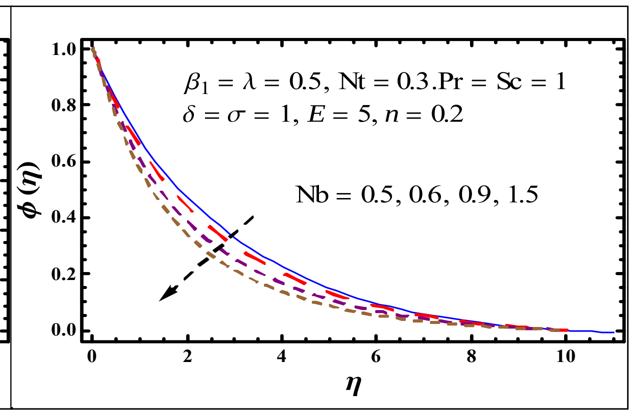

Fig. 2.13. Nb against $\phi(\eta)$.

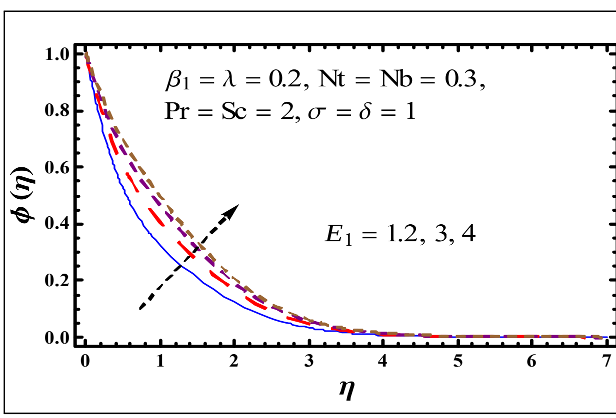

Fig. 2.14. E_1 against $\phi(\eta)$.

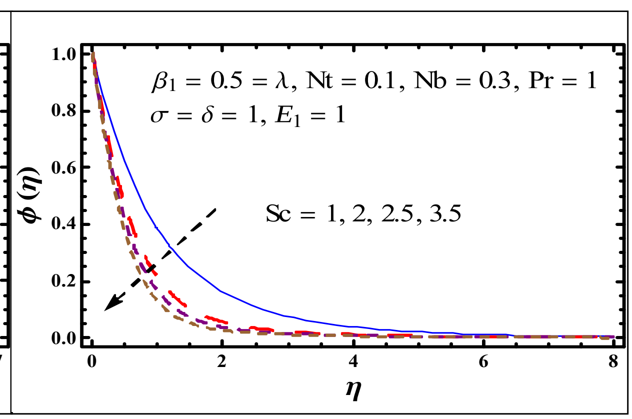

Fig. 2.15. Sc against $\phi(\eta)$.

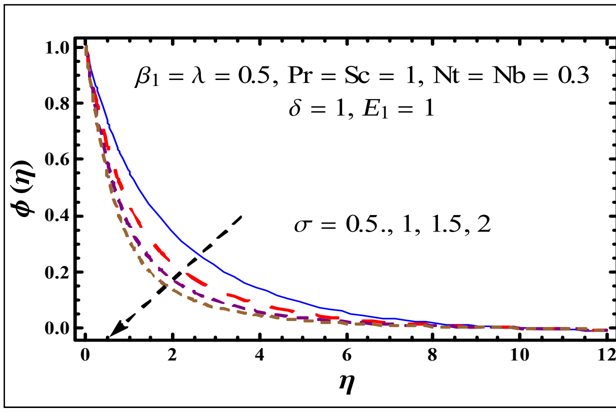

Fig. 2.16. σ against $\phi(\eta)$.

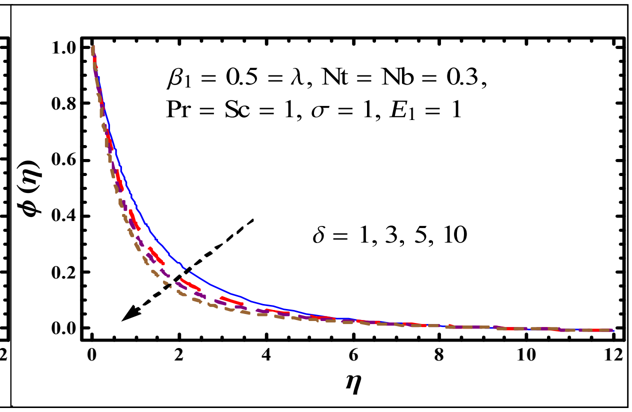

Fig. 2.17. δ against $\phi(\eta)$.

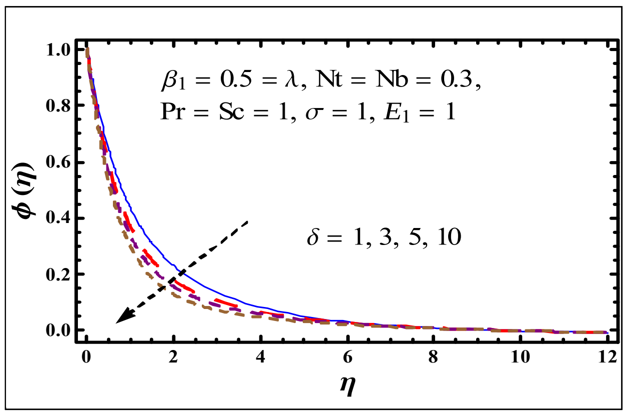

Fig. 2.17. δ against $\phi(\eta)$.

2.3 Conclusion

We have following main points.

- Larger β and λ exhibit decreasing trend for both velocities $f'(\eta)$ and $g(\eta)$.
- An increasing β_1 lead to to decay velocity $f'(\eta)$ whereas reverse is seen for $\theta(\eta)$.
- β and λ has increasing behavior for $\theta(\eta)$
- Have seen increasing behavior in θ and ϕ for larger Nt.
- Concentration field is decay for larger Sc and Nb.
- An increasing E_1 lead to to higher concentration whereas reverse is seen for σ.

- Nusselt number has lower impact for rising (λ, β_1) while, reverse behavior is observed for (Pr).

Chapter 3

Three dimensional rotating Darcy-Forcheimer flow with activation energy

Purpose of the article is to examine Darcy- Forchheimer in a rotating frame. Flow due to stretched sheet fills the porous space. Binary chemical reaction is entertained. Resulting system is numerically solved. The plots are arranged for rotational parameter, porosity parameter, coefficients of inertia, Prandtl number and Schmidt number. It is revealed that rotation on Velocity has opposite effects when compared with temperature and concentration distribution. Motion of the fluid reduces for higher porosity parameter and inertia coefficient. Concentration and temperature field have same behavior via inertia coefficient.

3.1 Formulation

Here we are interested to investigate rotating flow in a porous space. Dissipation and radiation effects are neglected. Due to absence of radiation effect there is no electromagnetic radiation generated by the thermal motion of charged particles in fluid. Effect of activation energy is studied. Stretching surface coincides with the plane $z \geq 0$.

$$\nabla.\mathbf{V}' = 0, \tag{3.1}$$

$$\rho\left[\left(\mathbf{V}'.\boldsymbol{\nabla}\right)\mathbf{V}'+(\boldsymbol{\Omega}\times(\boldsymbol{\Omega}\times\mathbf{r}))+\left(2\boldsymbol{\Omega}\times\mathbf{V}'\right)\right]=-\nabla p+\nabla.\mathbf{S}^{*}, \tag{3.2}$$

$$\rho c_{p}^{*}\left(\mathbf{V}'.\boldsymbol{\nabla}\right)=k\nabla^{2}T, \tag{3.3}$$

$$\left(\mathbf{V}'.\boldsymbol{\nabla}\right)=D\nabla^{2}C-k_{r}^{2}\left(\frac{T}{T_{\infty}}\right)^{n}e^{-\frac{Ea}{\kappa T}}\left(C-C_{\infty}\right). \tag{3.4}$$

Considering the velocity $\mathbf{V}'=[u(x,y,z),v(x,y,z),w(x,y,z)]$, temperature $T=T(x,y,z)$ and concentration $C=C(x,y,z)$ we obtain

$$\frac{\partial u}{\partial x}+\frac{\partial v}{\partial y}+\frac{\partial w}{\partial z}=0, \tag{3.5}$$

$$u\frac{\partial u}{\partial x}+v\frac{\partial u}{\partial y}+w\frac{\partial u}{\partial z}-2\Omega v=\nu\frac{\partial^{2}u}{\partial z^{2}}-\frac{\nu}{K}u-Fu^{2}, \tag{3.6}$$

$$u\frac{\partial v}{\partial x}+v\frac{\partial v}{\partial y}+w\frac{\partial v}{\partial z}+2\Omega u=\nu\frac{\partial^{2}v}{\partial z^{2}}-\frac{\nu}{K}v-Fv^{2}, \tag{3.7}$$

$$\left(u\frac{\partial T}{\partial x}+v\frac{\partial T}{\partial y}+w\frac{\partial T}{\partial z}\right)=\alpha_{m}\frac{\partial^{2}T}{\partial z^{2}}, \tag{3.8}$$

$$u\frac{\partial C}{\partial x}+v\frac{\partial C}{\partial y}+w\frac{\partial C}{\partial z}=D\nabla^{2}C-k_{r}^{2}\left(\frac{T}{T_{\infty}}\right)^{n}e^{-\frac{Ea}{\kappa T}}\left(C-C_{\infty}\right). \tag{3.9}$$

The related boundary condition are:

$$\left.\begin{array}{c}u=ax,\ v=0,\ w=0,\ T=T_{w},\ C=C_{w}\quad\textbf{at}\quad z=0\\ u\longrightarrow 0,\ v\longrightarrow 0,\ T\longrightarrow T_{\infty},\ C\longrightarrow C_{\infty}\quad\textbf{when}\quad z\rightarrow\infty\end{array}\right\}. \tag{3.10}$$

Considering

$$\left.\begin{array}{c}\eta=\sqrt{\frac{a}{v}}z,\ u=axf'(\eta),\ v=axg(\eta),\ w=-\left(a\nu\right)^{\frac{1}{2}}f(\eta),\\ \theta(\eta)=\frac{T-T_{\infty}}{T_{w}-T_{\infty}},\ \phi(\eta)=\frac{C-C_{\infty}}{C_{w}-C_{\infty}}.\end{array}\right\} \tag{3.11}$$

Eq. (3.5) is trivially verified and Eqs.(3.6 − 3.9) become:

Eq. (3.1) is trivially verified and Eqs.(3.2 − 3.6) become:

$$f'''+ff''-\beta f'+2\lambda g-\left(1+F_{r}\right)f'^{2}=0, \tag{3.12}$$

$$g''+fg'-f'g-2\lambda f'-\beta g-F_{r}g^{2}=0, \tag{3.13}$$

$$\theta'' + \Pr f\theta' = 0, \tag{3.14}$$

$$\phi'' + Scf\phi' - Sc\sigma\left[1+\delta\theta\right]^n \exp\left[-\frac{E_1}{1+\delta\theta}\right]\phi = 0, \tag{3.15}$$

with conditions

$$\left.\begin{array}{l} f = 0\ ,\quad f' = 1,\quad g = 0,\ \theta = \phi = 1 \quad \text{at } \eta = 0, \\ f' \longrightarrow 0,\quad g \to 0,\quad \theta \longrightarrow 0,\ \phi \longrightarrow 0 \quad \text{at } \eta \longrightarrow \infty. \end{array}\right\} \tag{3.16}$$

Skin friction coefficient and local Nusselt and Sherwood numbers are

$$\left.\begin{array}{c} Nu_x = \frac{xq_w}{k(Tw - T_\infty)}, \\ Sh_x = \frac{xj_w}{D(C_w - C_\infty)}, \\ C_f = \frac{T_w}{\rho U_w^2}, \\ T_w = \mu\left(\frac{\partial u}{\partial z}\right), \end{array}\right\} \tag{3.17}$$

with

$$\left.\begin{array}{c} q_w = -k\frac{\partial T}{\partial z}\mid_{z=o}, \\ j_w = -D\frac{\partial C}{\partial z}\mid_{z=o}. \end{array}\right\} \tag{3.18}$$

Finally we have

$$\left.\begin{array}{c} C_f\sqrt{\mathrm{Re}_x} = f''(0)\,, \\ \frac{Nu_x}{\sqrt{\mathrm{Re}_x}} = -\theta'(0)\,, \\ \frac{Sh_x}{\sqrt{\mathrm{Re}_x}} = -\phi'(0)\,. \end{array}\right\} \tag{3.19}$$

3.2 Solution methodology

Present problem seems difficult for exact solutions. Therefore numerical method NDSolve of MATHEMATICA is used. The function NDsolve discussed in Numerical Differential Equation to find numerical solutions to differential equations. NDsolve handles both single differential equations and sets of simultaneous differential equations. It can handle a wide range of ordinary differential equations as well as some partial differential equations. It is built in method which directly construct graphs for different embedded variables. Graphs are constructed for velocity, temperature and concentration.

3.3 Numerical results

Equations $(3.12 - 3.16)$ are solved numerically by utilizing NDSolve approach. This portion is prepared to examine variations of embedded parameters on $f'(\eta)$, $\theta(\eta)$ and $\phi(\eta)$. Fig. 3.1 depicts the rotation parameter λ effects on velocity distribution $f'(\eta)$. It is noticed that an increment in rotation parameter λ demonstrates a decrease in velocity $f'(\eta)$. Physically for larger λ the stretching rate of sheet reduces and so velocity diminishes. Fig. 3.2 explains variation of β on $f'(\eta)$. The results of β on $f'(\eta)$ are similar to that of λ. In fact for larger β the fluid becomes more viscous which produces resistance for fluid to flow. Hence $f'(\eta)$ reduces. Fig. 3.3 indicates velocity $f'(\eta)$ for increasing Fr. Here $f'(\eta)$ is decreased by Fr. Fig. 3.4 indicates variation of λ on $\theta(\eta)$ and thermal layer thickness. Both physical quantities are increasing function of λ. Fig. 3.5 explains temperature $\theta(\eta)$ against porosity parameter. We noted that temperature distribution has an increasing behavior for porosity. Physically we noted that due to higher viscosity and resistance between the particles more heat produces and consequently $\theta(\eta)$ enhances. Fig. 3.6 depicts behavior of Fr for temperature. Clearly θ is higher for Fr. Fig. 3.7 displayed Pr effects on $\theta(\eta)$. Here $\theta(\eta)$ is a decreasing function of Pr. As expected thermal diffusivity decreased for higher Prandtl number and so thermal layer also decays. Fig. 3.8 presents λ effects on concentration $\phi(\eta)$. concentration is increased for higher λ. Influence of β on $\phi(\eta)$ is plotted in Fig. 3.9. Clearly concentration is an increasing function of porosity parameter β. Fig. 3.10 displays effects of inertia coefficient Fr on concentration. It is seen that concentration distribution $\phi(\eta)$ is enhanced via large Fr. Fig.3.11 illustrates that larger Prandtl number Pr yield lower concentration distribution $\phi(\eta)$ and related layer thickness. Fig. 3.12. predicts outcome of activation energy E_1. Here E_1 enhanced concentration layer thickness. Fig. 3.13 demonstrated variation of δ on concentration $\phi(\eta)$. Clearly $\phi(\eta)$ is decreased by δ. Figs. 3.14 and 3.15 have been organized for n and σ on concentration $\phi(\eta)$. There is an increment in $\sigma[1+\delta\sigma]^n \exp\left[-\frac{E_1}{1+\delta\sigma}\right]$ when n or σ enhances. Physically as we enhance the values of σ the destructive rate of chemical reaction also increases. It is used to terminate or dissolve the liquid specie more effectively and hence concentration reduces. Impact of Schmidt number Sc on concentration can be seen from Fig. 3.16. Concentration larger thickness is decreased by Sc. Mass diffusivity reduces for larger Sc. This is responsible for decrease in $\phi(\eta)$. Numerical estimation of skin friction coefficient for different rotational parameter, porosity parameter and inertial coefficient is illustrated in Table 3.1. Here skin friction coefficient is more via β, λ, and Fr. Table 3.2 is prepared for $\frac{Nu_x}{\sqrt{\mathrm{Re}_x}}$. It shows that local Nusselt number decreases via porosity β and rotation λ parameters. Table 3.3 exhibits an improvement in local Sherwood number $\frac{Sh_x}{\sqrt{\mathrm{Re}_x}}$ when either reaction rate σ or Schmidt number Sc is increased. Sherwood number is decreasing function of porosity parameter β. Table 3.4 is constructed for validation of our problem. Good agreement is seen from previous literature.

Table 3.1: Skin friction coefficient via variation of β, λ and Fr.

λ	β	Fr	$-f''(0)$
1	0.2	1	1.58724
2			1.862267
3			2.10932
0.5	0.1	1	1.41806
	0.5		1.53031
	1		1.67153
0.3	0.1	1	1.36352
		2	1.58502
		4	1.96195

Table 3.2: Local Nusselt number $-\theta'(0)$ via β, λ and Pr.

β	λ	Fr	Pr	$-\theta'(0)$
0	0.5	1	1	0.508972
1				0.485852
2				0.45752
0.2	0.1	1	1	0.542198
	0.5			0.506965
	0.9			0.467794
0.2	0.5	1	2	0.811336
			3	1.06461
			4	1.1.27979
0.2	0.5	0	2	0.844615
		2		0.783173
		3		0.734272

Table 3.3: Estimation of local Showered number $-\phi'(0)$ for Sc, β, λ, E_1 and σ:

Sc	β	λ	E_1	σ	$-\phi'(0)$
1	0.2	0.5	1	1	0.701962
3					1.36565
5					1.83376
1	0.1	0.5	1	1	0.703102
	2				0.669718
	4				0.547447
0.2	0.2	0.5	1	1.5	0.506206
				2	0.573711
				2.5	0.635773
1	0.2	0.1	1	1	0.72246
		0.3			0.714078
		0.5			0.701962
1	0.2	0.1	2	0.3	0.645658
			3		0.600474
			4		0.574834

Table 3.4: Comparative values of $-f''(0)$ when $\beta = \lambda = Fr = 0$ with refs. [16] and [54].

	$-f''(0)$
Hayat et al. [10]	1.000000
Mugahed [11]	0.999978
Present	1.000000

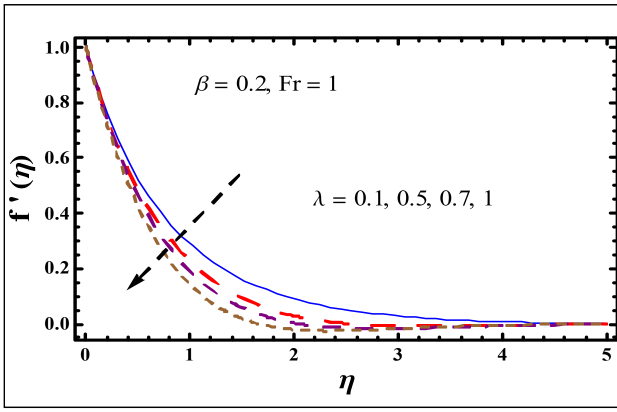

Fig. 3.1. λ variation on $f'(\eta)$.

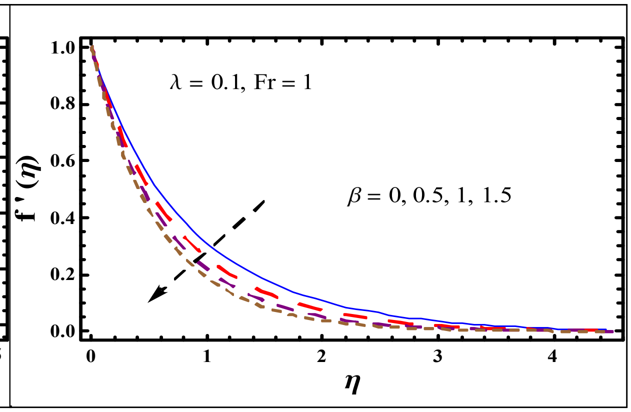

Fig. 3.2. β variation on $f'(\eta)$.

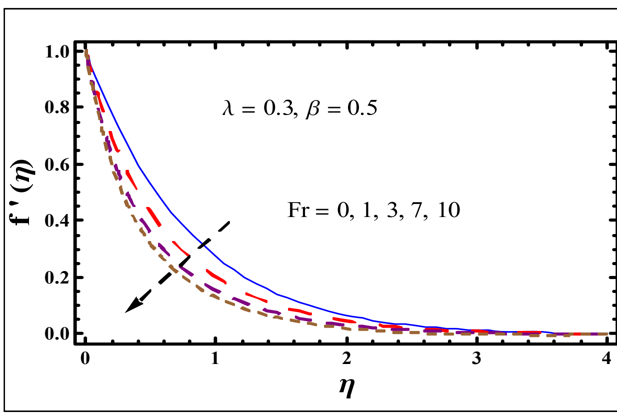

Fig. 3.3. Fr variation on $f'(\eta)$.

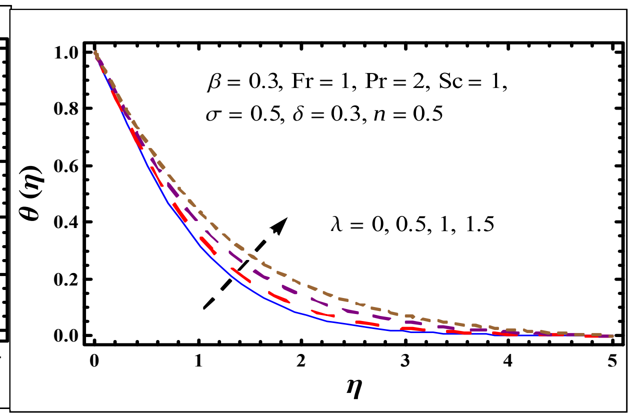

Fig. 3.4. λ variation on $\theta(\eta)$.

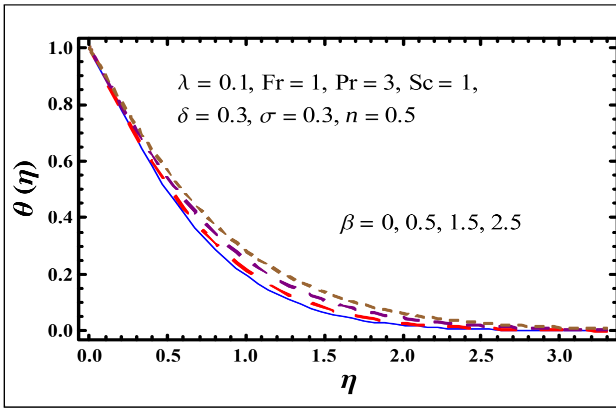

Fig. 3.5. β variation on $\theta(\eta)$.

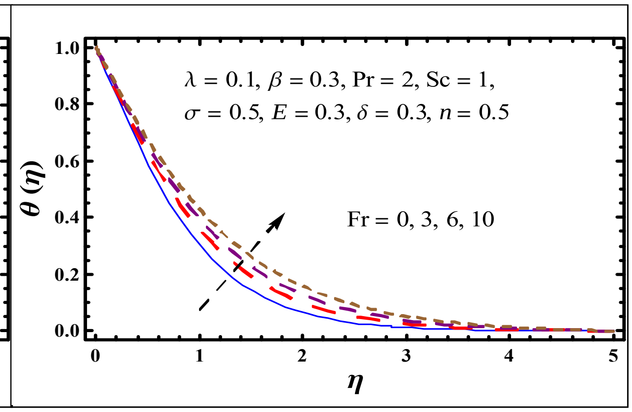

Fig. 3.6. Fr variation on $\theta(\eta)$.

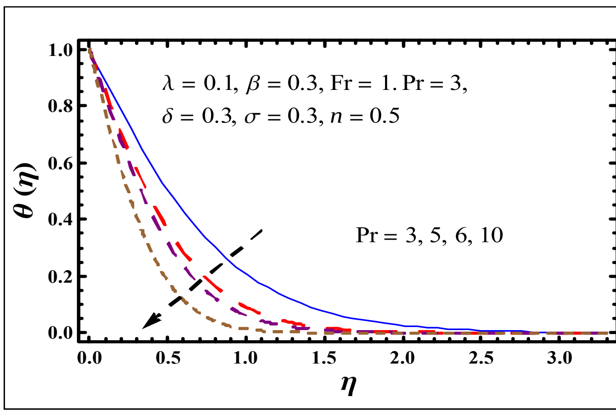

Fig. 3.7. Pr variation on $\theta(\eta)$

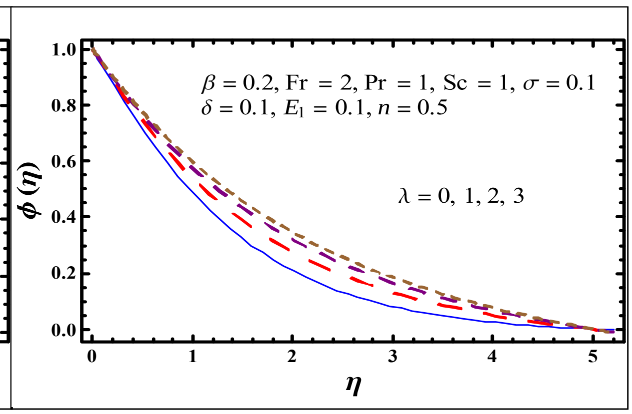

Fig. 3.8. λ variation on $\phi(\eta)$.

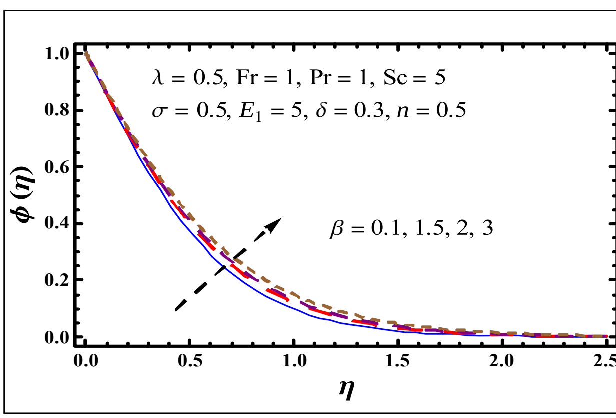

Fig. 3.9. β variation on $\phi(\eta)$.

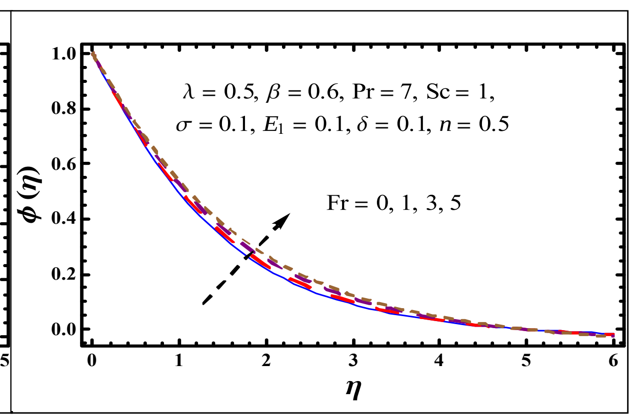

Fig. 3.10. Fr variation on $\phi(\eta)$.

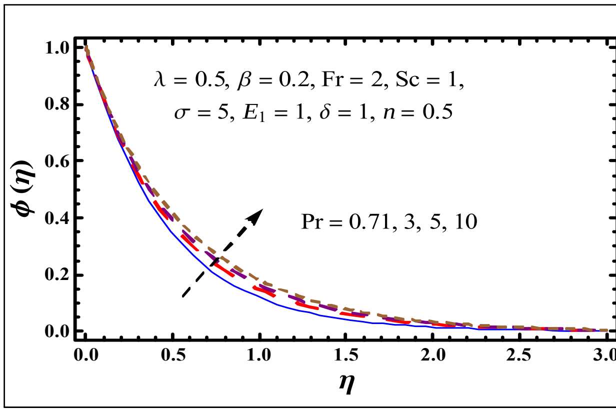

Fig. 3.11. Pr variation on $\phi\,(\eta)$

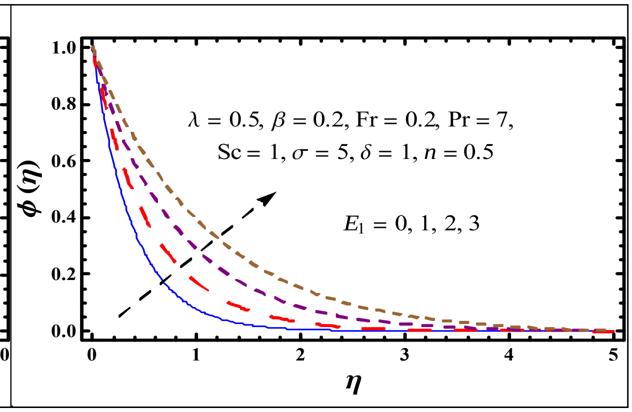

Fig. 3.12. E_1 variation on $\phi\,(\eta)$.

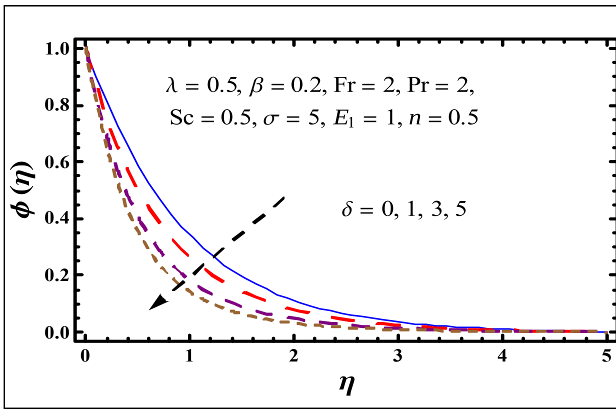

Fig. 3.13. δ variation on $\phi\,(\eta)$

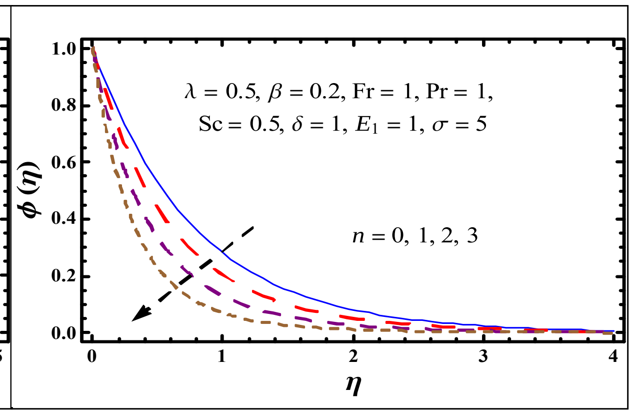

Fig. 3.14. n variation on $\phi\,(\eta)$

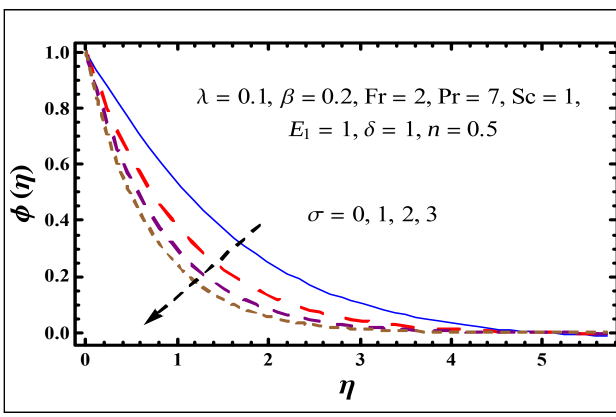

Fig. 3.15. σ variation on $\phi\,(\eta)$.

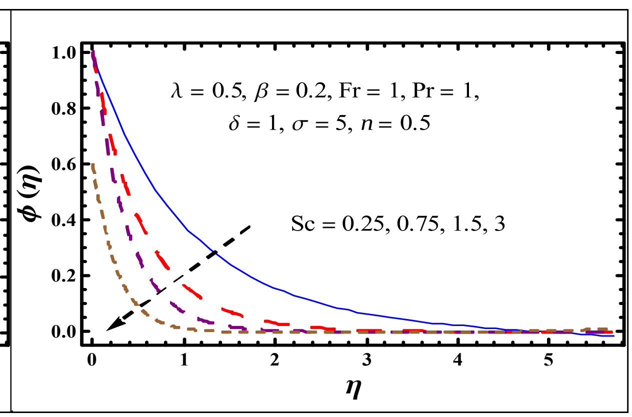

Fig. 3.16. Sc variation on $\phi\,(\eta)$.

3.4 Concluding remarks

The major findings here are

- An addition in porosity β causes decay in velocity $f'(\eta)$ besides we have seen reverse trend in $\theta(\eta)$ and $\phi(\eta)$ fields.
- Fr is decreasing function of $f'(\eta)$ and increasing function of $\theta(\eta)$ respectively.
- θ and ϕ via λ have similar results qualitatively.
- Opposite behavior of Pr is noticed on $\theta(\eta)$ and $\phi(\eta)$.
- Inverse behavior of β on ϕ and wall mass flux is noted.
- Concentration reduces when n or Sc enhances.
- Concentration ϕ is decreasing function of reaction rate constant σ.
- Skin friction coefficient has similar qualitative results for β and λ.
- Temperature gradient $-\theta'(0)$ is decreased by β and λ.

Chapter 4

Local similar solution for flow of an Oldroyd- B nanofluid with activation energy

Main purpose of present attempt is to examine outcome of activation energy in rotating flow of an Oldroyd-B nano liquid. Flow is generated due to stretched surface. Binary chemical reaction is studied. Brownian and thermophoresis effects are considered. The system of nonlinear ordinary differential equations are derived. Convergent series solutions are obtained by homotopy analysis method. The resulting profile for velocities, temperature and concentration are captured for different embedded parameters. It is found that velocities f' and g have decreasing effect when rotation parameter is enhanced. Brownian and thermophoresis are increasing functions of temperature and concentration. The physical quantities are sketched and discussed numerically. Concentration and temperature fields show decreasing behavior via Brownian and thermophoresis parameters.

4.1 Formulation

Here we have considered three-dimensional, incompressible steady nanomaterial flow of Oldroyd fluid. The flow is discussed in a rotating frame. Here sheet is rotating with angular speed Ω. The concept of activation energy related to chemical reaction is implemented for the explanation of mass concentration. The Oldroyd-B model describes the flow viscoelastic materials in nature. A three-dimensional flow assumes that a particle of liquid or fluid can go either up or down, forward or backward, left or right. All flows are three-dimensional, but some can be estimated to a two-dimensional or even one-dimensional flow to simplify the calculations without loss of much accuracy. Arrhenius equation gives the quantitative basis of relationship between the rate at which reaction proceeds through activation energy. In material chemistry binary reaction is a chemical reaction containing two different elements. Some binary phases reactions are molecular for example carbon tetrachloride. More typically binary phase refers to extended solids. Sheet in x-direction is stretched with stretching velocity $u_w = ax$. The surface temperature is T_w. Flow geometry is shown in Fig. 4.1. To explain the physical characteristics of nanofluid, Buongiorno model is used. The governing expressions in component forms are:

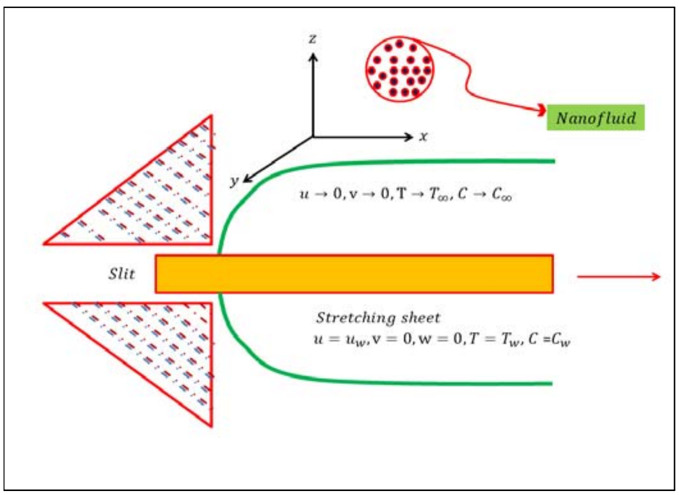

Fig. 4.1 : Flow geometry

$$\frac{\partial u}{\partial x} + \frac{\partial v}{\partial y} + \frac{\partial w}{\partial z} = 0, \tag{4.1}$$

$$\left.\begin{array}{c} u\frac{\partial u}{\partial x} + v\frac{\partial u}{\partial y} + w\frac{\partial u}{\partial z} - 2\Omega v + \lambda_1^* \left(\begin{array}{c} u^2\frac{\partial^2 u}{\partial x^2} + v^2\frac{\partial^2 u}{\partial y^2} + w^2\frac{\partial^2 u}{\partial z^2} + 2uv\frac{\partial^2 u}{\partial x \partial y} \\ +2vw\frac{\partial^2 u}{\partial y \partial z} + 2uw\frac{\partial^2 u}{\partial x \partial z} \\ -2\Omega\left(u\frac{\partial v}{\partial x} + v\frac{\partial v}{\partial y} + w\frac{\partial v}{\partial z}\right) + 2\Omega\left(v\frac{\partial u}{\partial x} - u\frac{\partial u}{\partial y}\right) \end{array} \right) = \\ \nu\left[\frac{\partial^2 u}{\partial z^2} + \lambda_2^* \left(\begin{array}{c} u\frac{\partial^3 u}{\partial x \partial z^2} + v\frac{\partial^3 u}{\partial y \partial z^2} + w\frac{\partial^3 u}{\partial z^3} \\ -\frac{\partial u}{\partial x}\frac{\partial^2 u}{\partial z^2} - \frac{\partial u}{\partial y}\frac{\partial^2 v}{\partial z^2} - \frac{\partial u}{\partial z}\frac{\partial^2 w}{\partial z^2} \end{array} \right)\right], \end{array}\right\} \tag{4.2}$$

$$\left.\begin{array}{c} u\frac{\partial v}{\partial x}+v\frac{\partial v}{\partial y}+w\frac{\partial v}{\partial z}+2\Omega u+\lambda_1^*\left(\begin{array}{c} u^2\frac{\partial^2 v}{\partial x^2}+v^2\frac{\partial^2 v}{\partial y^2}+w^2\frac{\partial^2 v}{\partial z^2} \\ +2uv\frac{\partial^2 v}{\partial x\partial y}+2vw\frac{\partial^2 v}{\partial y\partial z}+2uw\frac{\partial^2 v}{\partial x\partial z} \\ +2\Omega\left(u\frac{\partial u}{\partial x}+v\frac{\partial u}{\partial y}+w\frac{\partial u}{\partial z}\right)+2\Omega\left(v\frac{\partial v}{\partial x}-u\frac{\partial v}{\partial y}\right) \end{array}\right)= \\ \nu\left[\frac{\partial^2 v}{\partial z^2}+\lambda_2^*\left(\begin{array}{c} u\frac{\partial^3 v}{\partial x\partial z^2}+v\frac{\partial^3 v}{\partial y\partial z^2}+w\frac{\partial^3 v}{\partial z^3} \\ -\frac{\partial v}{\partial x}\frac{\partial^2 u}{\partial z^2}-\frac{\partial v}{\partial y}\frac{\partial^2 v}{\partial z^2}-\frac{\partial v}{\partial z}\frac{\partial^2 w}{\partial z^2} \end{array}\right)\right], \end{array}\right\} \tag{4.3}$$

$$u\frac{\partial T}{\partial x}+v\frac{\partial T}{\partial y}+w\frac{\partial T}{\partial z}=\alpha_m\frac{\partial^2 T}{\partial z^2}+\frac{(\rho c)_p}{(\rho c)_f}\left(D_B\left(\frac{\partial T}{\partial z}\frac{\partial C}{\partial z}\right)+\frac{D_T}{T_\infty}\left(\frac{\partial T}{\partial z}\right)^2\right), \tag{4.4}$$

$$u\frac{\partial C}{\partial x}+v\frac{\partial C}{\partial y}+w\frac{\partial C}{\partial z}=\frac{D_T}{T_\infty}\left(\frac{\partial^2 T}{\partial z^2}\right)+D_B\left(\frac{\partial^2 C}{\partial z^2}\right)-\kappa_r^2\left(\frac{T}{T_\infty}\right)^n e^{-\frac{-E_a}{KT}}\left(C-C_\infty\right). \tag{4.5}$$

Prescribed conditions are

$$\left.\begin{array}{c} u=u_w(x)=ax,\ v=0,\ w=0,\ T=T_w,\ C=C_w \text{ at } z=0, \\ u\longrightarrow 0,\ v\longrightarrow 0,\ T\longrightarrow T_\infty,\ C\longrightarrow C_\infty \text{ at } z\longrightarrow\infty. \end{array}\right\} \tag{4.6}$$

Considering

$$\left.\begin{array}{c} \eta=\sqrt{\frac{a}{v}}z,\ u=axf'(\eta),\ v=axg(\eta),\ w=-(av)^{\frac{1}{2}}f(\eta), \\ \theta(\eta)=\frac{T-T_\infty}{T_w-T_\infty},\ \phi(\eta)=\frac{C-C_\infty}{C_w-C_\infty}, \end{array}\right\} \tag{4.7}$$

applying Eqs. (4.7) continuity equation (4.1) is satisfied automatically while Eqs. (4.2) – (4.6) become

$$f'''+ff''-f'^2+2\lambda\left(g-\beta_1 fg'\right)+\beta_1\left(2ff'f''-f^2f'''\right)+\beta_2\left(f''^2-f'f^{iv}\right)=0, \tag{4.8}$$

$$\left.\begin{array}{c} g''+fg'-f'g-2\lambda\left(f'+\beta_1\left(f'^2-ff''+g^2\right)\right)+\beta_1\left(2ff'g'-f^2g''\right) \\ +\beta_2\left(f'g''-fg'''-gf'''+g'f''\right)=0, \end{array}\right\} \tag{4.9}$$

$$\theta''+\Pr\left(f\theta'+Nb\theta'\phi'+Nt\theta'^2\right)=0, \tag{4.10}$$

$$\phi''+Scf\phi'+\frac{Nt}{Nb}\theta''-Sc\sigma\left[1+\delta\theta\right]^n\exp\left[-\frac{E_1}{1+\delta\theta}\right]\phi=0, \tag{4.11}$$

with

$$\left.\begin{array}{c} f\left(0\right)=g\left(0\right)=0,\ f'\left(0\right),=1,\ \theta\left(0\right)=\phi\left(0\right)=1, \\ f'\left(\infty\right)\longrightarrow 0,\ g\left(\infty\right)\longrightarrow 0,\ \theta\left(\infty\right)\longrightarrow 0,\ \phi\left(\infty\right)\longrightarrow 0. \end{array}\right\} \tag{4.12}$$

The involved definitions are

$$\left.\begin{array}{c} \lambda=\frac{\Omega}{a},\ \beta_1=\lambda_1^* a,\ \beta_2=\lambda_2^* a,\ \ \Pr=\frac{v}{\alpha_m}, \\ Nb=\frac{(\rho c)_p D_B(C_w-C_\infty)}{(\rho c)_f \nu},\ Nt=\frac{(\rho c)_p D_T(T_w-T_\infty)}{(\rho c)_f v T_\infty}, \\ Sc=\frac{\nu}{D_B},\ E_1=\frac{E_a}{KT_\infty},\ \delta=\frac{T_w-T_\infty}{T_\infty},\ \sigma=\frac{k_r^2}{a}\ \ \mathrm{Re}_x=\frac{ax^2}{\nu}. \end{array}\right\} \tag{4.13}$$

Physical quantities are

$$\left.\begin{array}{c} \frac{Nu_x}{\sqrt{\mathrm{Re}_x}}=-\theta'\left(0\right), \\ \frac{Sh_x}{\sqrt{\mathrm{Re}_x}}=-\phi'\left(0\right). \end{array}\right\} \tag{4.14}$$

4.2 Homotopic solutions

Homotopy analysis method requires initial guesses. The initial guesses for homotopy analysis are $(f_0, g_0, \theta_0, \phi_0)$.

$$\left.\begin{array}{c} f_0\left(\eta\right)=1-e^{-\eta}, \\ g_0\left(\eta\right)=0, \\ \theta_0\left(\eta\right)=e^{-\eta} \\ \phi_0\left(\eta\right)=e^{-\eta}. \end{array}\right\} \tag{4.15}$$

4.3 Convergence of the series solution

The series solutions involve auxiliary parameters $\hbar_f$, $\hbar_g$, $\hbar_\theta$ and $\hbar_\phi$. $h-$curves in Figs. 2a and 2b have been displayed. The displayed figures witness that solutions convergence for $-1.5 \leq h_f \leq -0.2$, $-1.5 \leq h_g \leq -0.25$, $-1.5 \leq h_\theta \leq -0.4$, $-1.6 \leq h_\phi \leq -0.9$.

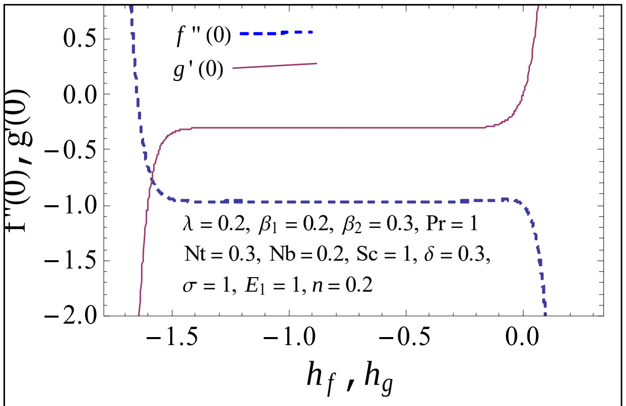

Fig. 4.2a $h-$curves for $f''(0)$ and $g'(0)$.

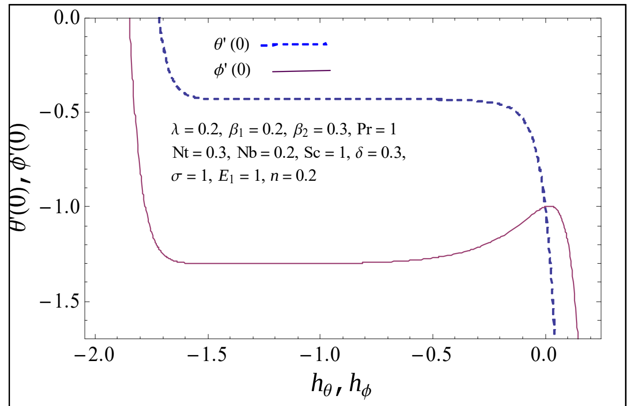

Fig. 4.2b $h-$curves for $\theta'(0)$ and $\phi'(0)$.

Table 4.1. Series solutions convergence for $\beta_1 = 0.2$, $\beta_2 = 0.3$, $Pr = 1$, $Nt = 0.3$, $Nb = 0.2$, $Sc = 1$,$\delta = 1$, $\sigma = 1$, $E_1 = 1$, $n = 0.2$, $h = -1$.

Order of approximations	$-f''(0)$	$-g'(0)$	$-\theta'(0)$	$-\phi'(0)$
1	0.94000	0.17400	0.70000	0.0123
5	0.95746	0.29941	0.46985	0.1243
10	0.96420	0.30414	0.44000	0.2136
15	0.96347	0.30375	0.43350	0.2588
20	0.96362	0.30396	0.43185	0.2810
25	0.96364	0.30389	0.43132	0.2919
30	0.96361	0.30391	0.43115	0.2973
35	0.96361	0.30391	0.43115	0.2973

4.3.1 Optimal convergence

OHAM is also applied to the nonlinear equations to construct the series solutions. To calculate the optimal estimations of $\hbar_f$, $\hbar_g$, $\hbar_\theta$ and $\hbar_\phi$ we have used the concept of average squared residual errors.

$$\varepsilon_{m^*}^f = \frac{1}{k^*+1} \sum_{j^*=0}^{k^*} \left[\mathcal{N}_f \left(\sum_{i=0}^{m^*} f(\eta), \sum_{i=0}^{m^*} g(\eta) \right)_{\eta = j^* \delta^* \eta} \right]^2, \tag{4.16}$$

$$\varepsilon_{m^*}^g = \frac{1}{k^*+1} \sum_{j^*=0}^{k^*} \left[\mathcal{N}_f \left(\sum_{i=0}^{m^*} f(\eta), \sum_{i=0}^{m^*} g(\eta) \right)_{\eta = j^* \delta^* \eta} \right]^2, \tag{4.17}$$

$$\varepsilon_{m^*}^{\theta} = \frac{1}{k^*+1} \sum_{j^*=0}^{k^*} \left[\mathcal{N}_{\theta} \left(\sum_{i=0}^{m^*} \theta(\eta), \sum_{i=0}^{m^*} f(\eta), \sum_{i=0}^{m^*} \phi(\eta) \right)_{\eta = j^* \delta^* \eta} \right]^2, \tag{4.18}$$

$$\varepsilon_{m^*}^{\phi} = \frac{1}{k^*+1} \sum_{j^*=0}^{k^*} \left[\mathcal{N}_{\phi} \left(\sum_{i=0}^{m^*} \phi(\eta), \sum_{i=0}^{m^*} \theta(\eta), \sum_{i=0}^{m^*} f(\eta), \right)_{\eta = j^* \delta^* \eta} \right]^2. \tag{4.19}$$

Total squared residual error is expressed as:

$$\varepsilon_{m^*}^{t} = \varepsilon_{m^*}^{f} + \varepsilon_{m^*}^{g} + \varepsilon_{m^*}^{\theta} + \varepsilon_{m^*}^{\phi}, \tag{4.20}$$

where $\varepsilon_{m^*}^{f}, \varepsilon_{m^*}^{g}, \varepsilon_{m^*}^{\theta}, \varepsilon_{m^*}^{\phi}$ represent squared residual error for velocity in x and y directions, temperature and concentration respectively and $\varepsilon_{m^*}^{t}$ is total squared residual error for whole flow at $\delta^*\eta = 0.5$ and $k^* = 20$. MATHEMATICA package BVPh2.0 is implemented to minimize the total average squared residual error. The optimal estimations of control variables at 2nd order are $h_f = -1.24552$, $h_g = -0.94552$, $h_\theta = -1.09587$ and $h_\phi = -1.248276$. The total squared averaged residual error is at 2nd order is $\varepsilon_m^t = 3.853053 \times 10^{-3}$.Table 4.2 and Fig. 4.3 show the residual errors for temperature, velocities and concentration. It can be seen that total residual error is decaying with larger approximations.

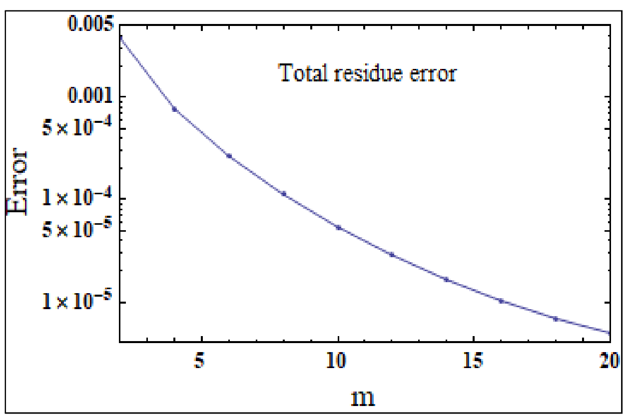

Fig. 4.3: Residual error.

Table. 4.2: Squared residual errors for velocities, temperature and concentration.

m^*	$\varepsilon_{m^*}^{f}$	$\varepsilon_{m^*}^{g}$	$\varepsilon_{m^*}^{\theta}$	$\varepsilon_{m^*}^{\phi}$
2	0.0000983233	0.0000491617	0.00356342	0.000142148
4	0.0000157594	0.0000078797	0.000738246	0.0000163182
8	0.0000032464	0.0000016232	0.000100889	7.07181*10^-6
10	0.0000020204	0.0000010102	0.0000465819	4.59887*10^-6
16	0.0000007357	3.6786666×10^{-7}	7.96709*10^-6	1.21654*10^-6
20	0.0000004519	2.25966667×10^{-7}	3.76384*10^-6	5.39439*10^-7

4.4 Discussion

This section is developed to investigate embedded parameters effection an Oldroyd-B fluid flow on nanofluid in rotating frame chemical reaction. Figs. $(4.4-4.21)$ and tables $(4.3-4.4)$ are constructed to show the influence of involved variables on temperature, concentration, velocities, Nusselt number and Sherwood number. Fig. 4.4 shows the trend of $f'(\eta)$ against rotational parameter (λ). Decrease in $(f'(\eta))$ is noticed for higher $(\lambda = 0, 0.2, 0.4, 0.5)$. As we increase (λ) the stretching rate in $x-$direction reduces which is responsible for decrease in $(f'(\eta))$. Velocity distribution $(f'(\eta))$ for (β_1) is plotted in Fig. 4.5. It is seen that when $(\beta_1 = 0, 0.3, 0.5, 0.7)$ increases than velocity field $(f'(\eta))$ decays and thinner momentum boundary layer occurs. (β_2) effects on $(f'(\eta))$ is described in Fig. 4.6. Behavior of (β_2) on velocity is quite opposite to that of (β_1). Physically $(\beta_2 = 0, 0.35, 0.5, 0.8)$ is directly related to retardation time so when particles move from equilibrium to perturbed system there is more disturbance which tends to increase the velocity. Rotation parameter (λ) effect on $(g(\eta))$ is presented in Fig. 4.7. Here we noticed that magnitude of $(g(\eta))$ enhances for higher $(\lambda = 0.1, 0.2, 0.3, 0.4)$. It is due to the reason that rotational frequency rises for larger (λ). Figs. 4.8 and 4.9 portray the effects of (β_1) and (β_2) on $(g(\eta))$. Behavior of $(g(\eta))$ indicated that flow is negative in y direction. It is seen that magnitude of $(g(\eta))$ enhances near the surface for both parameters while for higher (β_1) the velocity shows opposite effect away from the surface. Fig. 4.10 is portrayed for (β_1) impacts on the temperature $(\theta(\eta))$. It is observed that by enhancing $(\beta_1 = 0, 0.25, 0.65, 0.85)$ the temperature of fluid rises. Fig. 4.11 displayed (β_2) impact on $(\theta(\eta))$. Temperature and related boundary thickness are reduced for larger ($\beta_2 = 0, 0.25, 0.65, 0.85$). Fig. 4.12 is portrayed for impact of (Nt) on ($\theta(\eta)$). Increasing values of ($Nt = 0.1, 0.3, 0.5, 0.7$) tend to enhance the temperature field and thermal layer thickness. For larger (Nt) the thermophoresis force increases through which particles travels from hotter to the colder region and consequently temperature increases. Influence of (Nb) on temperature distribution is portrayed in Fig. 4.13. Here we have noticed that thermal boundary layer thickness and temperature are reduced for larger values of ($Nb = 0.1, 0.3, 0.5, 0.7$). Physically for higher Brownian effects the random motion of particles occurs that responsible for larger ($\theta(\eta)$). (Pr) effect on ($\theta(\eta)$) is described in Fig. 4.14. For higher ($\Pr = 1, 2, 2.5, 3$) thermal diffusivity of the fluid reduces. It means capability of fluid to conduct heat reduces and consequently temperature reduces. Impact of (Sc) on concentration field is depicted in Fig. 4.15. Schmidt number is the ratio of momentum to mass diffusivity so for larger ($Sc = 0, 3, 6, 9$) momentum diffusivity enhances and reduction in ($\phi(\eta)$) is seen. Impact of (Nt) for concentration distribution ($\phi(\eta)$) is sketched in Fig. 4.16. Here concentration distribution ($\phi(\eta)$) rises for larger values of thermophoresis parameters ($Nt = 0, 0.5, 1, 1.5$). Here ($\phi(\eta)$) is decreasing function of ($Nb = 0, 0.3, 0.6, 0.9$) showing in Fig. 4.17. Fig. 18 is prepared to describe the effects of activation energy (E_1) on ($\phi(\eta)$). We have noticed decay in ($\phi(\eta)$) for higher ($E_1 = 0, 0.4, 0.8, 1$). Figs. 4.19 and 4.20 are sketched for the impacts of δ and σ on concentration distribution ($\phi(\eta)$). Here we can see that ($\phi(\eta)$) increases near the surface for both parameters. Fig. 4.21 presents the impact of (β_1) on ($\phi(\eta)$).Here an increase in concentration for larger (β_1) is noticed.

Table 4.3 is prepared for numerical estimation of Nusselt number $-\theta'(0)$ via λ, β_1, β_2, Nt, Nb and Pr is shown. Decay in $-\theta'(0)$ is seen when λ, Nb, Nt and Pr are enhanced while opposite behavior is observed for β_1 and β_2. Table 4.4 shows the numerical value of local Sherwood number via β_1, β_2, Sc, E_1, δ and σ. We have noticed Sh_xhas larger and small values for increasing (Sc, E_1, β_1) and (Nt, Nb, β_2, σ) respectively. Table 4.5 shows the good agreement with previous literature.

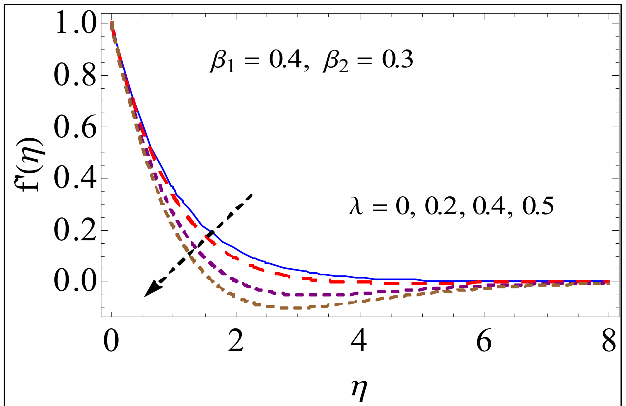

Fig. 4.4. $f'(\eta)$ against λ.

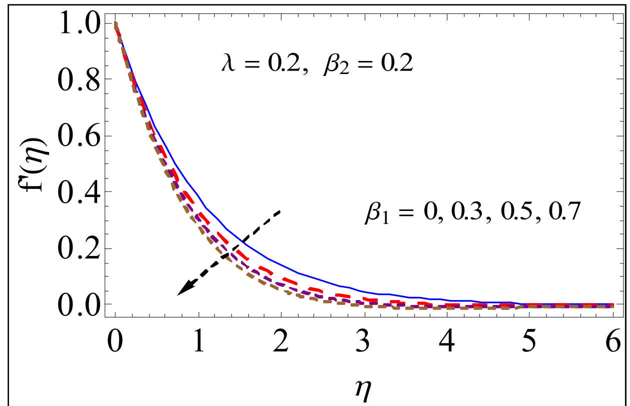

Fig. 4.5. $f'(\eta)$ against β_1.

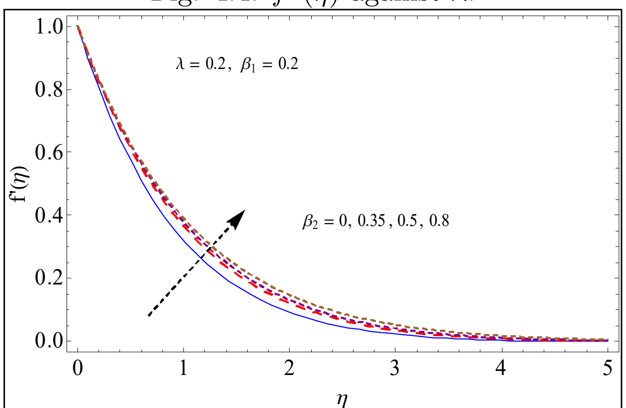

Fig. 4.6. $f'(\eta)$ against β_2.

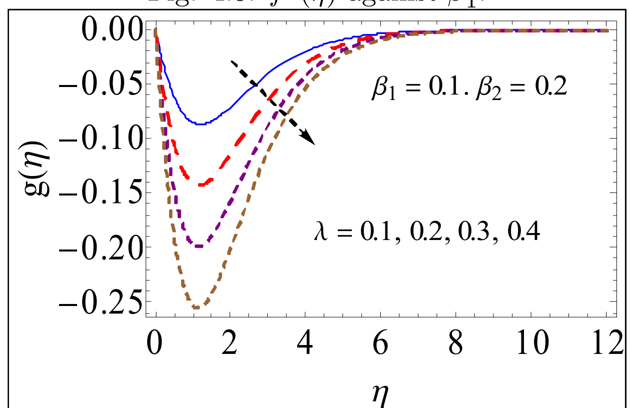

Fig. 4.7. $g(\eta)$ against λ.

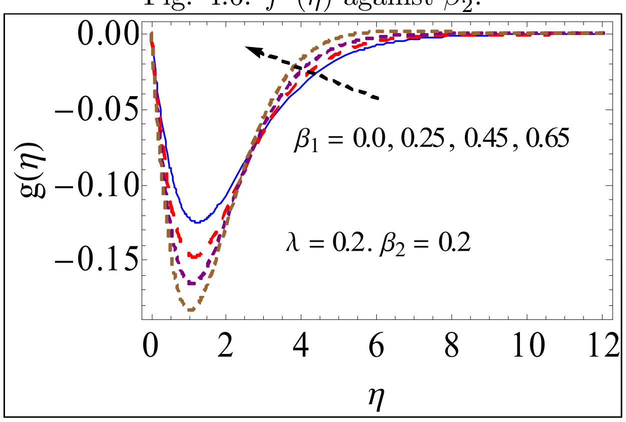

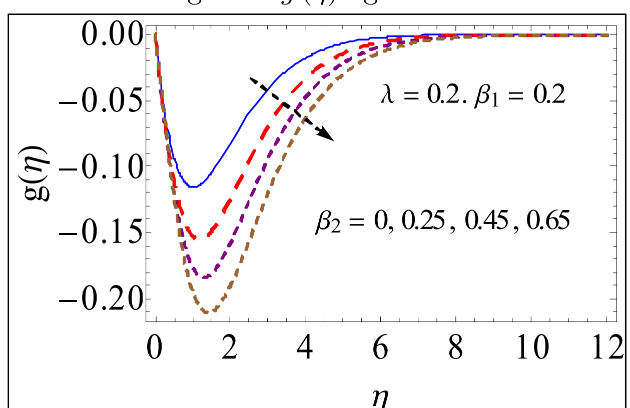

Fig. 4.9. $g(\eta)$ against β_2.

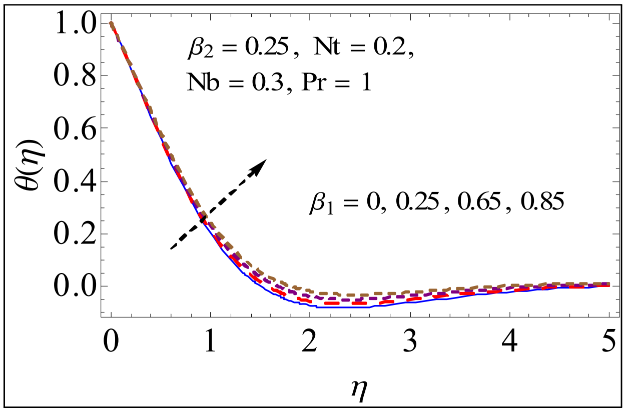

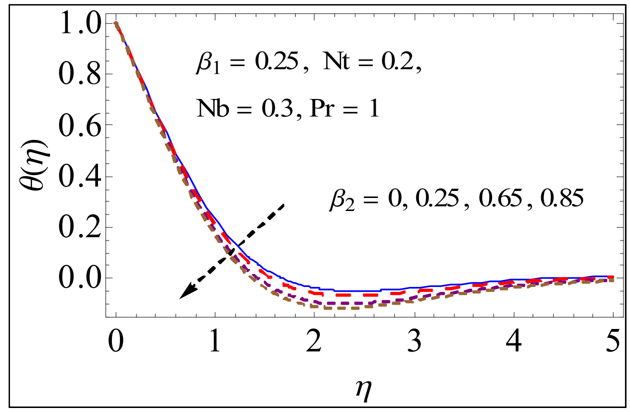

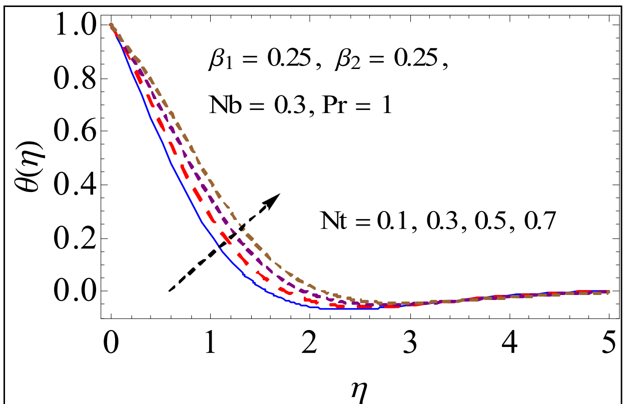

Fig. 4.12. $\theta(\eta)$ against Nt.

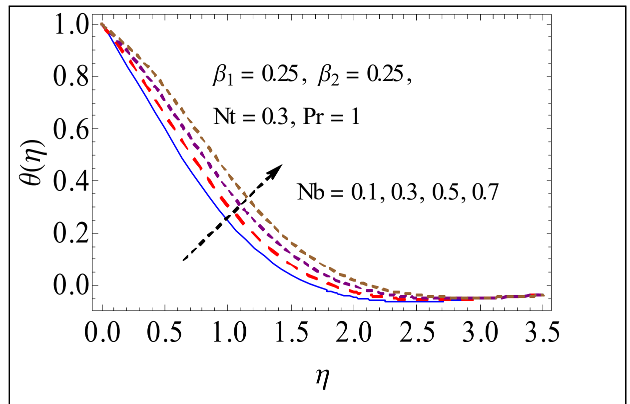

Fig. 4.13. $\theta(\eta)$ against Nb.

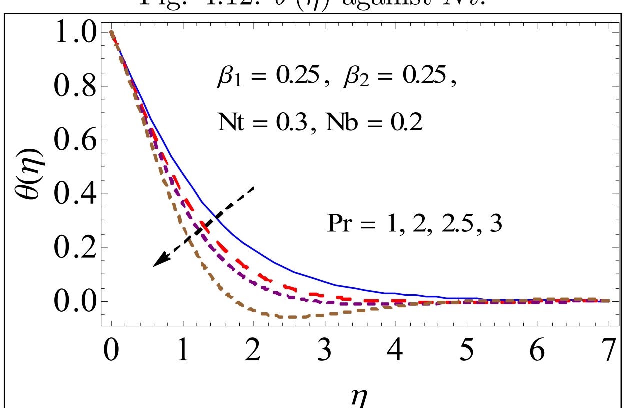

Fig. 4.14. $\theta(\eta)$ against Pr.

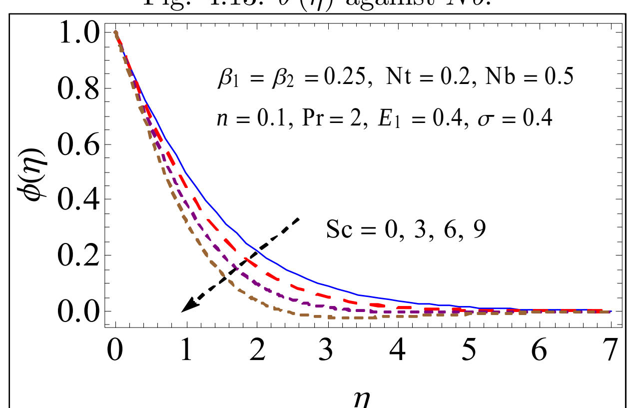

Fig. 4.15. $\phi(\eta)$ against Sc.

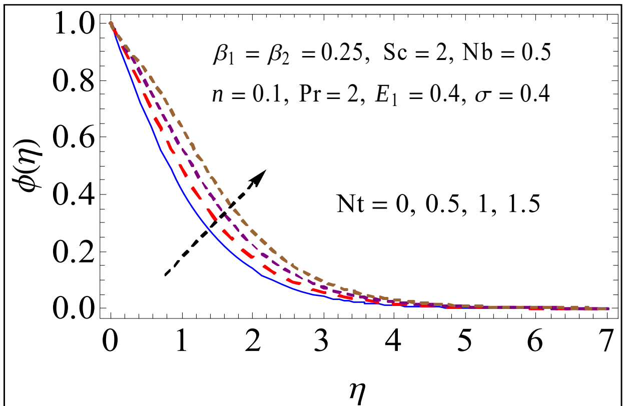

Fig. 4.16. $\phi(\eta)$ against Nt.

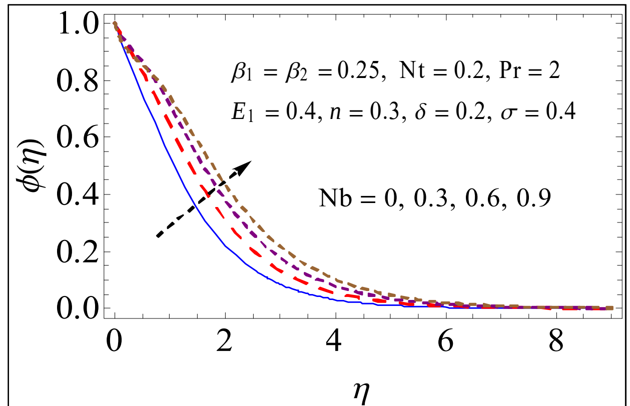

Fig. 4.17. $\phi(\eta)$ against Nb.

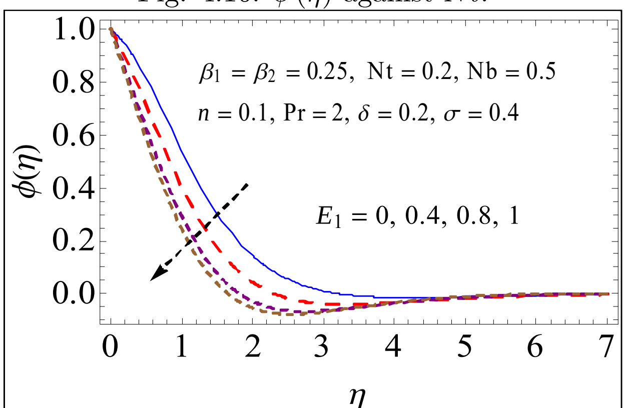

Fig. 4.18. $\phi(\eta)$ against E_1.

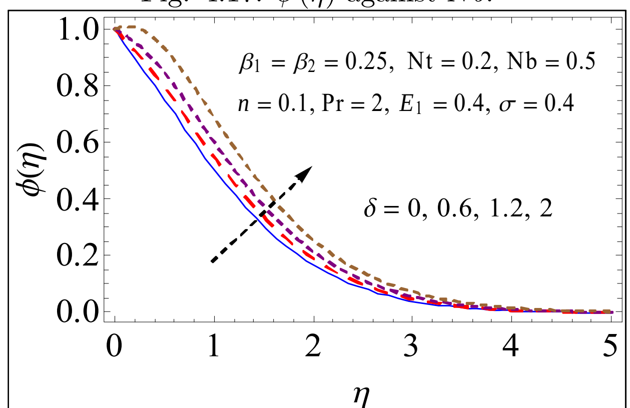

Fig. 4.19. $\phi(\eta)$ against δ

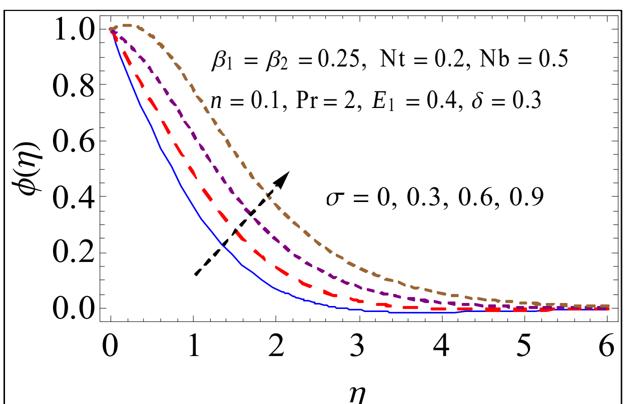

Fig. 4.20. $\phi(\eta)$ against σ

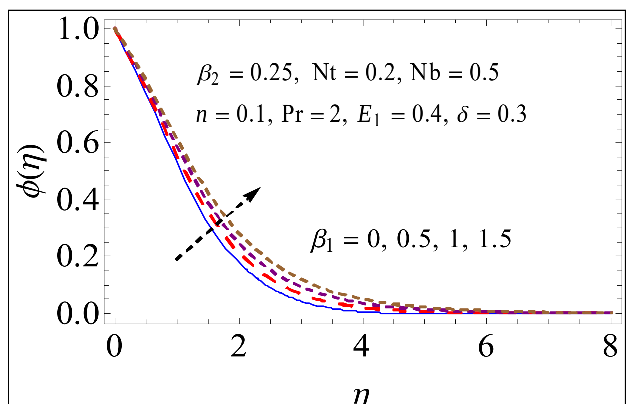

Fig. 4.21. $\phi(\eta)$ against β_1

Table 4.3: Nu_x estimation via different parameters.

λ	β_1	β_2	Nb	Nt	Pr	$-\theta'(0)$
0.1	0.2	0.4	0.1	0.2	1	0.51331
0.2						0.50183
0.4						0.47488
0.1	0	0.2	0.1	0.2	1	0.51423
	0.25					0.51721
	0.45					0.52770
0.1	0.25	0	0.1	0.2	1	0.48786
		0.25				0.50526
		0.45				0.51580
0.1	0.2	0.2	0.1	0.2	1	0.50141
					2	0.69530
					3	0.76608
0.1	0.2	0.2	0.1	0.1	1	0.52458
			0.3	0		0.47798
			0.4			0.45631
0.1	0.2	0.2	0.2	0.1	1	0.50044
				0.3		0.45959
				0.4		0.42413

Table 4.4: Numerical values of Sh_x via different parameters.

β_1	β_2	Nb	Nt	Sc	E_1	σ	$-\phi'(0)$
0	0.2	0.1	0.2	1	1	1	0.50681
0.25							0.53690
0.45							0.55397
0.2	0	0.1	0.2	1	1	1	0.54426
	0.25						0.54012
	0.45						0.53722
0.2	0.2	0.1	0.2	1	1	1	0.54090
		0.3					0.40776
		0.5					0.38663
0.2	0.2	0.2	0.1	1	1	1	0.53204
			0.3				0.37635
			0.5				0.29663
0.2	0.2	0.1	0.1	1	1	1	0.64628
				2			0.72232
				3			0.76496
0.2	0.2	0.1	0.1	1	0.7	1	0.56673
			0.3		0.9		0.62021
			0.4		1		0.64628
0.2	0.2	0.1	0.1	1	1	0.7	0.66353
						0.9	0.65203
						1	0.64628

Table 4.5: Comparison for validation of problem with [54, 55, 56] when $\lambda = \beta_2 = 0$.

β_2	Waqas et al. [54]	Abel et al. [55]	Megahed et al. [56]	Present work
0.0	1.000000	0.999962	0.999978	1.0000
0.2	1.051889	1.051948	1.051945	1.051890
0.4	1.101903	1.101850	1.101848	1.101903
0.6	1.150137	1.150163	1.150160	1.150137
0.8	1.196711	1.196692	1.196690	1.196712
1.2	1.285363	1.285257	1.285253	1.285361
1.6	1.368758	1.368641	1.368641	1.368755
2.0	1.447651	1.447617	1.447616	1.447653

4.5 Concluding remarks

Key point is presented as below:

- Boundary layer approximation is reducing function of λ for f' and g.
- β_1 and β_2 are increasing and decreasing function of g.
- Increasing value of Pr show decay in the θ.
- Opposite behavior of β_1 and β_2 are noticed for velocity f' and θ.
- Nt and Nb are increasing function of both θ and ϕ.
- Concentration profile ϕ is increasing function of β_1, δ and σ.
- Increasing activation energy parameter E_1 reduces concentration ϕ.
- Nusselt number (Nu_x) and Sherwood number have opposite behavior for (β_2).

Chapter 5

Magnetic effects in rotating flow of an Oldroyd-B fluid with chemical reaction and convective surface

Here, we have investigated $3D$ incompressible steady MHD flow of Oldroyd-B material in a rotating frame. The flow is caused through linearly stretched sheet. Applied magnetic field is accounted. Cubic autocatalytic chemical reaction is considered at the surface. Convective conditions at the boundary are considered for heat transport. Flow problem is modeled with the help of boundary layer approximations. Homotopy method (HAM) is utilized for the series solutions. Impacts of physical variable are interpreted through graph. Heat transfer rate is presented in tabulated form.

5.1 Problem Formulation

Here we have investigated $3D$ incompressible steady MHD flow of Oldroyd-B material in a rotating frame. Applied magnetic field is accounted. The flow is caused through linearly stretched sheet. Convective conditions at the boundary are considered for heat transport. Cubic autocatalytic chemical reaction is considered at the surface. Flow problem is modeled with the help of boundary layer approximations. The mathematical procedure for the cubic autocatalytic reactions are addressed as

$$A^* + 2B^* \rightarrow 3B^*,\ \text{rate} = k_c a^{**} b^2, \tag{5.1}$$

and

$$A^* \rightarrow B^*,\ \text{rate} = k_s a^{**}. \tag{5.2}$$

In components form, the flow equations are:

$$\frac{\partial u}{\partial x} + \frac{\partial v}{\partial y} + \frac{\partial w}{\partial z} = 0, \tag{5.3}$$

$$\left.\begin{array}{c} u\frac{\partial u}{\partial x} + v\frac{\partial u}{\partial y} + w\frac{\partial u}{\partial z} - 2\Omega v + \lambda_1^* \left(\begin{array}{c} u^2 \frac{\partial^2 u}{\partial x^2} + v^2 \frac{\partial^2 u}{\partial y^2} + w^2 \frac{\partial^2 u}{\partial z^2} + 2uv \frac{\partial^2 u}{\partial x \partial y} \\ +2vw \frac{\partial^2 u}{\partial y \partial z} + 2uw \frac{\partial^2 u}{\partial x \partial z} \\ -2\Omega \left(u\frac{\partial v}{\partial x} + v\frac{\partial v}{\partial y} + w\frac{\partial v}{\partial z} \right) + 2\Omega \left(v\frac{\partial u}{\partial x} - u\frac{\partial u}{\partial y} \right) \end{array} \right) = \\ \nu \left[\frac{\partial^2 u}{\partial z^2} + \lambda_2^* \left(\begin{array}{c} u\frac{\partial^3 u}{\partial x \partial z^2} + v\frac{\partial^3 u}{\partial y \partial z^2} + w\frac{\partial^3 u}{\partial z^3} \\ -\frac{\partial u}{\partial x}\frac{\partial^2 u}{\partial z^2} - \frac{\partial u}{\partial y}\frac{\partial^2 v}{\partial z^2} - \frac{\partial u}{\partial z}\frac{\partial^2 w}{\partial z^2} \end{array} \right) \right] - \frac{\sigma_1 B_0^2}{\rho_f}(u + \lambda_1^* w \frac{\partial u}{\partial z^2}), \end{array}\right\} \tag{5.4}$$

$$\left.\begin{array}{c} u\frac{\partial v}{\partial x} + v\frac{\partial v}{\partial y} + w\frac{\partial v}{\partial z} + 2\Omega u + \lambda_1^* \left(\begin{array}{c} u^2 \frac{\partial^2 v}{\partial x^2} + v^2 \frac{\partial^2 v}{\partial y^2} + w^2 \frac{\partial^2 v}{\partial z^2} \\ +2uv \frac{\partial^2 v}{\partial x \partial y} + 2vw \frac{\partial^2 v}{\partial y \partial z} + 2uw \frac{\partial^2 v}{\partial x \partial z} \\ +2\Omega \left(u\frac{\partial u}{\partial x} + v\frac{\partial u}{\partial y} + w\frac{\partial u}{\partial z} \right) + 2\Omega \left(v\frac{\partial v}{\partial x} - u\frac{\partial v}{\partial y} \right) \end{array} \right) = \\ \nu \left[\frac{\partial^2 v}{\partial z^2} + \lambda_2^* \left(\begin{array}{c} u\frac{\partial^3 v}{\partial x \partial z^2} + v\frac{\partial^3 v}{\partial y \partial z^2} + w\frac{\partial^3 v}{\partial z^3} \\ -\frac{\partial v}{\partial x}\frac{\partial^2 u}{\partial z^2} - \frac{\partial v}{\partial y}\frac{\partial^2 v}{\partial z^2} - \frac{\partial v}{\partial z}\frac{\partial^2 w}{\partial z^2} \end{array} \right) \right] - \frac{\sigma_1 B_0^2}{\rho_f}(v + \lambda_1^* w \frac{\partial v}{\partial z^2}), \end{array}\right\} \tag{5.5}$$

$$u\frac{\partial T}{\partial x} + v\frac{\partial T}{\partial y} + w\frac{\partial T}{\partial z} = \alpha_m \frac{\partial^2 T}{\partial z^2}, \tag{5.6}$$

$$u\frac{\partial a^{**}}{\partial x} + v\frac{\partial a^{**}}{\partial y} + w\frac{\partial a^{**}}{\partial z} = D_A \frac{\partial^2 a^{**}}{\partial z^2} - k_c a^{**} b^2, \tag{5.7}$$

$$u\frac{\partial b}{\partial x} + v\frac{\partial b}{\partial y} + w\frac{\partial b}{\partial z} = D_B \frac{\partial^2 a}{\partial z^2} + k_c a^{**} b^2, \tag{5.8}$$

with

$$\left.\begin{array}{c} u = u_w(x) = ax,\ v = 0,\ w = 0,\ \ -k\frac{\partial T}{\partial z} = \frac{h}{f}(T_f - T)\ \ \mathbf{at}\ \ z = 0, \\ D_A \frac{\partial a^{**}}{\partial z} = k_s a^{**},\ D_B \frac{\partial b}{\partial z} = -\mathbf{k}_s a^{**}\ \mathbf{at}\ \ z = 0, \\ u \longrightarrow 0,\ v \longrightarrow 0,\ w \longrightarrow 0,\ T \longrightarrow T_\infty,\ a^{**} \longrightarrow a_0,\ b \longrightarrow 0\ \mathbf{at}\ \ z = \infty. \end{array}\right\} \tag{5.9}$$

Considering

$$\left.\begin{array}{c} \eta = \sqrt{\frac{a}{v}}z,\ u = axf'(\eta),\ v = axg(\eta), \\ w = -(av)^{\frac{1}{2}} f(\eta),\ \theta(\eta) = \frac{T-T_\infty}{T_f - T_\infty}. \end{array}\right\} \tag{5.10}$$

One has using transformation, continuity equation (5.3) is satisfied while Eqs., (5.4) – (5.9) are converted into following differential equations

$$\left.\begin{array}{c} f''' + 2\lambda\left(g - \beta_1 f g'\right) + \beta_1\left(2ff'f'' - f^2 f''' + M^2 ff''\right) \\ +ff'' - f'^2 + \beta_2\left(f''^2 - f' f'^{iv}\right) - M^2 f' = 0, \end{array}\right\} \tag{5.11}$$

$$\left.\begin{array}{c} g'' + fg' - f'g - 2\lambda\left(f' + \beta_1\left(f'^2 - ff'' + g^2\right)\right) + \beta_1\left(2ff'g' - f^2 g'' + M^2 g'\right) \\ +\beta_2\left(f'g'' - fg''' - gf''' + g'f''\right) - M^2 g' = 0, \end{array}\right\} \tag{5.12}$$

$$\theta'' + \Pr f\theta' = 0, \tag{5.13}$$

$$\frac{1}{Sc}\phi'' + f\phi' - k_1 h^2 \phi = 0, \tag{5.14}$$

$$\frac{1}{Sc}h'' + fh' + k_1 h^2 \phi = 0, \tag{5.15}$$

$$\left.\begin{array}{c} f = 0 = g,\ \ f' = 1,\ \theta' = -\gamma\left[1 - \theta(0)\right], \\ \phi' = k_2\phi(0),\ \ \delta h'(0) = -k_2\phi(0) \ \text{ at } \eta = 0, \end{array}\right\} \tag{5.16}$$

$$f' \longrightarrow 0,\ g' \longrightarrow 0,\ \theta \longrightarrow 0,\ \phi \longrightarrow 1,\ h \longrightarrow 0 \text{ at } \eta \longrightarrow \infty, \tag{5.17}$$

the dimensionless parameters express in following definition

$$\left.\begin{array}{c} \lambda = \frac{\Omega}{a},\ \beta_1 = \lambda_1 a,\ \beta_2 = \lambda_2 a,\ M = \frac{B_0^2 \sigma^{**}}{\rho a},\ \ \Pr = \frac{v}{\alpha},\ \gamma = \frac{h_f}{k}\sqrt{\frac{v}{a}}, \\ Sc = \frac{v}{D_A},\ \delta = \frac{D_B}{D_A},\ k_1 = \frac{k_c a_0^2}{u_w},\ k_2 = \frac{k_s}{D_A}\sqrt{\frac{v}{a}}. \end{array}\right\} \tag{5.18}$$

For comparable mass diffusions we put D_A and D_B are equal, we have

$$\phi(\eta) + h(\eta) = 1, \tag{5.19}$$

now Eqs. (5.14) and (5.15) becomes

$$\frac{1}{Sc}\phi'' + f\phi' - k_1(1-\phi)^2\phi, \tag{5.20}$$

with boundary conditions

$$\phi'(0) = k_2\phi(0), \ \phi(\infty) \longrightarrow \mathbf{1}. \quad (5.21)$$

Local Nusselt number Nu_x is expressed by formula

Mathematically, we have

$$Nu_x = \frac{xq_w}{k(Tw - T_\infty)}, \quad (5.22)$$

where hall flux is defined as

$$q_w = -k\frac{\partial T}{\partial z}\mid_{z=o}. \quad (5.23)$$

Finally, one has

$$Nu_x(\mathrm{Re}_x)^{-o.5} = -\theta'(0). \quad (5.24)$$

5.2 Series solutions

Homotopy analysis procedure [76 − 83] requires the initial guesses and linear operators in the forms:

We have

$$\left.\begin{aligned} f_0(\eta) &= 1 - e^{-\eta}, \\ g_0(\eta) &= 0, \\ \theta_0(\eta) &= \tfrac{\gamma}{1+\gamma}e^{-\eta}, \\ \phi_0(\eta) &= 1 - \tfrac{1}{2}e^{-k_2\eta}, \end{aligned}\right\} \quad (5.25)$$

$$\left.\begin{aligned} \mathcal{L}_f(\eta) &= f''' - f', \\ \mathcal{L}_g &= g'' - g, \\ \mathcal{L}_\theta(\eta) &= \theta'' - \theta, \\ \mathcal{L}_\phi &= \phi'' - \phi, \end{aligned}\right\} \quad (5.26)$$

with the following characteristics

$$\left.\begin{array}{c}\mathcal{L}_f\left[A_{*1}+A_{*2}e^{-\eta}+A_{*3}e^{\eta}\right]=0,\\ \mathcal{L}_g\left[A_{*4}e^{-\eta}+A_{*5}e^{\eta}\right]=0,\\ \mathcal{L}_\theta\left[A_{*6}e^{-\eta}+A_{*7}e^{\eta}\right]=0,\\ \mathcal{L}_\phi\left[A_{*8}e^{-\eta}+A_{*9}e^{\eta}\right]=0,\end{array}\right\} \tag{5.27}$$

where A_{*i} $(i=1-9)$ designates are arbitrary constants

$$\left.\begin{array}{c}A_{*2}=A_{*4}=A_{*6}=A_{*8}=0,\\ A_{*1}=-A_{*3}-f^{*}_{m^*}(0),\ A_{*3}=\frac{\partial f^{\star}_{m^*}(\eta)}{\partial\eta}\ |_{\eta=0},\ A_{*5}=-\frac{\partial g^{\star}_{m^*}(\eta)}{\partial\eta}\ |_{\eta=0},\\ A_{*7}=\frac{1}{1+\gamma}\left[\frac{\partial\theta^{\star}_{m^*}(\eta)}{\partial\eta}\ |_{\eta=0}-\gamma\left(\theta^{\star}_{m^*}(0)\right)\right],\\ A_{*9}=\frac{1}{1+k_2}\left[\frac{\partial\phi^{\star}_{m^*}(\eta)}{\partial\eta}\ |_{\eta=0}-k_2\left(\phi^{\star}_{m^*}(0)\right)\right].\end{array}\right\} \tag{5.28}$$

5.3 Convergence of series solution

In convergence analysis, auxiliary variables $\hbar_f$, $\hbar_g$, $\hbar_\theta$, $\hbar_\phi$ play an important role to regulate the series solutions. Therefore, Figs. 1 and 2 are outlined for such purpose. The appropriate ranges for the velocities, temperature and concentration expressions are lies in the domain $-1.8\leq h_f\leq -0.1$, $-1.6\leq h_g\leq -0.1$, $-2.1\leq h_\theta\leq 0.1$, $-2.1\leq h_\phi\leq 0.1$.

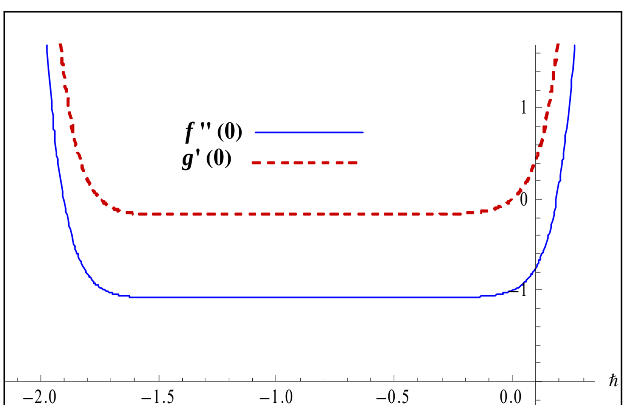

Fig. 5.1. h curves for $f''(0)$ and $g'(0)$

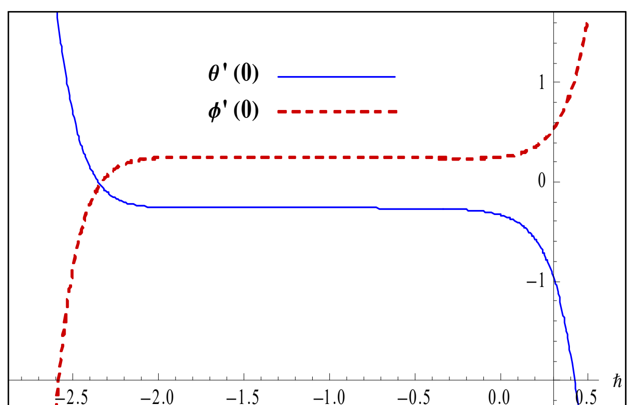

Fig. 5.2. h curves for $\theta'(0)$ and $\phi'(0)$

Table 5.1 is delineated for the numerical iterations of convergence portion. From this Table, it is noticed that 10th, 20th, 25th and 30th iterations are significant for the series convergence

Table 5.1. Different iterations for the series solutions when $\lambda = 0.1$, $\beta_1 = 0.1$, $\beta_2 = 0.1$, $M = 0.3$, $\Pr = 1, \gamma = 0.1$, $k_1 = 0.2$, $k_2 = 0.1$, $Sc = 1$

Order of approximations	$-f''(0)$	$-g'(0)$	$-\theta'(0)$	$\phi'(0)$
1	1.0215	0.12667	0.088154	0.049515
5	1.0313	0.14819	0.085496	0.052571
10	1.0318	0.14886	0.085094	0.060685
15	1.0318	0.14877	0.085059	0.066513
20	1.0318	0.14888	0.085050	0.073378
25	1.0318	0.14888	0.085048	0.079135
30	1.0318	0.14888	0.085048	0.082693
35	1.0318	0.14888	0.085048	0.082693

Table 5.2. Heat transfer rate analysis for various flow parameters

β_1	β_2	λ	M	Pr	γ	$\theta'(0)$
0	0.25	0.2	0.5	1	0.1	0.61123
0.25						0.60345
0.4						0.59305
0.25	0	0.2	0.5	1	0.1	0.67754
	0.2					0.68452
	0.4					0.74561
0.25	0.25		0	1	0.1	0.8219
			0.3			0.8117
			0.5			0.7806
0.25	0.25	0.2	0.5	1	0.1	0.7852
				2		0.9123
				3		1.2501.
0.25	0.25	0.2	0.5	1	0	0.55672
					0.1	0.78152
					0.3	0.82342

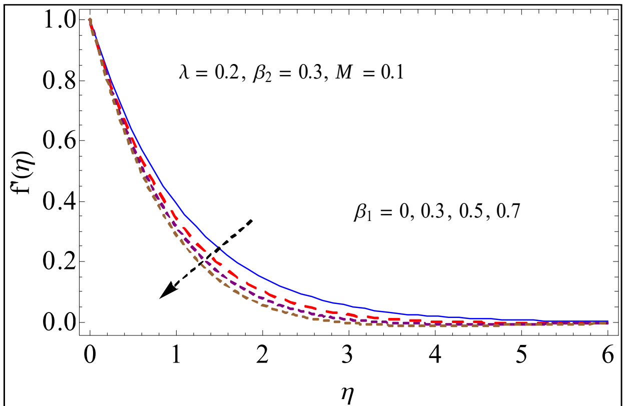

Fig. 5.3. $f'(\eta)$ versus β_1.

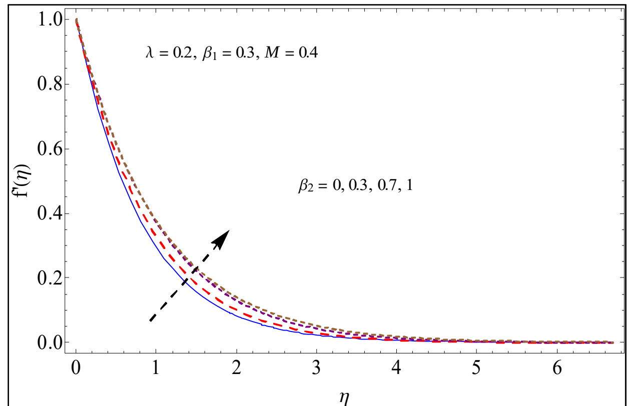

Fig. 5.4. $f'(\eta)$ versus β_2.

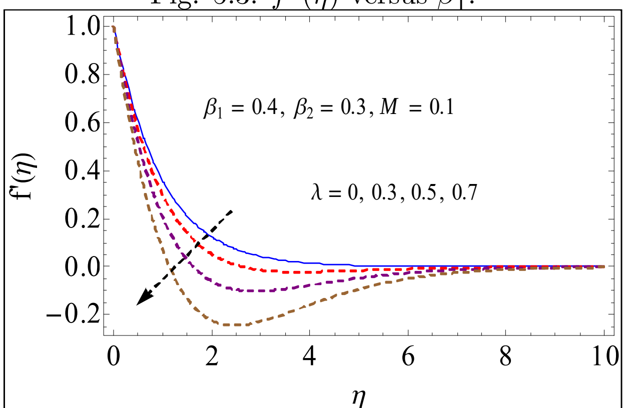

Fig. 5.5. $f'(\eta)$ versus λ.

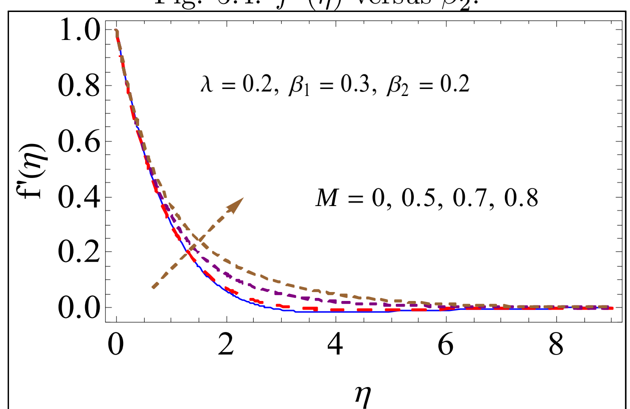

Fig. 5.6. $f'(\eta)$ versus M

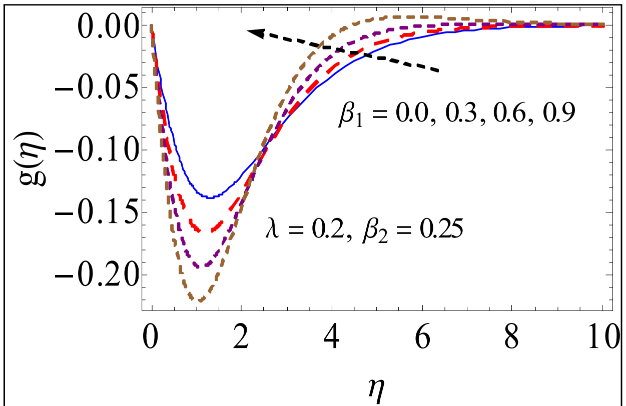

Fig. 5.7. $g(\eta)$ versus β_1.

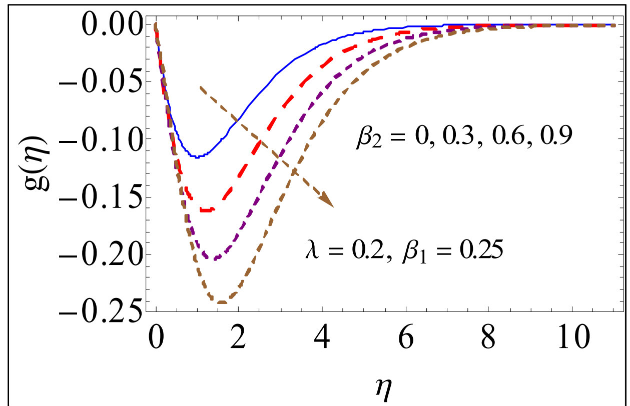

Fig. 5.8. $g(\eta)$ versus β_2.

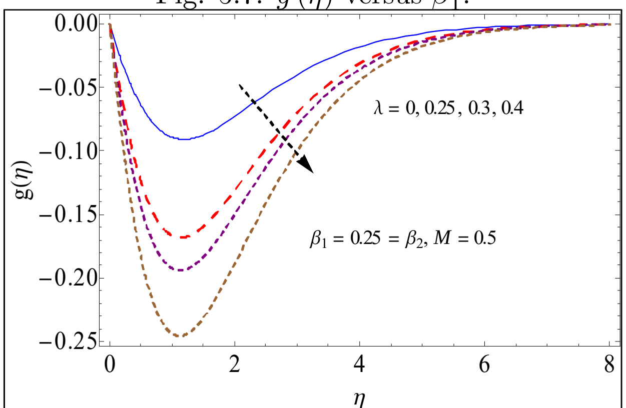

Fig. 5.9. $g(\eta)$ versus λ

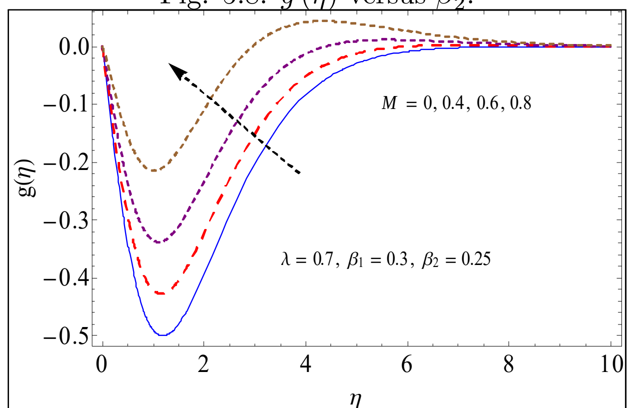

Fig. 5.10. $g(\eta)$ versus M

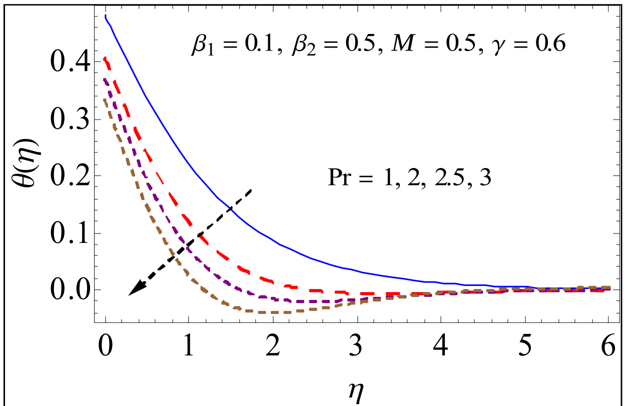

Fig. 5.11. $\theta(\eta)$ versus Pr

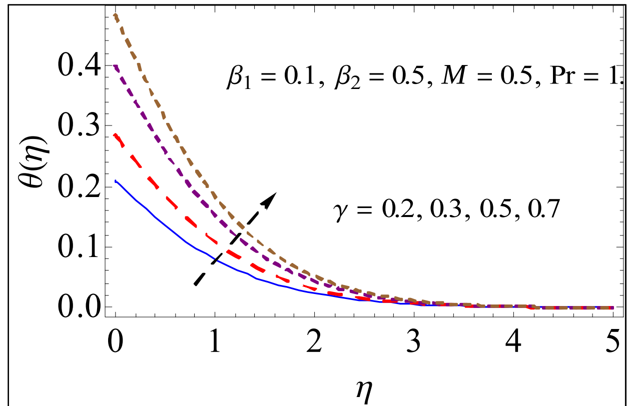

Fig. 5.12. $\theta(\eta)$ versus γ

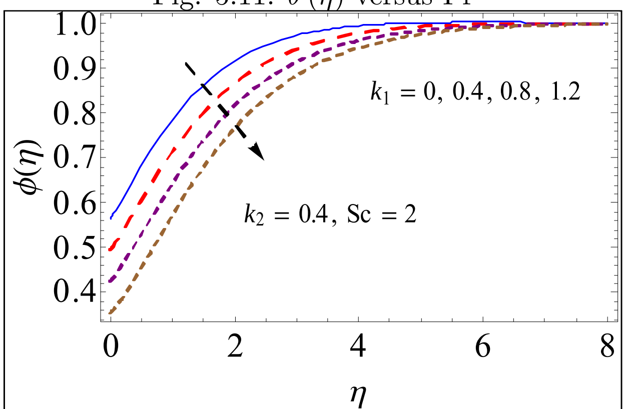

Fig. 5.13. $\phi(\eta)$ versus k_1.

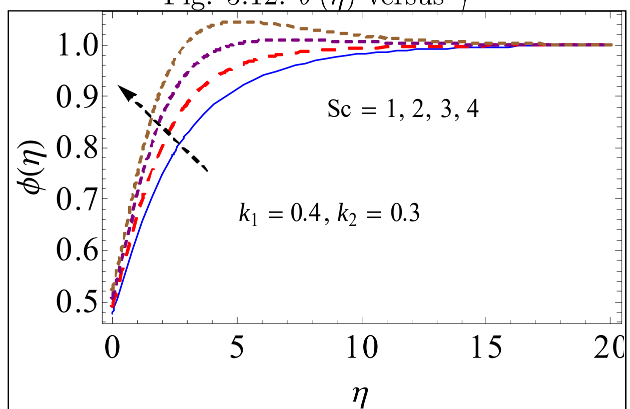

Fig. 5.14. $\phi(\eta)$ versus Sc.

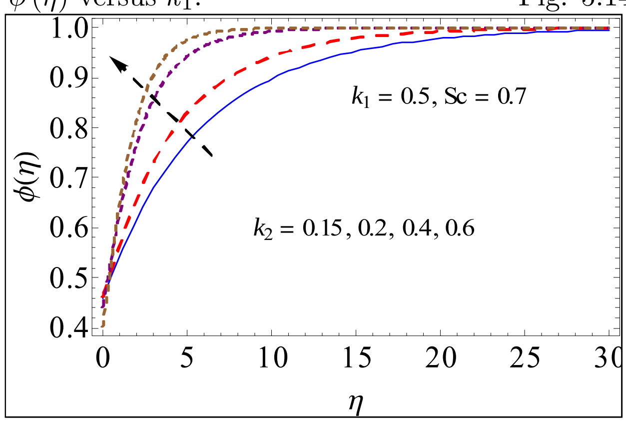

Fig. 5.15. $\phi(\eta)$ versus k_2.

5.3.1 Results and discussion

This segment is documented to explore the physical influences of interesting flow variables. For this determination, we have outlined Figs. For this we have plotted Fig. $(5.3 - 5.15)$. Figs. 5.1and 5.2 represent the convergence of series solutions in graphical form. Tables 5.1 and 5.2 highlight the iterations for convergence analysis and heat transfer rate respectively. In Fig. 5.3, we outlined the velocity profile versus different estimations of relaxation variable. Here we have seen that curves of velocity profile decay against larger relaxation parameter. Furthermore, layer thickness also declines via larger relaxation parameter. Fig.5. 4 portrayed for the impact of retardation variable on the velocity field. Here velocity field monotonically increases for the rising values of retardation variable. Also layer thickness enhances via higher retardation parameter. In Fig. 5.5, we have discussed the behavior of rotation variable on the velocity field. Here velocity monotonically declines versus rising estimations of rotation parameter. Magnetic parameter effects on velocity distribution $f'(\eta)$ is presented in Fig. 5.6. Here the velocity distribution is enhanced for larger value of magnetic parameter M. Behaviors of relaxation and retardation variables on the velocity distribution $g(\eta)$ are presented in Figs. 5.7 and 5.8. Initially $g(\eta)$ declines near the surface of sheet and then upsurges when the relaxation parameter increases ($see\ Fig.$5.7). In Fig. 5.8, velocity field decays in the whole portion versus higher values of retardation variable (see Fig.5.8). Moreover, layer thickness diminishes via larger retardation variable. Salient characteristic of rotation variable on the velocity field in g direction is portrayed in Fig. 5.9. Here same behavior is noticed for rotation variable is similar as Fig. 5.8. Fig. 5.10 is portrayed for the impacts of magnetic parameter M in velocity distribution $g(\eta)$. Fig. 5.11 is characterized for the variation of temperature field versus Prandtl number. Here temperature field declines versus higher impact of Prandtl number. Physically Prandtl number is ratio of viscous diffusion rate to thermal diffusion rate. Therefore, for larger Prandtl number, the thermal diffusion rate decays due to which viscous diffusion rate enhances and as a result thermal field decays. Also thermal layer declines through rising estimations of Prandtl number. Biot number attributes on the thermal profile is highlighted in Fig. 5.12. Physically, Biot number is the dimensionless quantity utilized in the heat transport calculations. Biot number gives a simple index of the ratio of heat transport resistances of and at the surface of stretchable sheet. This ratio governs whether or not temperatures inside a body will diverge meaningfully in space while the body cools or heats over time, from a thermal gradient applied to its stretchable surface. The Biot number has a variability of applications, with transient heat transport and utilizes in extended surface heat transport calculations. Here thermal field is an increasing behavior versus higher Biot number.

Figs. 5.13-5.15 are delineated to discuss the mass concentration versus Schmidt number, homogeneous reactive variable and heterogamous reactive variable respectively. In Fig. 5.13, we have examined that the mass concentration declines against higher estimations of homogenous reactive parameter. Fig. 5.14 is outlined the impact of Schmidt number on mass concentration. Here both mass concentration as well as solute layer increases against rising estimation of Schmidt number. Same behavior for the heterogeneous reactive variable is noticed on the mass concentration in Fig. 5.15 is similar as Fig. 5.14.

5.4 Concluding remarks

The key observations of present investigation are as follows:

- Velocity field shows contrast behavior against relaxation and retardation variables.
- Velocity distribution is enhanced for larger value of magnetic parameter M.
- Temperature of the system decays versus higher Prandtl number.
- Thermal field upsurges through rising values of Biot number.
- Concentration of species decays versus homogeneous reactive variable.
- For larger Schmidt number concentration enhances.
- Heat transfer rate is more against higher estimations of retardation parameter and Prandtl number.

Chapter 6

Theoretical description of Arrhenius energy in binary chemically rotating mixed convective flow with radiative flux

The main aim of present analysis is to study the three-dimensional rotating mixed convective flow of nanomaterial. Chemical reaction associated with Arrhenius energy is also accounted. Flow is created through exponential stretchable sheet. Slip mechanisms to nanomaterial like Brownian and thermophoresis diffusions are considered. Moreover, heat transfer analysis is developed in existence of heat source/sink and radiative flux. Similarity transformations are implemented to develop the system of nonlinear ordinary ones. Numerical approach ($Built-in-Shooting$) has been utilized to handle the governing mathematical system. Graphically impacts of pertinent parameters on the velocity, mass concentration and temperature are deliberated. Local Nusselt number and Sherwood number are examined and analyzed. It is noticed that temperature field enhances versus radiation and heat source/sink parameter while it decays through higher Prandtl number.

6.1 Mathematical description

Here we intend to investigate rotating flow of nanomaterials. The fluid is induced by an exponential stretching of surface. Slip mechanisms of thermophoresis and Brownian motion are considered. Let the sheet is stretched with velocity and rotating in axis with angular speed $\Omega = \Omega k$.

$$\frac{\partial u}{\partial x} + \frac{\partial v}{\partial y} + \frac{\partial w}{\partial z} = 0, \tag{6.1}$$

$$u\frac{\partial u}{\partial x} + v\frac{\partial u}{\partial y} + w\frac{\partial u}{\partial z} - 2\Omega v = \upsilon\frac{\partial^2 u}{\partial z^2} + g_{e\beta_0^*}\left(T - T_\infty\right) + g_{e\beta_0}\left(C - C_\infty\right), \tag{6.2}$$

$$u\frac{\partial v}{\partial x} + v\frac{\partial v}{\partial y} + w\frac{\partial v}{\partial z} + 2\Omega u = \upsilon\frac{\partial^2 v}{\partial z^2}, \tag{6.3}$$

$$\left.\begin{array}{c} u\frac{\partial T}{\partial x} + v\frac{\partial T}{\partial y} + w\frac{\partial T}{\partial z} = \alpha_m\frac{\partial^2 T}{\partial z^2} + \frac{(\rho c)_p}{(\rho c)_f}\left(D_B\left(\frac{\partial T}{\partial z}\frac{\partial C}{\partial z}\right) + \frac{D_T}{T_\infty}\left(\frac{\partial T}{\partial z}\right)^2\right) \\ +\frac{Q_0}{\rho c_p}\left(T - T_\infty\right) - \frac{1}{\rho c_p}\frac{\partial q_r}{\partial z}, \end{array}\right\} \tag{6.4}$$

$$u\frac{\partial C}{\partial x} + v\frac{\partial C}{\partial y} + w\frac{\partial C}{\partial z} = D_B\left(\frac{\partial^2 C}{\partial z^2}\right) - \kappa_r^2\left(\frac{T}{T_\infty}\right)^n e^{-\frac{Ea}{KT}}\left(C - C_\infty\right) + \frac{D_T}{T_\infty}\left(\frac{\partial^2 T}{\partial z^2}\right), \tag{6.5}$$

$$\left.\begin{array}{c} u = u_w\left(x\right) = U_0 \exp\left(\frac{x}{L}\right), v = 0, \quad w = 0, T = T_w, \quad C = C_w \textbf{ at } z = 0, \\ u \longrightarrow 0,\ v \longrightarrow 0,\ T \longrightarrow T_\infty,\ C \longrightarrow C_\infty \textbf{ at } z \longrightarrow \infty. \end{array}\right\} \tag{6.6}$$

Mathematically qr is expressed as

$$qr = -\frac{4\sigma^*}{3m}\frac{\partial\left(T^4\right)}{\partial z}. \tag{6.7}$$

We expand T^4 in Taylor series about T_∞ and neglecting higher term we have

$$T^4 = T_\infty^4 + 4T_\infty^3(T - T\infty) + 6T_\infty^2(T - T\infty)^2 + ... \tag{6.8}$$

or

$$T^4 = -3T_\infty^4 + 4T_\infty^3. \tag{6.9}$$

Then the radiative term becomes

$$\frac{\partial qr}{\partial z} = \frac{16\sigma^* T_\infty^3}{3m}\frac{\partial^2 T}{\partial z^2}, \tag{6.10}$$

and finally the energy expression is

$$\left.\begin{array}{c} u\frac{\partial T}{\partial x} + v\frac{\partial T}{\partial y} + w\frac{\partial T}{\partial z} = \alpha_m \frac{\partial^2 T}{\partial z^2} + \frac{(\rho c)_p}{(\rho c)_f}\left(D_B\left(\frac{\partial T}{\partial z}\frac{\partial C}{\partial z}\right) + \frac{D_T}{T_\infty}\left(\frac{\partial T}{\partial z}\right)^2\right) \\ +\frac{Q_0}{\rho c_p}\left(T - T_\infty\right) + \frac{16\sigma^* T_\infty^3}{3m}\frac{\partial^2 T}{\partial z^2}, \end{array}\right\} \tag{6.11}$$

considering

$$\left.\begin{array}{c} \eta = z\sqrt{\frac{u_0}{2vL}}\exp\left(\frac{x}{2L}\right)\;\; u = u_0\exp\left(\frac{x}{L}\right)f'(\eta),\;\; v = u_0\exp\left(\frac{x}{L}\right)g(\eta), \\ w = -\sqrt{\frac{vu_0}{2L}}\exp\left(\frac{x}{2L}\right)\left(f + \eta f'\right),.T = T_\infty + T_0\exp\left(\frac{Ax}{2L}\right), \\ C = C_\infty + C_0\exp\left(\frac{Bx}{2L}\right),\;\; \theta(\eta) = \frac{T - T_\infty}{T_w - T_\infty},\; \phi(\eta) = \frac{C - C_\infty}{C_w - C_\infty}. \end{array}\right\} \tag{6.12}$$

We have

$$f''' + ff'' - 2f'^2 + 4\lambda g = 0 + \lambda_1\left(\theta + N\phi\right) = 0, \tag{6.13}$$

$$g'' + fg' - 2f'g' - 4\lambda f' = 0, \tag{6.14}$$

$$\left(1 + R\right)\theta'' + \Pr\left(f\theta' - Af'\theta + Nb\theta'\phi' + Nt\theta'^2 + S\theta\right) = 0,$$

$$\phi'' + Sc\left(f\phi' - f'\phi B\right) + \frac{Nt}{Nb}\theta'' - Sc\sigma\left[1 + \delta\sigma\right]^n\exp\left[-\frac{E_1}{1 + \delta\sigma}\right]\phi = 0, \tag{6.16}$$

with boundary condition

$$\left.\begin{array}{c} f\left(0\right) = g\left(0\right) = 0,\; f'\left(0\right),= 1,\;\; \theta\left(0\right) = \phi\left(0\right) = 1, \\ f'\left(\infty\right) \longrightarrow 0,\;\; g\left(\infty\right) \longrightarrow 0,\;\; \theta\left(\infty\right) \longrightarrow 0,\; \phi\left(\infty\right) \longrightarrow 0. \end{array}\right\} \tag{6.17}$$

These variables are expressed as

$$\left.\begin{array}{c}\lambda=\frac{\Omega}{U_w},\ \lambda_1=\frac{Gr}{\mathrm{Re}^2},\ Pr=\frac{v}{\alpha_m},\\ Nb=\frac{(\rho c)_p D_b(C_w-C_\infty)}{(\rho c)_f\nu},\ Nt=\frac{(\rho c)_p D_T(T_w-T_\infty)}{(\rho c)_f vT_\infty},N=\frac{\beta_0^* C_0\exp\left(\frac{Bx}{2L}\right)}{\beta_0 T_0\exp\left(\frac{Ax}{2L}\right)},\\ R=\frac{16\sigma^* T_\infty^3}{3m},\ S=\frac{2Q_0L}{(\rho c)_f U_w},\ \mathrm{Re}_x=\frac{U_wL}{\nu},\ Sc=\frac{\nu}{D_B},\\ Sc=\frac{\nu}{D_B},\ E_1=\frac{E_a}{\kappa T_\infty},\ \delta=\frac{Tw-T_\infty}{T_\infty},\ \sigma=\frac{2k_r^2L}{U_w}.\end{array}\right\} \tag{6.18}$$

$$\left.\begin{array}{c}Nu_x\,\mathrm{Re}_x^{-0.5}=-\left(1+R\right)\theta'\left(0\right),\\ Sh_x\,\mathrm{Re}_x^{-0.5}=-\phi'\left(0\right).\end{array}\right\} \tag{6.19}$$

6.2 Graphical presentations

This section of article is established to elaborate the different pertinent flow variables on the non-dimensional velocities $f'(\eta)$, $g(\eta)$, $\theta\,(\eta)$ and $\phi(\eta)$. λ_1 effects on velocity $f'(\eta)$ is presented in Fig. 6.1. Here we can see that velocity enhanced in existence of buoyancy force. For $\lambda_1 > 0$ assisting flow while $\lambda_1 < 0$ the opposing flow situation. Fig. 6.2 displayed λ_1 impacts on θ. Here sharp growth in thermal layer versus higher λ_1. Fig. 6.3 indicates temperature for increasing R. Here temperature is enhanced by increasing R. Physically heat flux provide more heat which shows an increment in temperature and also thermal layer thickness. Impacts of Pr on θ is presented in Fig. 6.4. Fig. 6.5 predicts outcome of S. Here we have seen θ and thermal layer thickness are enhanced for heat source as compare to heat sink. Fig. 6.6 shows that the θ is increased via increasing Brownian motion Nb. Fig. 6.7 demonstrated variation of thermophoresis parameter Nt on θ. Here we have observed that the temperature function boosts up versus rising Nt. Fig. 6.8 depicts temperature exponent variable A effects on the temperature θ. Fig. 6.9 depicted thermophoretic effect on nanoparticle concentration ϕ. As thermophoresis parameter Nt is enhances, an increment is occurred in the nanoparticle concentration ϕ. Fig. 6.10 is illustrated for the behavior of Nb on ϕ. Here nanoparticle concentration decays when an enhancement is occurred in the Brownian variable. Fig. 6.11 is depicted for relationship among activation energy E_1 and ϕ. There is enhancement in concentration layer thickness for larger E_1. 6.12 predicts that nanoparticle concentration declines through larger Sc. Fig. 6.13 displayed variation in chemical reaction variable on ϕ. Here we observed a reduction in ϕ when chemical reaction variable $\sigma > 0$ is increased. Fig. 6.14 depicted marginal rise in ϕ via fitted rate constant n is varied. Salient Aspects of temperature difference δ on ϕ has been depicted in Fig. 6.15. Here larger value of δ lead to decay in Concentration ϕ.

Tables 6.1 and 6.2 are established to show the numerical iterations for Nusselt and Sherwood numbers versus different estimations of λ_1, N, R, S, Nb, Nt, Pr, Sc and E_1, σ, δ, n. As expected, when λ_1 and Nb are enhanced the magnitude of $Nu_x \, \mathrm{Re}_x^{-0.5}$ enhances. While reverse impact is noticed for $Sh_x \, \mathrm{Re}_x^{-0.5}$ versus larger radiation and temperature variables. An enhancement in Nt occurred degeneration in $Nu_x \, \mathrm{Re}_x^{-0.5}$ local and $Sh_x \, \mathrm{Re}_x^{-0.5}$ Sherwood numbers.

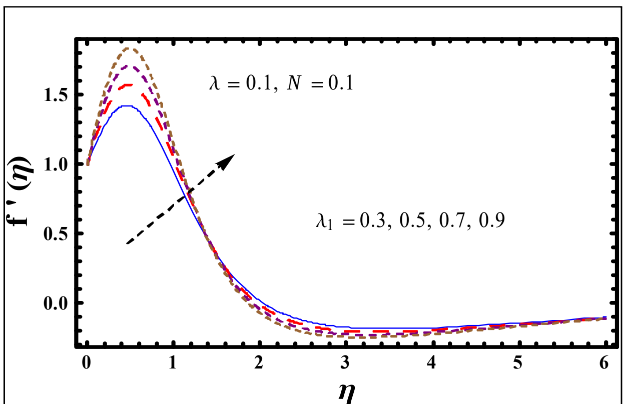

Fig. 6.1. λ_1 effercs on $f'(\eta)$.

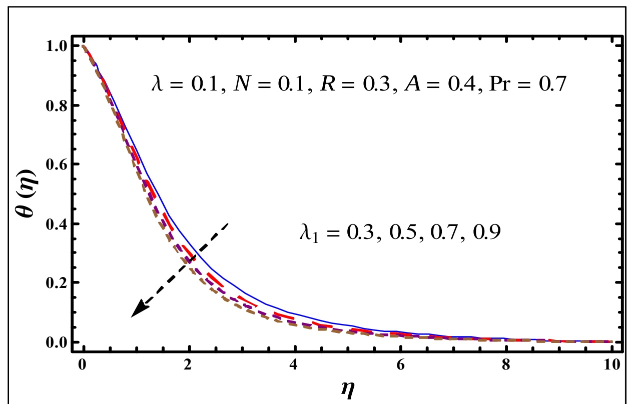

Fig. 6.2. λ_1 effercs on $\theta(\eta)$.

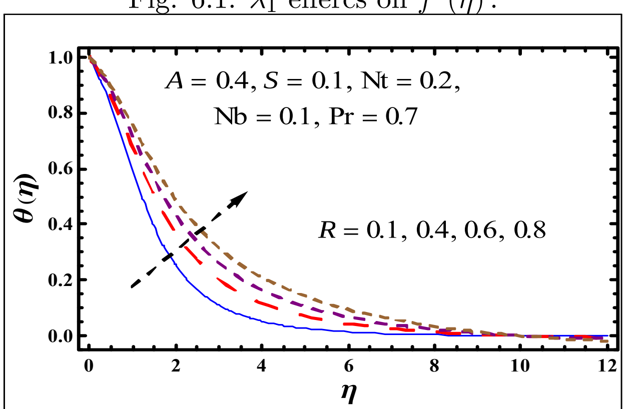

Fig. 6.3. R effercs on $\theta(\eta)$.

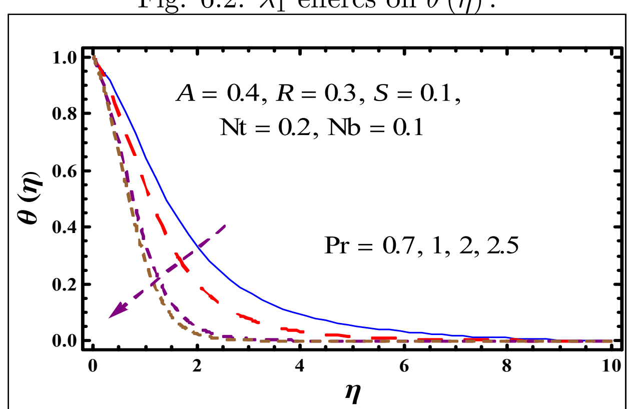

Fig. 6.4. Pr effercs on $\theta(\eta)$

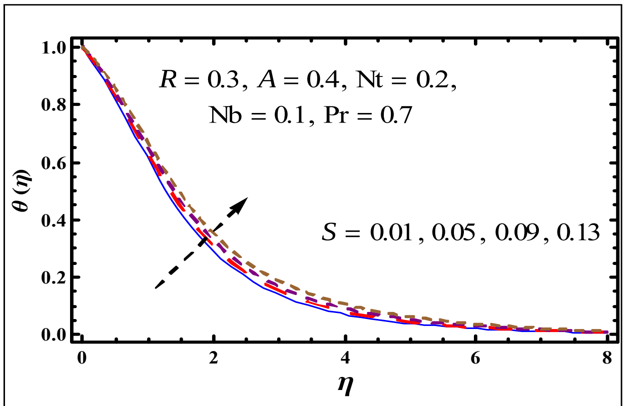

Fig. 6.5. S effercs on $\theta(\eta)$

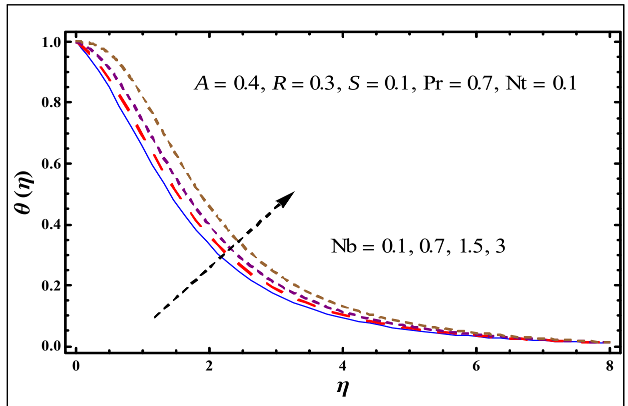

Fig. 6.6. Nb effercs on $\theta(\eta)$

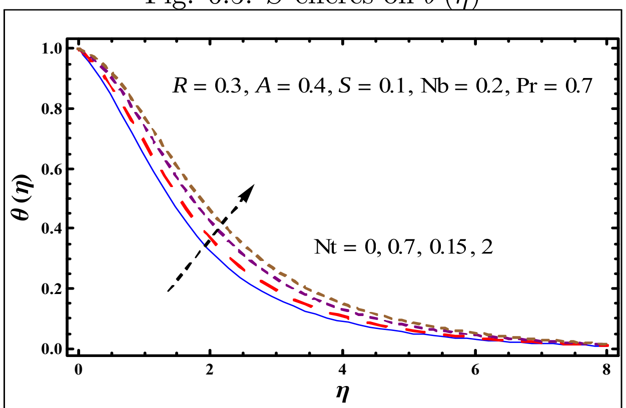

Fig. 6.7. Nt effercs on $\theta(\eta)$

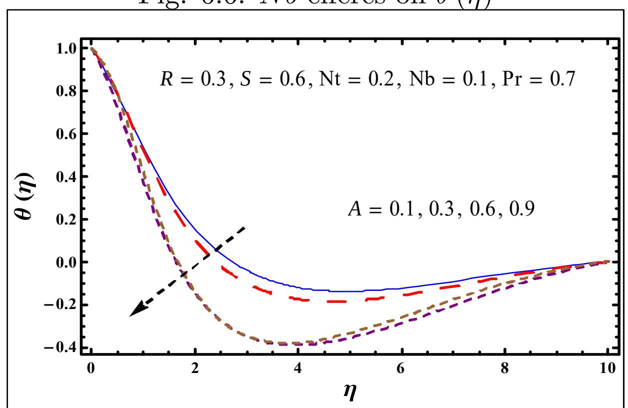

Fig. 6.8. A effercs on $\theta(\eta)$

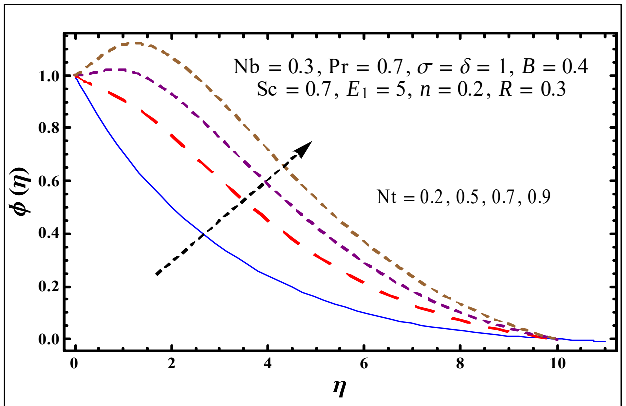

Fig. 6.9. Nt effercs on $\phi(\eta)$.

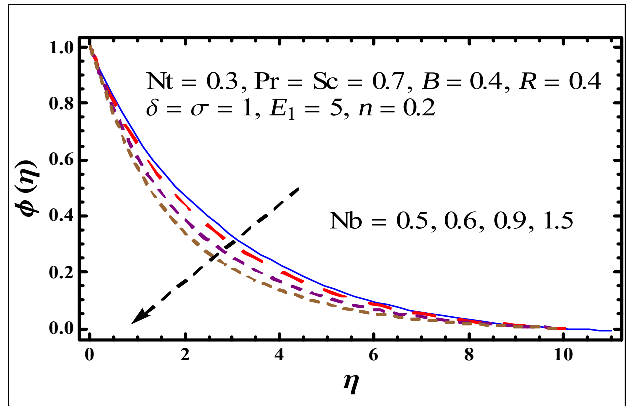

Fig. 6.10. Nb effercs on $\phi(\eta)$.

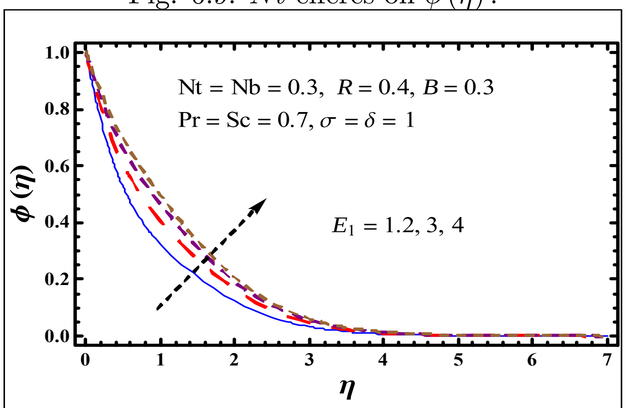

Fig. 6.11. E_1 effercs on $\phi(\eta)$.

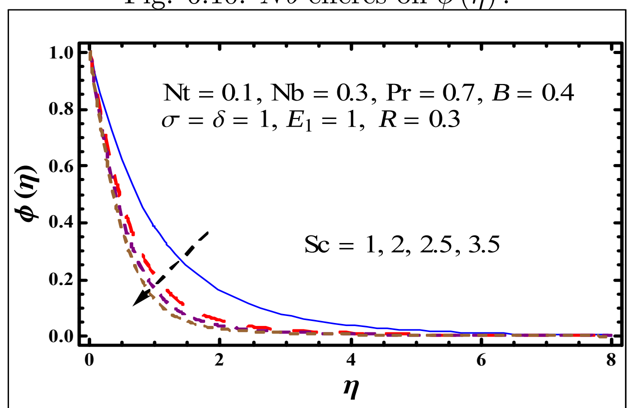

Fig. 6.12. Sc effercs on $\phi(\eta)$.

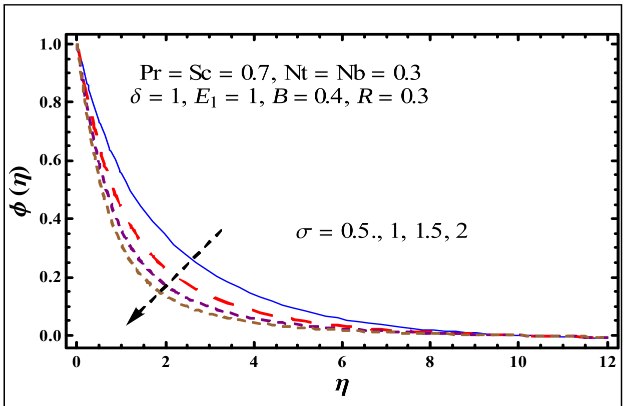

Fig. 6.13. σ effercs on $\phi(\eta)$.

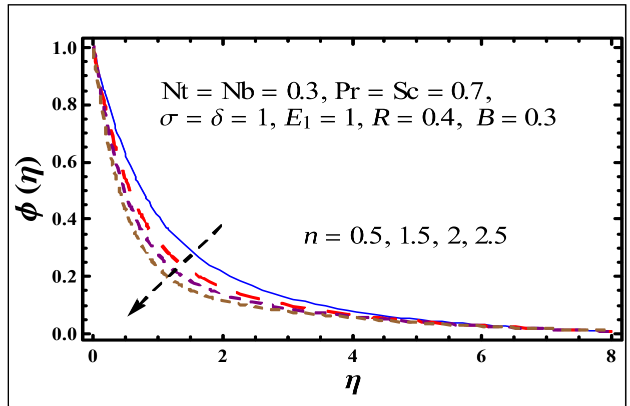

Fig. 6.14. n effercs on $\phi(\eta)$.

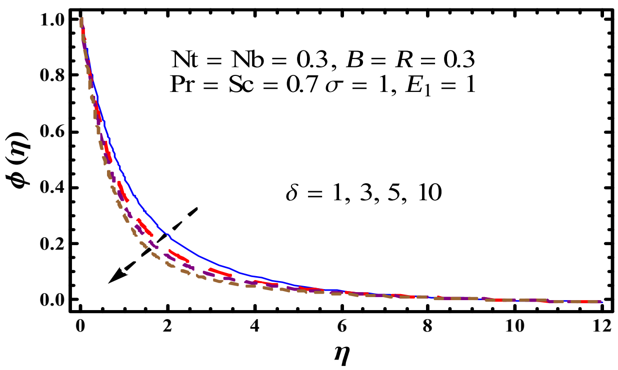

Fig. 6.15. δ effercs on $\phi(\eta)$.

Table. 6.1: Numerical computations of $Nu_x \, \mathrm{Re}_x^{-0.5}$

λ_1	R	S	Nt	Nb	$-\theta'(0)$
0.1	1.0	0.1	0.2	0.1	0247272
0.3					0.2799348
0.6					0.315281
0.3	0.1	0.1	0.2	0.1	0.279934
	0.4				0.217172
	0.6				0.185516
0.3	0.4	0.1	0.2	0.1	1.06447
		0.3			0.158539
		0.5			0.0593043
0.3	0.4	0.2	0.2	0.1	0.155239
					0.113359
					1.55569
0.3	0.4	0.2	0.2	0.1	0.495425
				0.3	0.440829
				0.5	0.390917

Table 6.2: Numerical computations of $Sh_x \, \mathrm{Re}_x^{-0.5}$

Sc	δ	E_1	σ	B	R	Nt	$-\phi'(0)$
1.0	0.3	1.0	1.0	0.3	0.2	0.2	0.710795
3.0							1.37655
5.0							1.84207
1.0	0.1	1.0	1.0	0.3	0.2	0.2	0.714662
	0.3						0.494606
	0.5						0.49365
1.0	0.2	2.0	1.5	0.3	0.2	0.2	0.492867
		4.0					0.565425
		6.0					0.60443
1	0.3	1	1.5	0.3	0.2	0.2	0.4720555
			2.0				0.71743
			2.5				0.716795
1	0.3	1	1.5	0.1	0.2	0.2	0.309259
				0.5			0.561866
				0.7			0.651723
1	0.3	1	1	0.1	0.1	0.2	0.309259
					0.3		0.295926
					0.5		0.147104
1	0.3	1	1	0.3	0.2	0.1	0.6070015
						0.3	0.40694
						0.5	0.349741

6.3 Concluding remarks

Key points of present analysis are

- Larger λ_1 and Nt exhibit increasing trend in θ.
- Thermal layer thickness are enhanced for heat source as compare to heat sink.
- Concentration decays when an enhancement is occurred in the Brownian variable Nt.
- Larger values of S and R decline in θ and ϕ.
- Temperature exponent A shows decreasing behavior in θ.
- Local Nusselt number and Sherwood number have decreasing behavior via large values of R and opposite behavior is seen for Nb

Chapter 7

Darcy-Forchheimer flow of Maxwell fluid with activation energy and thermal radiation over an exponential surface

The main purpose of this article is to investigate three-dimensional steady rotating flow of rate type fluid (Maxwell fluid) over an exponential stretching surface. The Maxwell fluid saturates the porous space via Darcy-Forchheimer relation. Flow caused by the exponential stretchable surface of sheet. Chemical reaction along with Arrhenius energy is considered at the surface. Energy expression is modeled subject to heat source/sink and radiation flux. Appropriate transformations leads to ordinary ones. Homotopy method is implemented for the series solutions. Pertinent parameters are discussed graphically. Special consideration is given to the engineering quantities like Sherwood and Nusselt numbers and discussed numerically through tabular form. Temperature distribution enhances versus higher radiation and heat source/sink parameter while decays for larger Prandtl number. Furthermore velocity shows decreasing trend through larger porosity and Deborah number.

7.1 Modeling

Here $3D$ rotating Darcy-Forchheimer flow of Maxwell liquid is considered. Fluid is saturated through Darcy-Forchheimer relation. Effects of Joule heating and dissipations effects are neglected. The flow expressions in compact form is addressed as

$$\nabla.\mathbf{V}' = 0, \tag{7.1}$$

$$\rho\left[\left(\mathbf{V}'.\boldsymbol{\nabla}\right)\mathbf{V}' + (\boldsymbol{\Omega}\times(\boldsymbol{\Omega}\times\mathbf{r})) + \left(2\boldsymbol{\Omega}\times\mathbf{V}'\right)\right] = -\nabla p + \nabla.\mathbf{S}^*, \tag{7.2}$$

$$\rho c_p^*\left(\mathbf{V}'.\boldsymbol{\nabla}\right) = k\nabla^2 T, \tag{7.3}$$

$$\left(\mathbf{V}'.\boldsymbol{\nabla}\right) = D\nabla^2 C - k_r^2\left(\frac{T}{T_\infty}\right)^n e^{-\frac{Ea}{\kappa T}}\left(C - C_\infty\right). \tag{7.4}$$

In components form we have

$$\frac{\partial u}{\partial x} + \frac{\partial v}{\partial y} + \frac{\partial w}{\partial z} = 0, \tag{7.5}$$

$$\left.\begin{array}{c} u\frac{\partial u}{\partial x} + v\frac{\partial u}{\partial y} + w\frac{\partial u}{\partial z} - 2\Omega v = \nu\frac{\partial^2 u}{\partial z^2} - \frac{\nu}{K}u - Fu^2 \\ +\lambda_1^*\left(\begin{array}{c} u^2\frac{\partial^2 u}{\partial x^2} + v^2\frac{\partial^2 u}{\partial y^2} + w^2\frac{\partial^2 u}{\partial z^2} + 2uv\frac{\partial^2 u}{\partial x\partial y} \\ +2vw\frac{\partial^2 u}{\partial y\partial z} + 2uw\frac{\partial^2 u}{\partial x\partial z} \\ -2\Omega\left(u\frac{\partial v}{\partial x} + v\frac{\partial v}{\partial y} + w\frac{\partial v}{\partial z}\right) + 2\Omega\left(v\frac{\partial u}{\partial x} - u\frac{\partial u}{\partial y}\right) \end{array}\right) \end{array}\right\} \tag{7.6}$$

$$\left.\begin{array}{c} u\frac{\partial v}{\partial x} + v\frac{\partial v}{\partial y} + w\frac{\partial v}{\partial z} + 2\Omega u = \nu\frac{\partial^2 v}{\partial z^2} - \frac{\nu}{K}v - Fv^2 \\ +\lambda_1^*\left(\begin{array}{c} u^2\frac{\partial^2 v}{\partial x^2} + v^2\frac{\partial^2 v}{\partial y^2} + w^2\frac{\partial^2 v}{\partial z^2} + 2uv\frac{\partial^2 v}{\partial xy} \\ +2vw\frac{\partial^2 v}{\partial xz} + 2uw\frac{\partial^2 v}{\partial x\partial z} \\ +2\Omega\left(u\frac{\partial u}{\partial x} + v\frac{\partial u}{\partial y} + w\frac{\partial u}{\partial z}\right) + 2\Omega\left(v\frac{\partial v}{\partial x} - u\frac{\partial v}{\partial y}\right) \end{array}\right) \end{array}\right\} \tag{7.7}$$

$$u\frac{\partial T}{\partial x} + v\frac{\partial T}{\partial y} + w\frac{\partial T}{\partial z} = \alpha_m\frac{\partial^2 T}{\partial z^2} + \frac{Q_0}{\rho c_p}\left(T - T_\infty\right) - \frac{1}{\rho c_p}\frac{\partial q_r}{\partial z}, \tag{7.8}$$

$$u\frac{\partial C}{\partial x} + v\frac{\partial C}{\partial y} + w\frac{\partial C}{\partial z} = D\left(\frac{\partial^2 C}{\partial z^2}\right) - \kappa_r^2\left(\frac{T}{T_\infty}\right)^n e^{-\frac{Ea}{KT}}\left(C - C_\infty\right). \tag{7.9}$$

Mathematically qr is expressed as

$$qr = -\frac{4\sigma^*}{3m}\frac{\partial\left(T^4\right)}{\partial z}. \tag{7.10}$$

After Taylor series we have

$$T^4 = T_\infty^4 + 4T_\infty^3(T - T\infty) + 6T_\infty^2(T - T\infty)^2 + ... \tag{7.11}$$

neglecting higher order terms we have

$$T^4 = -3T_\infty^4 + 4T_\infty^3, \tag{7.12}$$

$$\frac{\partial qr}{\partial z} = \frac{16\sigma^* T_\infty^3}{3m}\frac{\partial^2 T}{\partial z^2}. \tag{7.13}$$

Using Eq. (7.13) in Eq. (7.8) we get

$$u\frac{\partial T}{\partial x} + v\frac{\partial T}{\partial y} + w\frac{\partial T}{\partial z} = \alpha_m \frac{\partial^2 T}{\partial z^2} + \frac{Q_0}{\rho c_p}(T - T_\infty) + \frac{16\sigma_1 T_\infty^3}{3m}\frac{\partial^2 T}{\partial z^2}. \tag{7.14}$$

With boundary constrains we have

$$\left.\begin{array}{c} u = U_w(x) = U_0 \exp\left(\frac{x}{L}\right),\ v = 0,\ w = 0,\ T = T_w,\ C = C_w \textbf{ at } z = 0, \\ u \longrightarrow 0,\ v \longrightarrow 0,\ T \longrightarrow T_\infty,\ C \longrightarrow C_\infty \textbf{ at } z \longrightarrow \infty. \end{array}\right\} \tag{7.15}$$

Considering

$$\left.\begin{array}{c} \eta = z\sqrt{\frac{u_0}{2vL}} \exp\left(\frac{x}{2L}\right)\ \ u = u_0 \exp\left(\frac{x}{L}\right) f'(\eta),\ v = u_0 \exp\left(\frac{x}{L}\right) g(\eta), \\ w = -\sqrt{\frac{vu_0}{2L}} \exp\left(\frac{x}{2L}\right)(f + \eta f'),\ T = T_\infty + T_0 \exp\left(\frac{Ax}{2L}\right), \\ C = C_\infty + C_0 \exp\left(\frac{Bx}{2L}\right),\ \theta(\eta) = \frac{T - T_\infty}{T_w - T_\infty},\ \phi(\eta) = \frac{C - C_\infty}{C_w - C_\infty}. \end{array}\right\} \tag{7.16}$$

One have

$$\left.\begin{array}{c} 2f''' + 2\lambda(4g - 2\beta_1(fg' + \eta f'' g)) - \beta_1\left(4f'^3 - \eta f'^2 f'' + f^2 f''' - 6ff'g'\right) \\ +2ff'' - 2\beta f' - 2(1 + Fr) f'^2 = 0, \end{array}\right\} \tag{7.17}$$

$$\left.\begin{array}{c} 2g'' + 2fg' - 2f'g - 2\lambda\left(-f' + 2\beta_1\left(-f'^2 - g^2 + \eta g g' + ff''\right)\right) \\ -\beta_1\left(4f'^2 g - \eta f'^2 g' + f^2 g'' - 6ff'g'\right) - 2\beta\Lambda g - 2Frg^2 = 0, \end{array}\right\} \tag{7.18}$$

$$3\theta'' + 4R\theta'' + 3\Pr\left(f\theta' - Af'\theta + S\theta\right) = 0, \tag{7.19}$$

$$\phi'' + Sc\left(f\phi' - f'\phi B\right) - Sc\sigma\left[1+\delta\sigma\right]^n \exp\left[-\frac{E_1}{1+\delta\sigma}\right]\phi = 0. \tag{7.20}$$

These parameters are expressed as

$$\left.\begin{array}{c} \lambda = \frac{\Omega}{U_w},\ \beta_1 = \frac{\lambda_1^*}{LU_w},\ \beta = \frac{L}{KU_w},\ Fr = \frac{C_b L}{K^{\frac{1}{2}}} \\ \Pr = \frac{v}{\alpha_m},\ R = \frac{4\sigma^* T_\infty^3}{3m},\ S = \frac{2Q_0 L}{(\rho c)_f U_w},\ Sc = \frac{\nu}{D_B},\ \mathrm{Re}_x = \frac{U_w L}{\nu}, \\ Sc = \frac{\nu}{D},\ E_1 = \frac{E_a}{\kappa T_\infty},\ \delta = \frac{Tw - T_\infty}{T_\infty},\ \sigma = \frac{2k_r^2 L}{U_w}. \end{array}\right\} \tag{7.21}$$

Local Nusselt number Nu_x and Sherwood number Sh_x are expressed by formula

$$\left.\begin{array}{c} Nu_x = -\frac{x}{(Tw - T_\infty)}\frac{\partial T}{\partial z}\mid_{z=o} = -\frac{x}{L}\sqrt{\frac{\mathrm{Re}_x}{2}}\left(1+R\right)\theta'\left(0\right), \\ Sh_x = -\frac{x}{(Tw - T_\infty)}\frac{\partial C}{\partial z}\mid_{z=o} = -\frac{x}{L}\sqrt{\frac{\mathrm{Re}_x}{2}}\phi'\left(0\right). \end{array}\right\} \tag{7.22}$$

7.2 Homotopic solutions

The initial approximations and linear operators are requires for series solution. Here $(f_0, g_0, \theta_0, \phi_0)$ are initial guesses and linear operators $\left(\mathcal{L}_f^*,\ \mathcal{L}_g^*,\ \mathcal{L}_\theta^*,\ \mathcal{L}_\phi^*\right)$ which are selected in the forms

$$\left.\begin{array}{c} f_0^*\left(\eta\right) = 1 - e^{-\eta} \\ g_0^*\left(\eta\right) = 0, \\ \theta_0^*\left(\eta\right) = e^{-\eta}, \\ \phi_0^*\left(\eta\right) = e^{-\eta}, \end{array}\right\} \tag{7.23}$$

$$\left.\begin{array}{c} \mathcal{L}_f^* = f^{*'''} - f^*, \\ \mathcal{L}_g^* = g^{*\prime\prime} - g^*, \\ \mathcal{L}_\theta^{**} = \theta^{*\prime\prime} - \theta^*, \\ \mathcal{L}_\phi^* = \phi^{*\prime\prime} - \phi^*, \end{array}\right\} \tag{7.24}$$

with

$$\left.\begin{array}{c} \mathcal{L}_f^*\left[A_{*1} + A_{*2}e^{-\eta} + A_{*3}e^{\eta}\right] = 0, \\ \mathcal{L}_g^*\left[A_{*4}e^{-\eta} + A_{*5}e^{\eta}\right] = 0, \\ \mathcal{L}_\theta^*\left[A_{*6}e^{-\eta} + A_{*7}e^{\eta}\right] = 0, \\ \mathcal{L}_\phi^*\left[A_{*8}e^{-\eta} + A_{*9}e^{\eta}\right] = 0, \end{array}\right\} \tag{7.25}$$

where A_{*i} $(i = 1 - 9)$ signify the arbitrary constants

7.2.1 Convergence analysis

Series solution involves the auxiliary parameters $\hbar_f$ $\hbar_g.h_\theta$ and h_ϕ. The $h-$ curve in Fig. 1 and 2 show graphically the convergence region. It is clear from this figures that the convergence lies within the domain $-0.1 \leq h_f \leq -0.4$, $-0.1 \leq h_g \leq -0.45$, $-0.1 \leq h_\theta \leq -0.4$, $-1.0 \leq h_\phi \leq -0.4$.

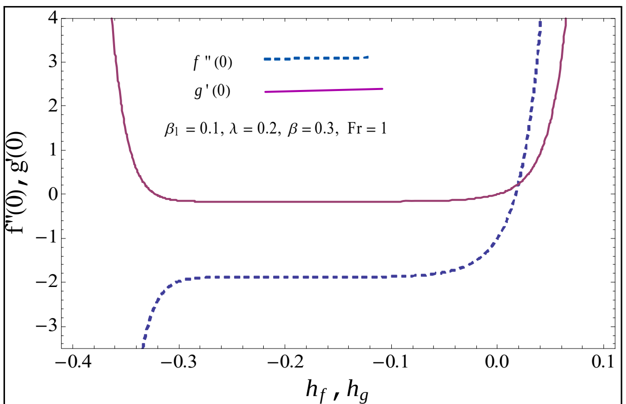

Fig. 7.1. $h-$curves for f and g.

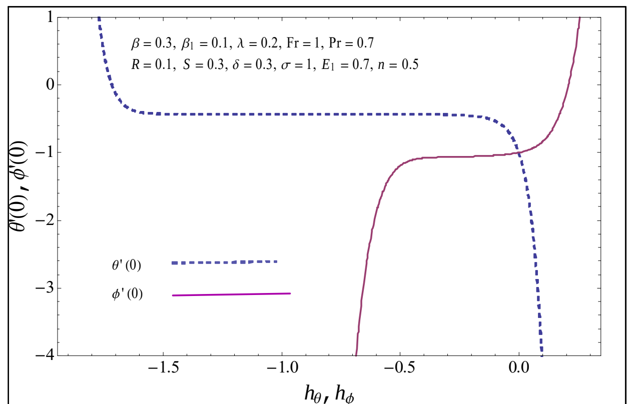

Fig. 7.2. $h-$curves for θ and ϕ

Table 7.1. Convergence iterations for flow expressions versus various pertinent parameters

Order of approximations	$-f''(0)$	$-g'(0)$	$-\theta'(0)$	$-\phi'(0)$
1	1.2548	0.044000	0.78100	1.0777
5	1.6289	0.11210	0.36826	1.2517
10	1.8335	0.15374	0.36124	1.4466
15	1.8710	0.16253	0.36011	1.5281
20	1.8818	0.16531	0.35768	1.5738
25	1.8850	0.16621	0.35423	1.6010
30	1.89766	0.17654	0.3163	1.7564
35	1.89766	0.17654	0.3163	1.7564

Table 7.2. Numerical results for Nusselt number

β_1	β	Fr	A_1	S	R	Pr	$\theta'(0)$
0	0.3	1	0.3	0.2	0.2	1	0.15098
0.25							0.15434
0.45							0.15923
0.25	0	1	0.3	0.2	0.2	1	0.13747
	0.3						0.14868
	0.5						0.15348
0.25	0.2	1	0.3	0.2	0.2	1	0.14337
		2					0.15240
		4					0.16566
0.25	0.2	1	0.1	0.2	0.2	1	0.061208
			0.2				0.10195
			0.4				0.18549
0.25	0.2	1	0.2	0.1	0.2	1	0.021850
				0.4			0.078896
				0.6			0.13759
0.25	0.2	1	0.3	0.2	0.2	1	0.15434
					0.3		0.040617
					0.4		0.022277
0.25	0.2	1	0.3	0.2	0.2	1	0.14337
						2	0.25775
						3	0.30917

Table 7.3. Numerical approximations for local Sherwood number

Sc	δ	E_1	S	R	σ	$-\phi'(0)$
1.0	0.3	1.0	0.2	0.5	1.0	1.6563
3.0						2.3471
5.0						2.9159
1.0	0.2	1.0	0.2	0.5	1.0	1.9482
	0.4					1.9639
	0.5					2.0119
1.0	0.2	2.0	0.2	0.5	1.5	2.3279
		4.0				2.8722
		5.0				3.2793
1	0.2	1	0.2	0.5	1.5	1.9429
					2.0	2.3389
					2.5	2.4981
1	0.2	1	0.1	0.5	1	1.6150
			0.3			1.6476
			0.5			1.6680
1	0.2	1	0.2	0.1	1	1.6212
				0.3		1.6302
				0.5		1.6584

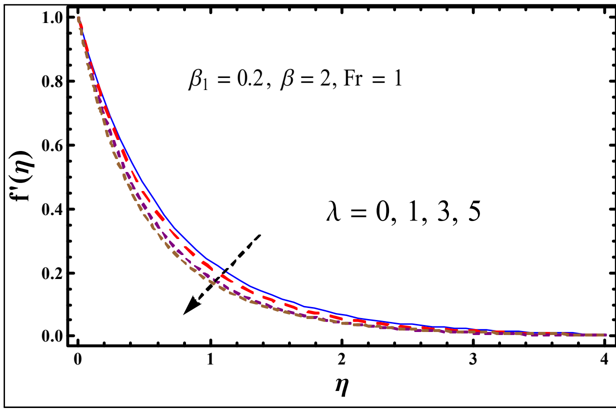

Fig. 7.3. $f'(\eta)$ against λ

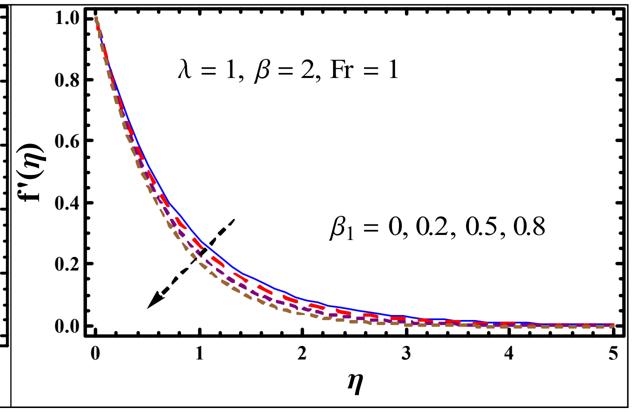

Fig. 7.4. $f'(\eta)$ against β_1.

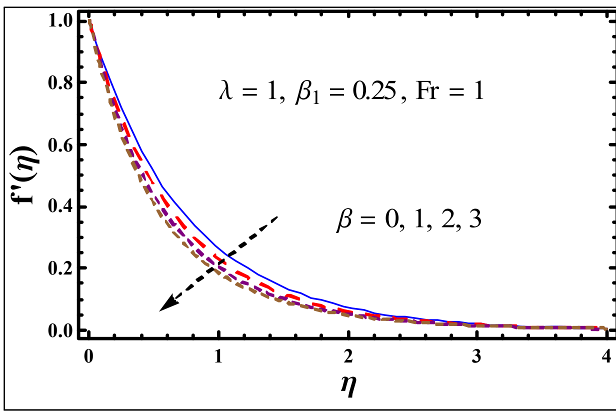

Fig. 7.5. $f'(\eta)$ against β.

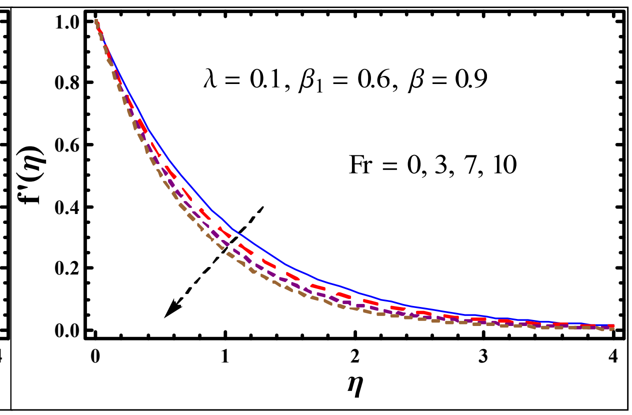

Fig. 7.6. $f'(\eta)$ against Fr.

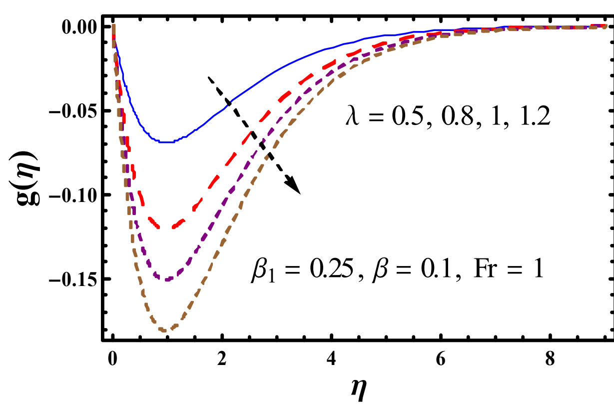

Fig. 7.7. $g(\eta)$ against λ.

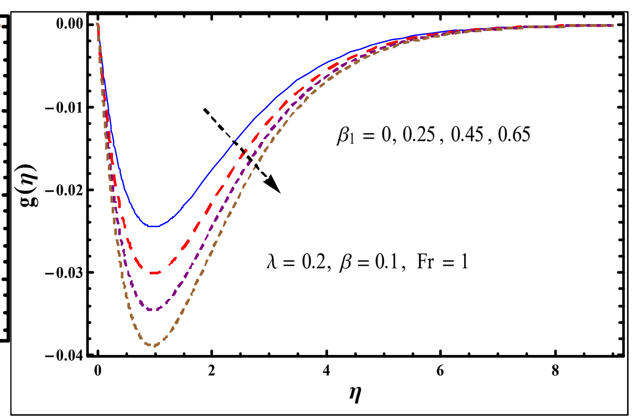

Fig. 7.8. $g(\eta)$ against β_1.

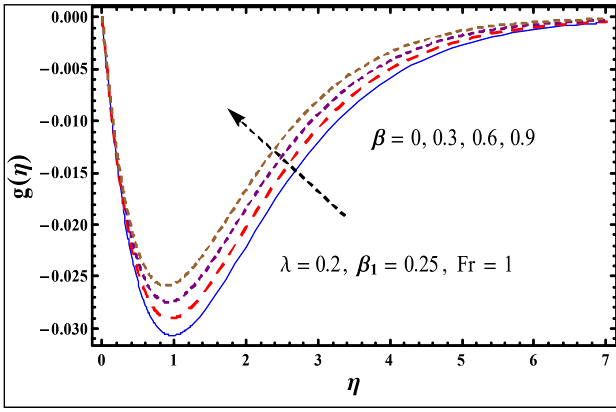

Fig. 7.9. $g(\eta)$ against β.

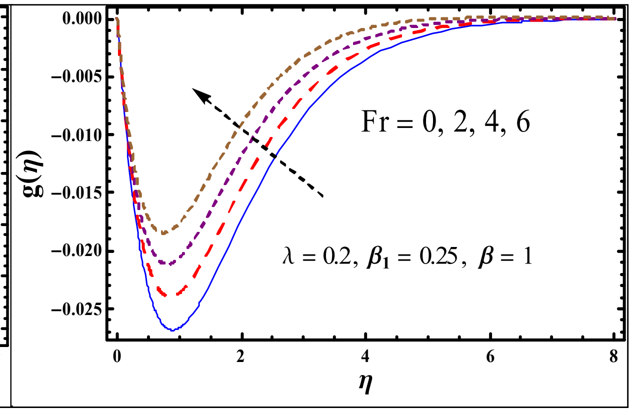

Fig. 7.10. $g(\eta)$ against Fr.

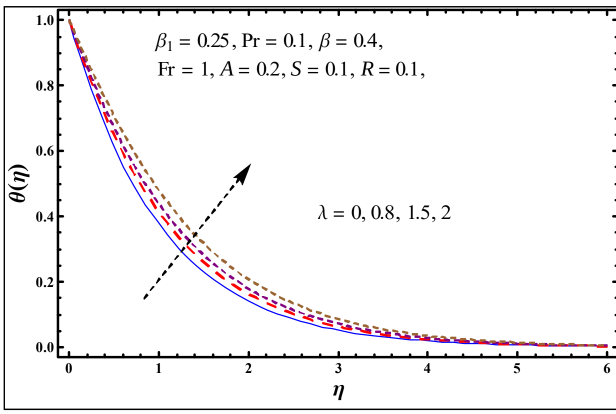

Fig. 7.11. $\theta(\eta)$ against λ.

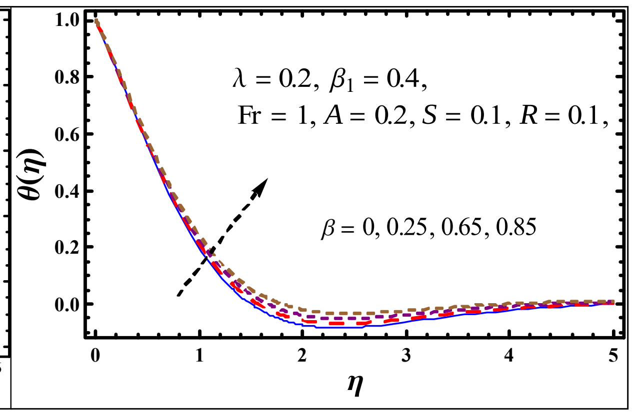

Fig. 7.12. $\theta(\eta)$ against β.

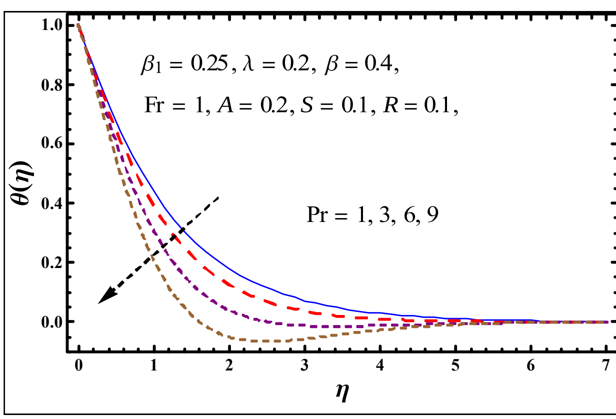

Fig. 7.13. $\theta(\eta)$ against $\Pr$.

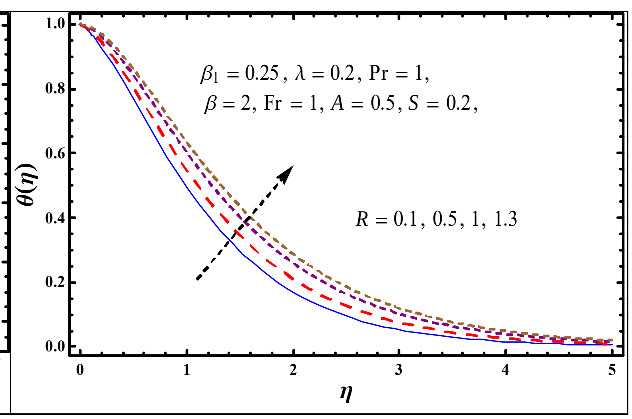

Fig. 7.14. $\theta(\eta)$ against R.

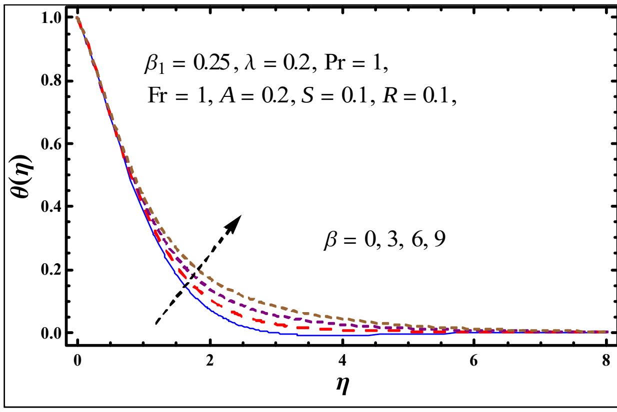

Fig. 7.15. $\theta(\eta)$ against β.

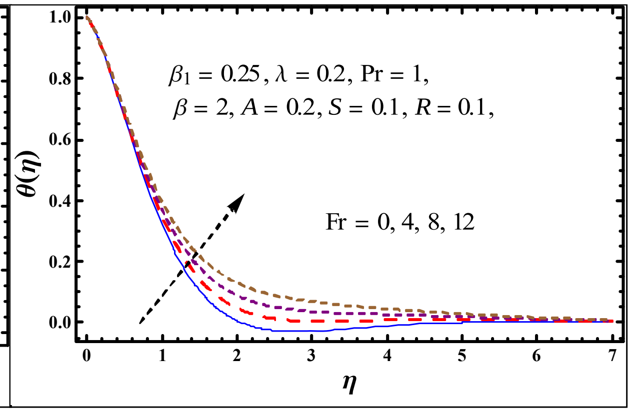

Fig. 7.16. $\theta(\eta)$ against Fr.

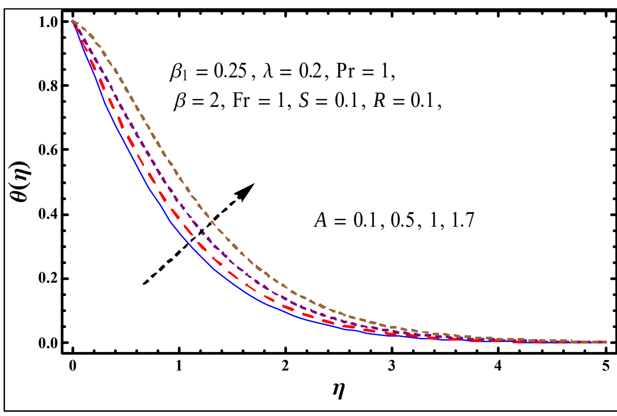

Fig. 7.17. $\theta(\eta)$ against A.

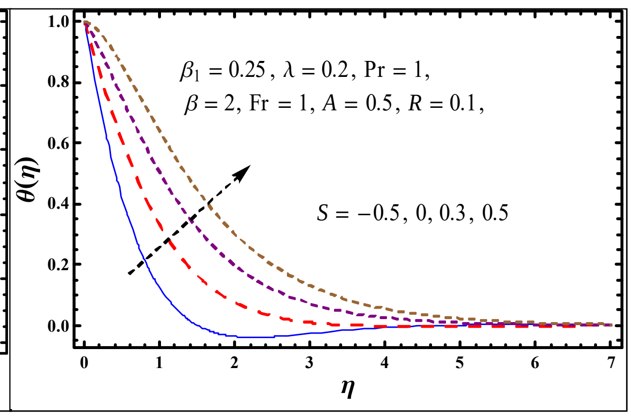

Fig. 7.18. $\theta(\eta)$ against S.

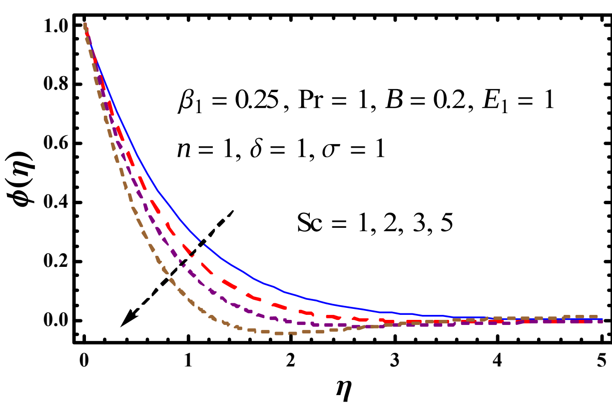

Fig. 7.19. $\phi(\eta)$ against Sc.

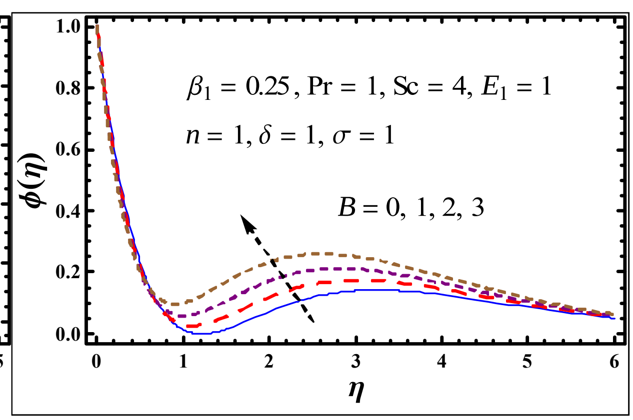

Fig. 7.20. $\phi(\eta)$ against B.

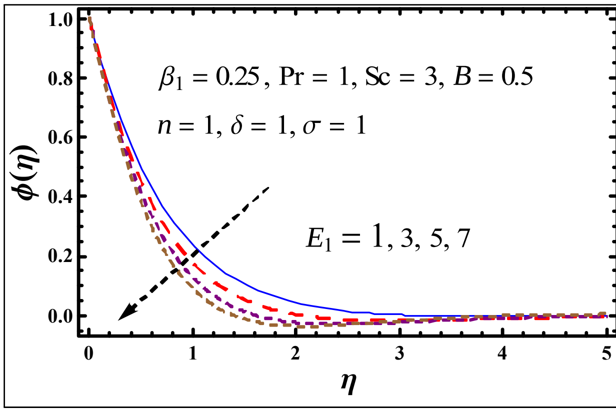

Fig. 7.21. $\phi(\eta)$ against E_1.

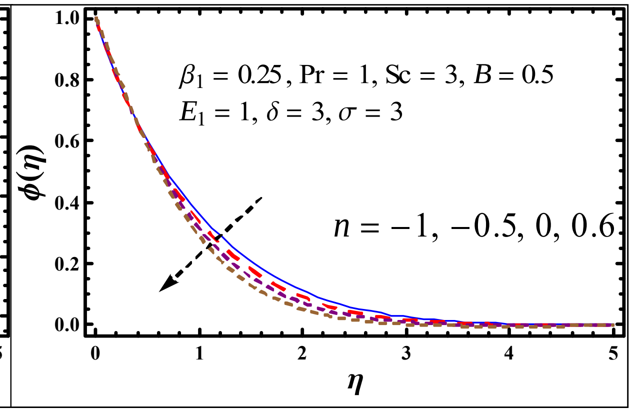

Fig. 7.22. $\phi(\eta)$ against n.

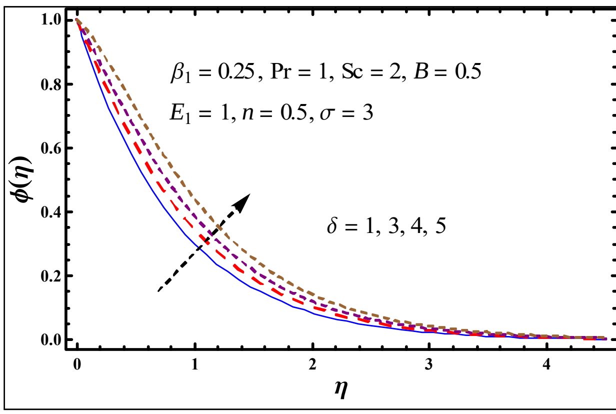

Fig. 7.23. $\phi(\eta)$ against δ.

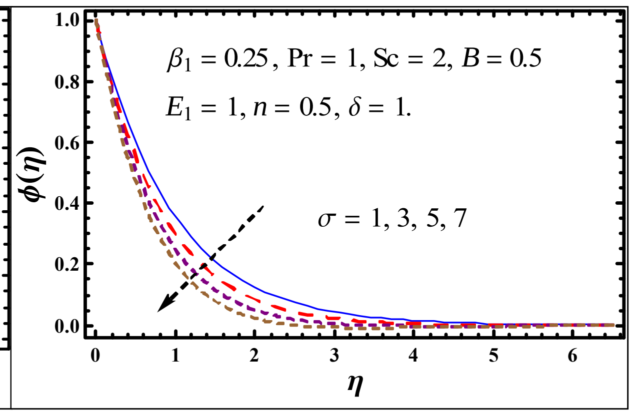

Fig. 7.24. $\phi(\eta)$ against σ.

7.3 Discussion

Here we investigate the impact of embedded parameters on the Darcy-Forchheimer Maxwell fluid flow in rotating frame with activation energy. For this purpose Figs. 7.3-7.24 are plotted. Table 1, it is observed that the 30th iteration is sufficient for all the flow expressions. Tables 7.2 and 7.3 are plotted to analysis the Nu_x and Sh_x numerically. Impact of rotation parameter on $f'(\eta)$ is presented in Fig. 7.3. Here velocity decays versus rotation parameter. Physically stretching rate decreases for rising estimations of rotation parameter and thus velocity field is declined. Velocity field via larger β_1 in highlighted in Fig. 7.4. Similarly velocity of fluid particles decays through higher β_1. It is due to fact that stretching velocity decays through larger values of β_1 .Fig. 7.5 explains the variation of β on $f'(\eta)$. The results of β is similar on velocity field as Figs. 7.3 and 7.4. Fig. 7.6 indicates the velocity field for increasing Fr. Here velocity is decreased by larger Fr. Physically resistive force enhances when an increment is occurred in Fr. Behavior of rotating parameter on $g(\eta)$ in Fig. 7.7. Here we can that $g(\eta)$ is decreased versus rotation parameter. Similar impact on $g(\eta)$ is observed through rising estimations of β in Fig. 7.8. Fig. 7.9 is presented to discuss the salient behavior of β on $g(\eta)$. Here we noticed that $g(\eta)$ is an increasing function of porosity variable. Same behavior of $g(\eta)$ versus Fr is sketched in Fig. 7.10. Fig. 7.11 shows the salient characteristics of λ on θ Fig. 7.11. Here both thermal layer and temperatur. Fig. 7.13 is prepared to point out the impact of Prandtl number on temperature distribution. Here we can see that both thermal field and associated layer decline versus higher Prandtl number field increase versus higher values of λ. Fig. 7.12. is portrayed for the influence of β_1 on temperature field. ere sharp growth in thermal field is seen when β_1 attend the maximum range. . Fig. 7.14 designates temperature field against higher radiation variable. Here curves of thermal field boosts up through rising radiative variable. Also thermal layer boost up versus higher radiative parameter. Fig. 7.15 elucidates temperature field against β. Fig. 7.16 illustrates the performance of Fr on thermal field. Clearly thermal distribution enhances against Fr. Temperature exponent influence on thermal field is existed in Fig. 7.17. Clearly thermal field enhances via larger temperature exponent parameter. Fig. 7.18 predicts the salient outcome of heat S on thermal field. Here $S > 0$ shows the heat source and $S < 0$ designate the heat sink and $S = 0$ signpost there is no heat source/sink. Here we have noticed that both θ and thermal layer enhanced versus larger heat source/sink parameter. Inspiration of Sc on concentration field is portrayed in Fig. 7.19. Since Schmidt number is the ratio of momentum to mass diffusivity, so an increase in the values of Schmidt number the mass concentration decays. Fig. 7.20 clearly designates that an enhancement in concentration exponent B, there is a reduction in the concentration field. Also mass concentration thickness decays versus larger concentration exponent. Fig. 7.21 is organized to deliberate the salient features of activation energy variable on concentration. Clearly mass concentration decays through higher values of activation energy variable. Also concentration layer thickness declines versus this parameter. Figs. 7.22 is organized for the impact of n on concentration. Here it is noticed that concentration distribution decreases for higher fitted rate constant variable. Figs. 7.23 and 7.24 arranged to examine the effects of

δ and σ on $\phi(\eta)$. Here contrast behavior of concentration distribution is observed for higher estimations of these variable. Clearly concentration of fluid particles boosts against larger δ (*see* Fig.7.23). But decreasing behavior is noticed for chemical rate parameter (*see* Fig.7.24).

7.4 Concluding remarks

Key points are presented as below

- Velocity decays versus larger estimations of λ, β and Fr.
- Velocity of liquid particles decreases in g direction through rising values of β_1 and λ.
- Curves of thermal field boosts up through rising radiative variable R.
- Fluid temperature enhances against larger radiation, heat source/sink parameters.
- Concentration of fluid particles boosts up versus higher values of δ.
- Decreasing behavior is noticed for chemical rate parameter σ.
- Concentration decays via larger E_1 and n.
- Rotation parameter has opposite performance on Sherwood and Nusselt numbers.

Chapter 8

Theoretical and analytical analysis of shear rheology of Oldroyd-B fluid with homogeneous-heterogeneous reactions

This research article communicates an analytical investigation for $(3D)$ steady incompressible Oldroyd-B fluid flow subject to stretchable surface. The flow of material induced through stretchable surface with Darcy-Forchheimer medium. Homogeneous-heterogeneous reactions are considered. Convective boundary conditions and heat source/sink effects are considered for the heat transport. Boundary layer concept is used in the development of flow problem. Series solutions are obtained of the nonlinear system through homotopy technique. Physical significance of pertinent parameters are discussed and plotted graphically. Heat transfer rate is discussed numerically.

8.1 Formulation

The cubic autocatalysis at the surface is defined as

$$A^* + 2B^* \rightarrow 3B^*, \text{ rate} = k_c a^{**} b^2, \tag{8.1}$$

and

$$A^* \to B^*,\ \text{rate} = k_s a^{**}, \tag{8.2}$$

where a^{**} and b respectively indicate the concentrations of species A^* and B^* and k_c and k_s are the rate constants.

In components form, the flow equations are

$$\frac{\partial u}{\partial x} + \frac{\partial v}{\partial y} + \frac{\partial w}{\partial z} = 0, \tag{8.3}$$

$$\left.\begin{array}{c} u\frac{\partial u}{\partial x} + v\frac{\partial u}{\partial y} + w\frac{\partial u}{\partial z} + \lambda_1^* \begin{pmatrix} u^2\frac{\partial^2 u}{\partial x^2} + v^2\frac{\partial^2 u}{\partial y^2} + w^2\frac{\partial^2 u}{\partial z^2} + 2uv\frac{\partial^2 u}{\partial x \partial y} \\ +2vw\frac{\partial^2 u}{\partial y \partial z} + 2uw\frac{\partial^2 u}{\partial x \partial z} \end{pmatrix} = \\ \nu\left[\frac{\partial^2 u}{\partial z^2} + \lambda_2^* \begin{pmatrix} u\frac{\partial^3 u}{\partial x \partial z^2} + v\frac{\partial^3 u}{\partial y \partial z^2} + w\frac{\partial^3 u}{\partial z^3} \\ -\frac{\partial u}{\partial x}\frac{\partial^2 u}{\partial z^2} - \frac{\partial u}{\partial y}\frac{\partial^2 v}{\partial z^2} - \frac{\partial u}{\partial z}\frac{\partial^2 w}{\partial z^2} \end{pmatrix}\right] - \frac{\nu}{K}u - Fu^2, \end{array}\right\} \tag{8.4}$$

$$\left.\begin{array}{c} u\frac{\partial v}{\partial x} + v\frac{\partial v}{\partial y} + w\frac{\partial v}{\partial z} + \lambda_1^* \begin{pmatrix} u^2\frac{\partial^2 v}{\partial x^2} + v^2\frac{\partial^2 v}{\partial y^2} + w^2\frac{\partial^2 v}{\partial z^2} \\ +2uv\frac{\partial^2 v}{\partial x \partial y} + 2vw\frac{\partial^2 v}{\partial y \partial z} + 2uw\frac{\partial^2 v}{\partial x \partial z} \end{pmatrix} = \\ \nu\left[\frac{\partial^2 v}{\partial z^2} + \lambda_2^* \begin{pmatrix} u\frac{\partial^3 v}{\partial x \partial z^2} + v\frac{\partial^3 v}{\partial y \partial z^2} + w\frac{\partial^3 v}{\partial z^3} \\ -\frac{\partial v}{\partial x}\frac{\partial^2 u}{\partial z^2} - \frac{\partial v}{\partial y}\frac{\partial^2 v}{\partial z^2} - \frac{\partial v}{\partial z}\frac{\partial^2 w}{\partial z^2} \end{pmatrix}\right] - \frac{\nu}{K}v - Fv^2, \end{array}\right\} \tag{8.5}$$

$$u\frac{\partial T}{\partial x} + v\frac{\partial T}{\partial y} + w\frac{\partial T}{\partial z} = \alpha_m \frac{\partial^2 T}{\partial z^2} + \frac{Q_0}{\rho c_p}\left(T - T_\infty\right), \tag{8.6}$$

$$u\frac{\partial a^{**}}{\partial x} + v\frac{\partial a^{**}}{\partial y} + w\frac{\partial a^{**}}{\partial z} = D_A \frac{\partial^2 a^{**}}{\partial z^2} - k_c a^{**} b^2, \tag{8.7}$$

$$u\frac{\partial b}{\partial x} + v\frac{\partial b}{\partial y} + w\frac{\partial b}{\partial z} = D_B \frac{\partial^2 a}{\partial z^2} + k_c a^{**} b^2, \tag{8.8}$$

with

$$\left.\begin{array}{c} u = u_w\left(x\right) = ax,\ v = 0,\ w = 0,\ \ -k\frac{\partial T}{\partial z} = \frac{h}{f}\left(T_f - T\right)\ \textbf{at}\ \ z = 0, \\ D_A\frac{\partial a^{**}}{\partial z} = k_s a^{**},\ D_B\frac{\partial b}{\partial z} = -\mathbf{k}_s a^{**}\ \textbf{at}\ z = 0, \\ u \longrightarrow 0,\ v \longrightarrow 0,\ w \longrightarrow 0,\ T \longrightarrow T_\infty,\ a^{**} \longrightarrow a_0,\ b \longrightarrow 0\ \textbf{at}\ \ z = \infty. \end{array}\right\} \tag{8.9}$$

Considering

$$\left.\begin{array}{c} \eta = \sqrt{\frac{a}{v}}z,\ u = axf'(\eta),\ v = axg(\eta), \\ w = -\left(av\right)^{\frac{1}{2}} f(\eta),\ \ \theta(\eta) = \frac{T - T_\infty}{T_f - T_\infty}. \end{array}\right\} \tag{8.10}$$

Continuity equation (8.3) is trivially satisfied while Eqs., (8.4) – (8.8) becomes

$$\left.\begin{aligned} f''' + \beta f' + \beta_1 \left(2ff'f'' - f^2 f'''\right) + ff'' \\ +\beta_2 \left(f''^2 - f' f'^{iv}\right) - \left(1 + F_r\right) f'^2 = 0, \end{aligned}\right\} \tag{8.11}$$

$$\left.\begin{aligned} g'' - \beta g + fg' - f'g + \beta_1 \left(2ff'g' - f^2 g''\right) \\ +\beta_2 \left(f'g'' - fg''' - gf''' + g'f''\right) - F_r g^2 = 0, \end{aligned}\right\} \tag{8.12}$$

$$\frac{1}{Sc}\phi'' + f\phi' - k_1 h^2 \phi = 0, \tag{8.13}$$

$$\frac{1}{Sc}h'' + fh' + k_1 h^2 \phi = 0, \tag{8.14}$$

$$\left.\begin{gathered} f = 0 = g,\ f' = 1,\ \theta' = -\gamma \left[1 - \theta(0)\right],\ \phi' = k_2 \phi(0), \\ \delta h'(0) = -k_2 \phi(0) \ \text{ at } \eta = 0, \\ f' \longrightarrow 0,\ g' \longrightarrow 0,\ \theta \longrightarrow 0,\ \phi \longrightarrow 1,\ h \longrightarrow 0 \text{ at } \eta \longrightarrow \infty. \end{gathered}\right\} \tag{8.15}$$

For comparable mass diffusions we put D_A and D_B are equal, we have

$$\phi(\eta) + h(\eta) = 1, \tag{8.16}$$

now Eqs. (8.13) and (8.14) becomes

$$\frac{1}{Sc}\phi'' + f\phi' - k_1 (1 - \phi)^2 \phi, \tag{8.17}$$

with

$$\phi'(0) = k_2 \phi(0),\ \ \phi(\infty) \longrightarrow \mathbf{1}. \tag{8.18}$$

The heat transfer rate is mathematically defined as

$$Nu_x = \frac{x q_w^*}{k\left(Tw - T_\infty\right)}, \tag{8.19}$$

where hall flux is defined as

$$q_w^* = -k\frac{\partial T}{\partial z}\ |_{z=o}\ . \tag{8.20}$$

Finally, one has

$$Nu_x \left(\mathrm{Re}_x\right)^{-0.5} \tag{8.21}$$

8.2 Homotopic solutions

Initial guesses and linear operators are requires in homotopy analysis method

$$\left.\begin{array}{c} f_0(\eta) = 1 - e^{-\eta}, \\ g_0(\eta) = 0, \\ \theta_0(\eta) = \frac{\gamma}{1+\gamma} e^{-\eta}, \\ \phi_0(\eta) = 1 - \frac{1}{2} e^{-k_2 \eta}, \end{array}\right\} \tag{8.22}$$

$$\left.\begin{array}{c} \mathcal{L}_f(\eta) = f''' - f', \\ \mathcal{L}_g = g'' - g, \\ \mathcal{L}_\theta(\eta) = \theta'' - \theta, \\ \mathcal{L}_\phi = \phi'' - \phi, \end{array}\right\} \tag{8.23}$$

with the following characteristics

$$\left.\begin{array}{c} \mathcal{L}_f\left[A_{*1} + A_{*2} e^{-\eta} + A_{*3} e^{\eta}\right] = 0, \\ \mathcal{L}_g\left[A_{*5} e^{-\eta} + A_{*5} e^{\eta}\right] = 0, \\ \mathcal{L}_\theta\left[A_{*6} e^{-\eta} + A_{*7} e^{\eta}\right] = 0, \\ \mathcal{L}_\phi\left[A_{*8} e^{-\eta} + A_{*9} e^{\eta}\right] = 0, \end{array}\right\} \tag{8.24}$$

where A_{*i} $(i = 1 - 9)$ designates are arbitrary constants

$$\left.\begin{array}{c} A_{*2} = A_{*4} = A_{*6} = A_{*8} = 0, \\ A_{*1} = -A_{*3} - f_m^*(0),\ A_{*3} = \frac{\partial f_m^\star(\eta)}{\partial \eta}\ |_{\eta=0},\ A_{*5} = -\frac{\partial g_m^\star(\eta)}{\partial \eta}\ |_{\eta=0}, \\ A_{*7} = \frac{1}{1+\gamma}\left[\frac{\partial \theta_m^\star(\eta)}{\partial \eta}\ |_{\eta=0} - \gamma\left(\theta_m^\star(0)\right)\right], \\ A_{*9} = \frac{1}{1+k_2}\left[\frac{\partial \phi_m^\star(\eta)}{\partial \eta}\ |_{\eta=0} - k_2\left(\phi_m^\star(0)\right)\right]. \end{array}\right\} \tag{8.25}$$

8.2.1 Convergence analysis

In series solutions auxiliary variables $\hbar_f$, $\hbar_g$, $\hbar_\theta$ and $\hbar_\phi$ play an important role to adjust the convergence portion. Therefore we have plotted $h-$curves for such analysis in Figs. 1 and 2. From these plots the valuable ranges are $-1.8 \leq h_f \leq -0.1$, $-1.6 \leq h_g \leq -0.1$, $-2.1 \leq h_\theta \leq 0.1$, $-2.1 \leq h_\phi \leq 0.1$.

Table 1 is sketched for the numerical iterations of convergence analysis.

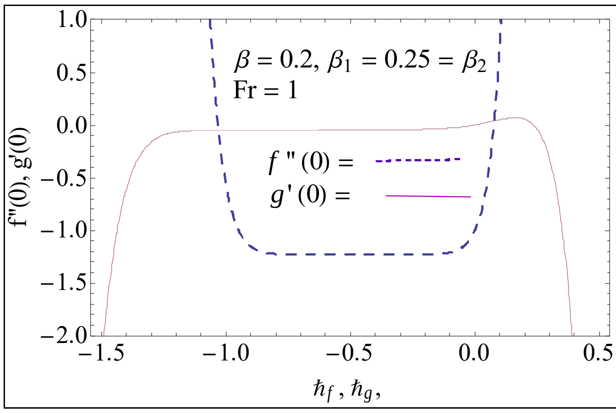

Fig. 8.1. $h-$curves for $f''(0)$ and $g'(0)$.

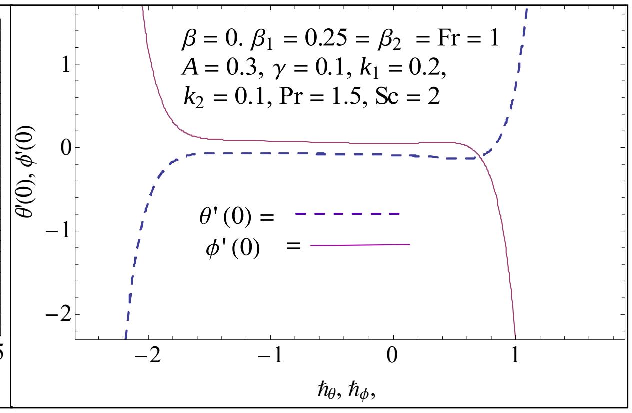

Fig. 8.2. $h-$curves for $\theta'(0)$ and $\phi'(0)$

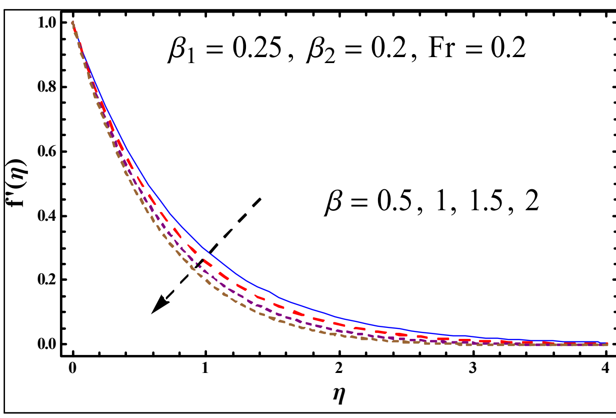

Fig. 8.3. f' versus β.

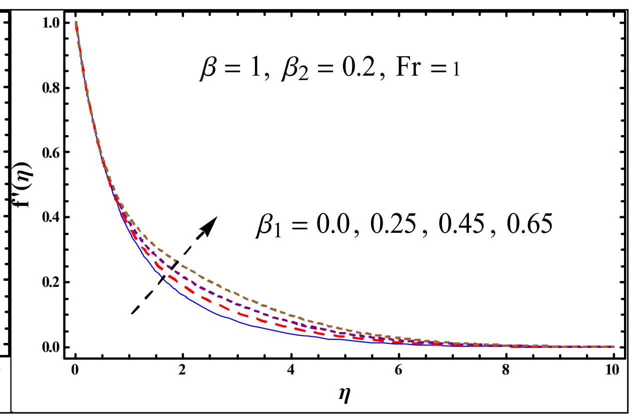

Fig. 8.4. f' versus β_1.

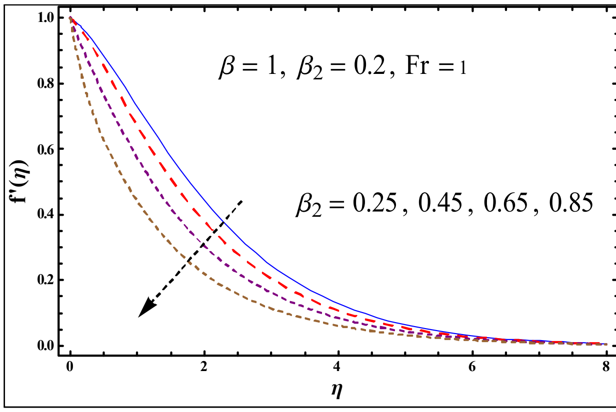

Fig. 8.5. f' versus β_2.

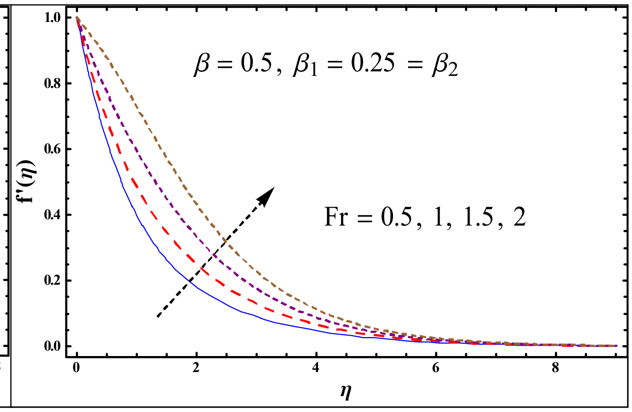

Fig. 8.6. f' versus Fr.

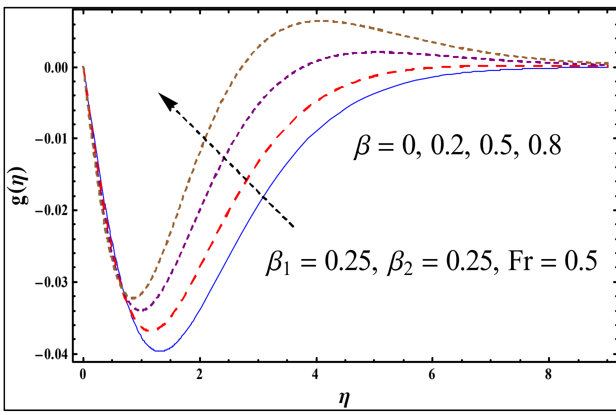

Fig. 8.7. g versus β

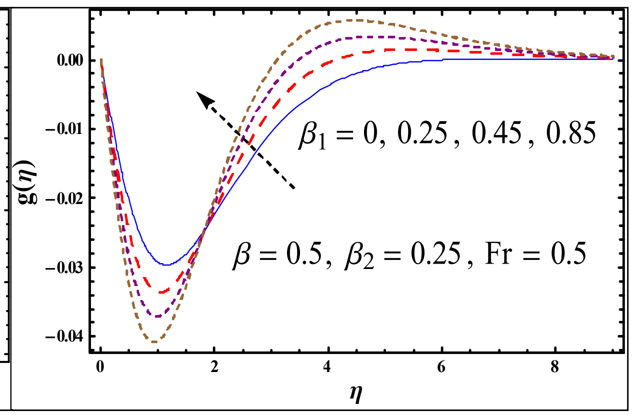

Fig. 8.8. g versus β_1.

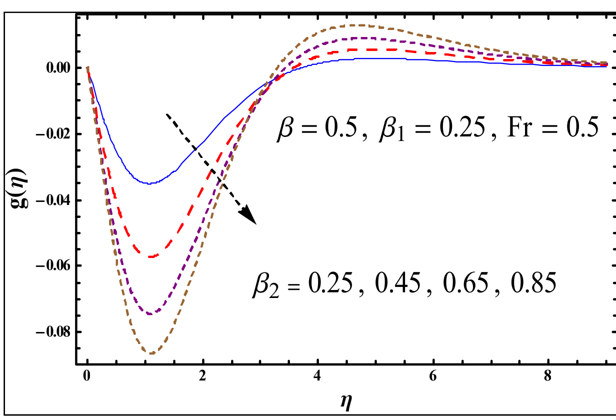

Fig. 8.9. g versus β_2.

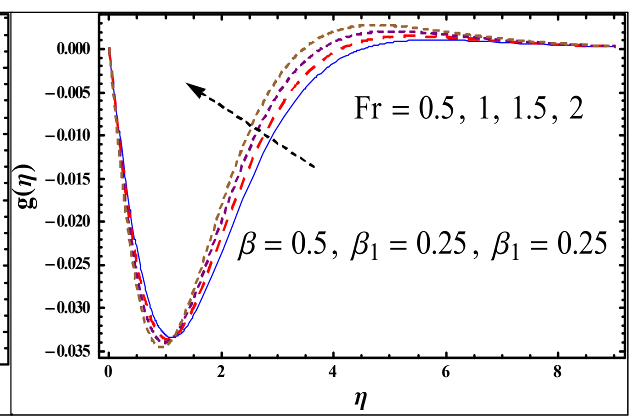

Fig. 8.10. g versus Fr.

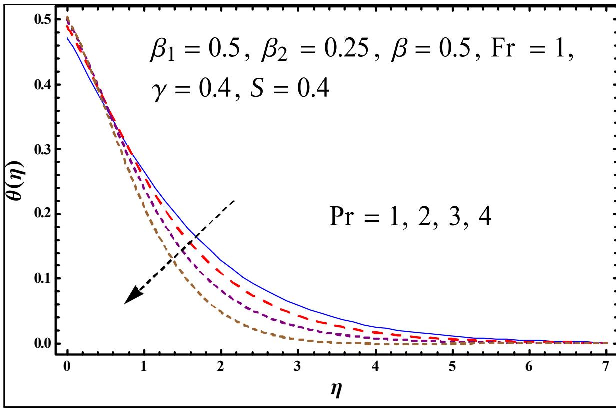

Fig. 8.11. θ versus Pr.

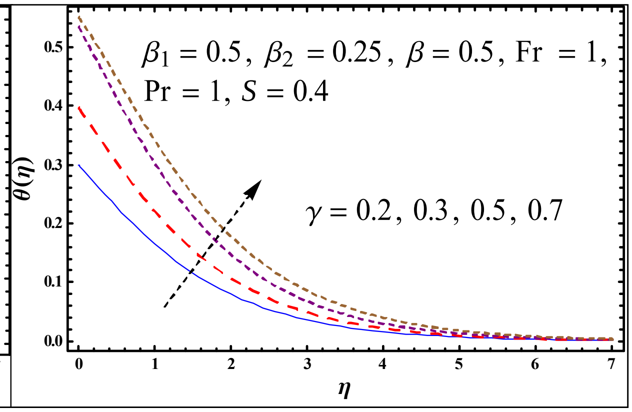

Fig. 8.12. θ versus γ.

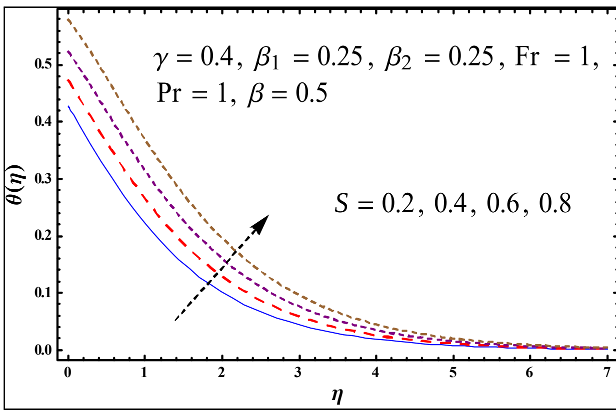

Fig. 8.13. θ versus S.

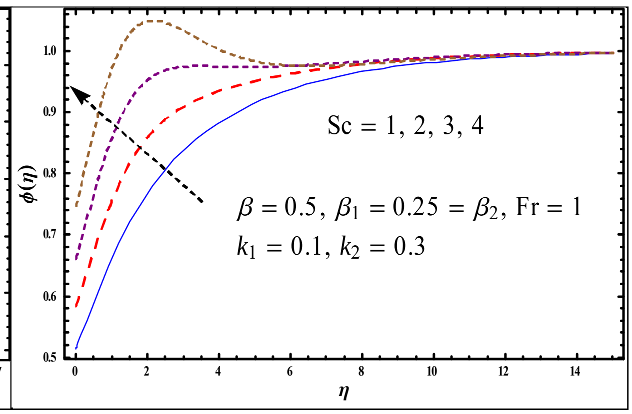

Fig. 8.14. ϕ versus Sc.

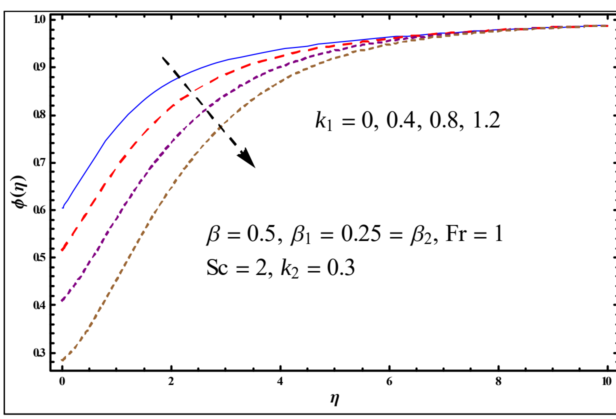

Fig. 8.15. ϕ versus k_1.

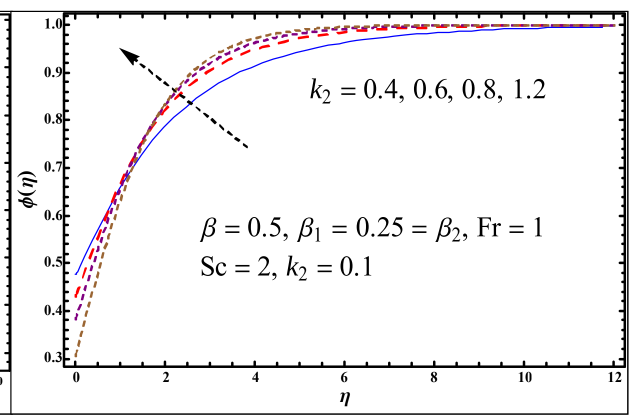

Fig. 8.16. ϕ versus k_2.

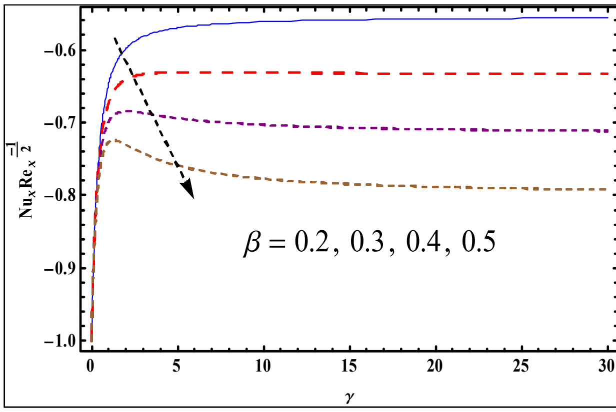

Fig. 8.17. Nusselt number versus β and γ.

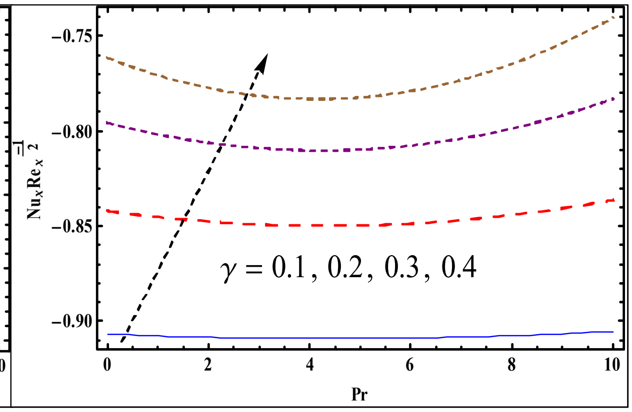

Fig. 8.18. Nusselt number versus γ and Pr.

Table 8.1. Different iterations for series solutions when $\beta = 0.1$, $\beta_1 = 0.1$, $\beta_2 = 0.1$, $Fr = 0.3$, $\Pr = 1, \gamma = 0.1$, $k_1 = 0.2$, $k_2 = 0.1$, $Sc = 1$

Order of approximations	$-f''(0)$	$-g'(0)$	$-\theta'(0)$	$\phi'(0)$
1	1.0215	0.12667	0.088154	0.049515
5	1.0313	0.14819	0.085496	0.052571
10	1.0318	0.14886	0.085094	0.060685
15	1.0318	0.14877	0.085059	0.066513
20	1.0318	0.14888	0.085050	0.073378
25	1.0318	0.14888	0.085048	0.079135
30	1.0318	0.14888	0.085048	0.082693
35	1.0318	0.14888	0.085048	0.082693

8.2.2 Discussion

This section is established to explore the impacts of interesting variables on velocity, temperature and concentration fields. For this purpose we have plotted Figs.(8.3 – 8.18). Porosity variable behavior on velocity $f'(\eta)$ is presented in Fig. 8.3. Velocity diminishes versus larger porosity variable. Physically, due to porous media more resistance occurred to the flow particles which make the velocity of fluid weaker. In Fig. 8.4, we have plotted the impact of fluid relaxation variable on velocity field. Here we observed that the velocity of material particles enhances versus larger relaxation variable. Furthermore, boundary layer shows an increasing impact against larger relaxation variable. Fig. 8.5 is outlined to show the velocity field against retardation variable. Here we noticed that velocity field declines via higher retardation parameter. Inertia variable impact on velocity field is highlighted in Fig. 8.6. Here velocity curves slowly increases when the inertia variable takes the maximum range. Also layer thickness upsurges versus larger inertia variable. Inspiration of porosity variable on $g(\eta)$ is depicted in Fig. 8.7. Here initially velocity of liquid particles increases and then show decreasing impact when the porosity variable take the maximum values. Salient aspects of relaxation and retardation variable on is outlined in Figs. 8.8 and 8.9. From these sketches we can see that velocity field monotonically decays initially near the stretchable surface and then monotonically upsurges against larger relaxation and retardation variables. Fig. 8.10 is revealed for the impact of Forchheimer number or inertia coefficient variable on $g(\eta)$. Here we noticed that velocity component in y-direction upsurges versus larger Forchheimer number. It is also noticed that layer thickness enhances against larger Forchheimer number. Behavior of Prandtl number on thermal field is recorded in Fig. 8.11. Lesser thermal field is noticed against higher Prandtl number. Characteristics of Biot number on thermal field is shown in Fig. 8.12. Here temperature is an increasing function of larger Biot number. Physically, larger Biot number increases the convection process at the stretchable surface which leads to upsurges the temperature field. Fig. 8.13 predicts the salient attributes of heat generation/absorption or heat source/sink variable on the thermal field. In this study, $S > 0$ highlights the heat generation or heat source and $S < 0$ signifies the absorption or sink and $S = 0$ signposts there is no heat generation/absorption or heat source/sink. But here we have only presents the effect of heat generation on the thermal field. Thermal field is an increasing behavior against heat generation variable. Fig. 8.14 highlights the salient attributes of Schmidt number on mass concentration field. Physically, Schmidt number is the combination of momentum and mass diffusivity. Here mass concentration increases against higher Schmidt number. Also concentration layer thickness upsurges versus rising estimations of Schmidt number. Attributes of homogeneous reactive variable on mass concentration is sketched in Fig. 8.15. Here we have examined reduction in solutal layer and as well as in mass concentration via higher homogeneous reactive variable. Behavior of heterogeneous reactive variable on mass concentration is revealed in Fig. 8.16. From this sketch, we have examined that concentration of reaction species at the surface upsurges against higher estimation of heterogeneous reactive variable. Graphical sketch of heat transfer rate against various flow variables like porosity parameter, Biot number and Prandtl number is highlighted in Figs. 8.17 and 8.18. From these sketches, we have noticed that magnitude of heat transfer decays versus higher estimations of porosity parameter and Biot number.

8.3 Concluding remarks

The valuable results of the presented problem are recorded below:

- Velocity of material particles in x-direction decays against higher porosity variable.
- Velocity shows contrast impact against relaxation and retardation variables.
- Thermal declines versus Prandtl number.
- Temperature is an increasing function of larger Biot number.
- Higher heat generation variable upsurge the temperature of material particles.
- Schmidt number is increasing function of concentration.
- Concentration presents contrast impact against homogeneous and heterogeneous reactive parameters.
- Magnitude of heat transfer rate decays against larger porosity parameter and Biot number.

Chapter 9

Future work

Our intention in this chapter is to modeling and analysis for nonlinear flow due to stretched surface through several possible directions. It is worthmentioning that results of modeled problems are useful in processes relating to metallurgy, polymer extrusion, glass fiber, food processing industries and paper production etc.

The attempted problem can further be modeled and scrutinized through following characteristic.

- Flow considering activation energy analysis in entropy generating.
- Rotating flow with homogeneous-heterogeneous reaction over an exponentially surface with convective boundary.
- Buoyancy effects in chemical reaction with Cattaneo-Christov heat flux and porous surface.

Bibliography

[1] S. U. S. Choi, Enhancing thermal conductivity of fluids with nanoparticles, USA, ASME, FED 231/MD, 66 (1995) 99 – 105.

[2] J. Buongiorno, Convective transport in nanofluids, ASME J. Heat Transf., 128 (2006) 240 – 250.

[3] T. Hayat, M. Shafique, A. Tanveer, A. Alsaedi, Hall and ion slip effects on peristaltic flow of Jeffrey nanofluid with Joule heating, J. Magn. Magn. Mater. 407 (2016) 51 – 59.

[4] T. Hayat, S. Qayyum, M. Imtiaz, A. Alsaedi, Comparative study of silver and copper water nanofluids with mixed convection and nonlinear thermal radiation, Int. J. Heat Mass Transf. 102 (2016) 723 – 732.

[5] O. D. Makinde and A. Aziz, Boundary layer flow of a nanofluid past a stretching sheet with a convective boundary condition, Int. J. Thermal Sci., 50 (2011) 1326 – 1332.

[6] S. Rashidi, S. Akar, M. Bovand and R. Ellahi, Volume of fluid model to simulate the nanofluid flow and entropy generation in a single slope solar still, Renew. Energy, 115 (2018) 400 – 410.

[7] T. Hayat, M. I. Khan, M. Waqas and A. Alsaedi, On the performance of heat absorption/generation and thermal stratification in mixed convective flow of an Oldroyd-B fluid, Nuclear Eng. Tech., 49 (2017) 1645 – 1653.

[8] M. Hassan, M. Marin, A. Alsharif and R. Ellahi, Convection heat transfer flow of nanofluid in a porous medium over wavy surface, Phys. Lett. A, 382 (2018) 2749 – 2753.

[9] T. Hayat, S. Ahmed, M. I. Khan and A. Alsaedi, Modeling the chemically reactive flow of Sutterby nano fluid by a rotating disk in the presence of heat generation/absorption, Commu. Theoret. Phys., 69 (2018) 569-576.

[10] M. Akbarzadeh, S. Rashidi, N. Karimi and R. Ellahi, Convection of heat and thermodynamic irreversibilities in two-phase, turbulent nanofluid flows in solar heaters by corrugated absorber plates, Adv. Powder Tech., 29 (2018) 2243 – 2254.

[11] M. I. Khan, S. Ullah, T. Hayat, M. Waqas, M. I. Khan and A. Alsaedi, Salient aspects of entropy generation optimization in mixed convection nanomaterial flow, Int. J. Heat Mass Transf., 126 (2018) 1337 – 1346.

[12] S. Z.Alamri, R. Ellahi, N. Shehzad and A. Zeeshan, Convective radiative plane Poiseuille flow of nanofluid through porous medium with slip: An application of Stefan blowing, J. Mol. Liq., 273 (2019) 292 - 304.

[13] S. Z. Alamri, R. Ellahi, N. Shehzad and A. Zeeshan, Convective radiative plane Poiseuille flow of nanofluid through porous medium with slip: An application of Stefan blowing, J. Mol. Liq., 273 (2019) 292 – 304.

[14] M. I. Khan, T. A. Khan, S. Qayyum, T. Hayat, M. I. Khan and A. Alsaedi, Entropy generation optimization and activation energy in nonlinear mixed convection flow of tangent hyperbolic nanofluid, Plus Eur. Phys. J. Plus, 133 (2018) 329.

[15] T. Hayat, M. Z. Kayani, A. Alsaedi, M. I. Khan and I. Ahmad, Mixed convective three-dimensional flow of Williamson nanofluid subject to chemical reaction, Int. J. Heat Mass Transf., 127 (2018) 422 – 429.

[16] T. Hayat, T. Muhammad, M. Mustafa and A. Alsaedi, An optimal study for three-dimensional flow of Maxwell nanofluid subject to rotating frame, J. Mol. Liq., 229 (2017) 541 – 547.

[17] A. Megahed, Variable fluid properties and variable heat flux effects on the flow and heat transfer in a non-Newtonian Maxwell fluid over an unsteady stretching sheet with slip velocity, Chinese Physica B, Vol. 22 (2013) 094701.

[18] M. I. Khan, S. Qayyum, T. Hayat, M. I. Khan and A. Alsaedi, Entropy optimization in flow of Williamson nanofluid in the presence of chemical reaction and Joule heating, Int. J. Heat Mass Transf., 133 (2019) 959 – 967.

[19] R. Ellahi, M. Hassan, A. Zeeshan and A. A. Khan, The shape effects of nanoparticles suspended in HFE-7100 over wedge with entropy generation and mixed convection, Appl. NanoSci., 6 (2016) 641 – 651.

[20] M. Rashid, M. I. Khan, T. Hayat, M. I. Khan and A. Alsaedi, Entropy generation in flow of ferromagnetic liquid with nonlinear radiation and slip condition, J. Mol. Liq., 276 (2019) 441 – 452.

[21] R. Ellahi, S. U. Rahman, S. Nadeem and N. S. Akbar, Blood flow of nanofluid through an artery with composite stenosis and permeable walls, Appl. NanoSci., 4 (2014) 919 – 926.

[22] T. Hayat, F. Shah, M. I. Khan and A. Alsaedi, Numerical simulation for aspects of homogeneous and heterogeneous reactions in forced convection flow of nanofluid, Results Phys., 8 (2018) 206 – 212.

[23] R. Ellahi, R. Riaz and S. Nadeem, A theoretical study of Prandtl nanofluid in a rectangular duct through peristaltic transport, Appl. NanoSci., 4 (2014) 753 – 760.

[24] M. I. Khan, S. Qayyum, T. Hayat and A. Alsaedi, Entropy generation minimization and statistical declaration with probable error for skin friction coefficient and Nusselt number, Chinese J. Phys., 56 (2018) 1525 – 1546.

[25] M. M. Rashidi, M. Ali, N. Freidoonimehr, B. Rostami and A. Hossian, Mixed convection heat transfer for viscoelastic fluid flow over a porous wedge with thermal radiation, Adv. Mech. Eng., 204 (2014) 735939.

[26] S. Mukhopadhyay, Slip effects on MHD boundary layer flow over an exponentially stretching sheet with suction/blowing and thermal radiation, Ain Sham. Eng. J., 4 (2013) 485 – 91.

[27] M. Sajid and T. Hayat, Influence of thermal radiation on the boundary layer flow due to an exponentially stretching sheet, Int. Comm. Heat Mass Transf., 35 (2008) 347 – 356.

[28] M. M. Nandeppanavar, K. Vajravelu and M. S. Abel, Heat transfer in MHD viscoelastic boundarylayer flow over a stretching sheet with thermal radiation and non-uniform heat source/sink, Comm. Nonlinear Sci. Numer. Simul., 16 (2011) 3578 − 3590.

[29] K. Bhattacharyya, S. Mukhopadhyay, G. C. Layek and I. Pop, Effects of thermal radiation on micropolar fluid flow and heat transfer over a porous shrinking sheet, Int. J. Heat Mass Transf., 55 (2012) 2945 − 52.

[30] O. D. Makinde, Second law analysis for variable viscosity hydromagnetic boundary layer flow with thermal radiation and Newtonian heating, Entropy, 13 (2011) 1446 − 64.

[31] T. Hayat, M. I. Khan, M. Farooq, A. Alsaedi, M. Waqas and T. Yasmeen, Impact of Cattaneo-Christov heat flux model in flow of variable thermal conductivity fluid over a variable thicked surface, Int. J. Heat Mass Transf., 99 (2016) 702 − 710.

[32] N. B. Khan, Z. Ibrahim, M. F. Javed and M. Jameel, Numerical investigation of the vortex-induced vibration of an elastically mounted circular cylinder at high Reynolds number ($Re = 104$) and low mass ratio using the RANS code, PloS one, 12 (2017) $e0185832$.

[33] T. Hayat, M. I. Khan, M. Farooq, T. Yasmeen and A. Alsaedi, Stagnation point flow with Cattaneo-Christov heat flux and homogeneous-heterogeneous reactions, J. Mol. Liq., 220 (2016) 49 − 55.

[34] M. F. Javed, M. I. Khan, N. B. Khan, R. Muhammad, M. U. Rehman, S. W. Khan and T. A. Khan, Axisymmetric flow of Casson fluid by a swirling cylinder, Results Phys., 9 (2018) 1250 − 1255.

[35] M. I. Khan, M. Waqas, T. Hayat and A. Alsaedi, A comparative study of Casson fluid with homogeneous-heterogeneous reactions, J. Colloid Interface Sci., 498 (2017) 85 − 90.

[36] M. F. Javed, N. B. Khan, M. I. Khan, R. Muhammad, M. U. Rehman, S. W. Khan and T. A. Khan, Optimization of SWCNTs and MWCNTs (single and multi-wall carbon nanotubes) in peristaltic transport with thermal radiation in a non-uniform channel, J. Mol. Liq., 273 (2018) 383 − 391.

[37] T. Hayat, M. I. Khan, S. Qayyum and A. Alsaedi, Entropy generation in flow with silver and copper nanoparticles, Colloid. Surfaces A: Physicochemical Eng. Aspect.,539 (2018) 335 − 346.

[38] N. B. Khan, Z. Ibrahim, A. B. B. M. Badry, M. Jameel and M. F. Javed, Numerical investigation of flow around cylinder at Reynolds number = 3900 with large eddy simulation technique: Effect of spanwise length and mesh resolution, Proceed. Instit. Mech. Eng. Part M: J. Eng. Maritime Environ., (2018) ,$DOI.org$/10.1177/1475090217751326.

[39] M. I. Khan, T. Hayat, M. I. Khan and A. Alsaedi, Activation energy impact in nonlinear radiative stagnation point flow of Cross nanofluid, Int. Comm. Heat Mass Transf., 91 (2018) 216 − 224.

[40] T. Hayat, S. Qayyum, M. I. Khan and A. Alsaedi, Entropy generation in magnetohydrodynamic radiative flow due to rotating disk in presence of viscous dissipation and Joule heating, Phys. Fluid., 30 (2018) 017101.

[41] N. B. Khan, Z. Ibrahim, M. I. Khan, T. Hayat and M. F. Javed, VIV study of an elastically mounted cylinder having low mass-damping ratio using RANS model, Int. J. Heat Mass Transf., 121 (2018) 309 − 314.

[42] M. I. Khan, T. Yasmeen, M. I. Khan, M. Farooq and M. Wakeel, Research progress in the development of natural gas as fuel for road vehicles: A bibliographic review (1991–2016), Renew. Sustain. Energy Review., 66 (2016) 702 − 741.

[43] M. I. Khan, M. Waqas, T. Hayat, A. Alsaedi and M. I. Khan, Significance of nonlinear radiation in mixed convection flow of magneto Walter-B nanoliquid, Int. J. Hydrogen Energy, 42 (2017) 26408 − 26416.

[44] S. Qayyum, M. I. Khan, T. Hayat and A. Alsaedi, A framework for nonlinear thermal radiation and homogeneous-heterogeneous reactions flow based on silver-water and copper-water nanoparticles: A numerical model for probable error, Results Phys., 7 (2017) 1907 − 1914.

[45] Y. Zhang, M. Zhang and Y. Bai, Flow and heat transfer of an Oldroyd-B nanofluid thin film over an unsteady stretching sheet, J. Mol. Liq., 220 (2016) 665 − 670.

[46] I. S. Shivakumara, M. Dhananjaya and C.O. Ng, Thermal convective instability in an Oldroyd-B nanofluid saturated porous layer, Int. J Heat Mass Transf., 84 (2015) 167−177.

[47] M. S. Hashmi, N. Khan, T. Mahmood and S. A. Shehzad, Effect of magnetic field on mixed convection flow of Oldroyd-B nanofluid induced by two infinite isothermal stretching disks, Int. J. Ther. Sci., 111 (2017) 463 − 474.

[48] Y. Zhang, B. Yuan, Y. Bai, Y. Cao and Y. Shen, Unsteady Cattaneo-Christov double diffusion of Oldroyd-B fluid thin film with relaxation-retardation viscous dissipation and relaxation chemical reaction, Powder Tech., 338 (2018) 975 − 982.

[49] S. A. Shehzad, A. Alsaedi, T. Hayat and M. S. Alhuthali, Thermophoresis particle deposition in mixed convection three-dimensional radiative flow of an Oldroyd-B fluid, J. Taiwan Inst. Chemical Eng., 45 (2014) 787 − 794.

[50] K. G. Kumar, G. K. Ramesh, B. J. Gireesha and R. S. R. Gorla, Characteristics of Joule heating and viscous dissipation on three-dimensional flow of Oldroyd B nanofluid with thermal radiation, Alexandria Eng. J., 57 (2018) 2139 − 2149.

[51] K. Das, T. Chakraborty and P. K. Kundu, Effect of magnetic field on Oldroyd-B type nanofluid flow over a permeable stretching surface, Propulsion and Power Res., 7 (2018) 238 − 246.

[52] B. J. Gireesha, K. G. Kumar, G. K. Ramesh and B. C. Prasannakumara, Nonlinear convective heat and mass transfer of Oldroyd-B nanofluid over a stretching sheet in the presence of uniform heat source/sink, Results Phy., 9 (2018) 1555 − 1563.

[53] N. Khan and T. Mahmood, Thermophoresis particle deposition and internal heat generation on MHD flow of an Oldroyd-B nanofluid between radiative stretching disks, J. Mol. Liq., 216 (2016) 571 − 582.

[54] M. Waqas, M. Ijaz Khan, T. Hayat and A. Alsaedi, Stratified flow of an Oldroyd-B nanoliquid with heat generation, Results Phy., 7 (2017) 2489 − 2496.

[55] M. S. Abel, J. V. Tawade and M. M. Nandeppanavar, MHD flow and heat transfer for the upper-convected Maxwell fluid over a stretching sheet, Meccanica 47 (2012) 385–393.

[56] A. M. Megahed, Variable fluid properties and variable heat flux effects on the flow and heat transfer in a non-Newtonian Maxwell fluid over an unsteady stretching sheet with slip velocity, Chin. Phys. B 22 (2013) 094701.

[57] S. A. Shehzad, Magnetohydrodynamic Jeffrey nanoliquid flow with thermally radiative Newtonian heat and mass species, Revista Mexicana de F´ısica, 64 (2018) 628 − 633.

[58] T. Hayat, M. I. Khan, M. Farooq, A. Alsaedi, M. Waqas and T. Yasmeen, Impact of Cattaneo-Christov heat flux model in flow of variable thermal conductivity fluid over a variable thicked surface, Int. J. Heat and Mass Trans., 99 (2016) 702 − 710.

[59] M. I. Khan, M. Waqas, T. Hayat and A. Alsaedi, A comparative study of Casson fluid with homogeneous-heterogeneous reactions, J. Colloid And Interface Sci., 498 (2017) 85 − 90.

[60] T. Muhammad, A. Alsaedi, T. Hayat and S. A. Shehzad, A revised model for Darcy-Forchheimer three-dimensional flow of nanofluid subject to convective boundary condition, Results Phys., 7 (2017) 2791 − 2797.

[61] M. I. Khan, T. Hayat, M. I. Khan and A. Alsaedi, A modified homogeneous-heterogeneous reactions for MHD stagnation flow with viscous dissipation and Joule heating, Int. J. of Heat Mass Transf., 113 (20178) 310 − 317.

[62] T. Hayat, M. I. Khan, S. Qayyum and A. Alsaedi, Entropy generation in flow with silver and copper nanoparticles, Colloids and Surfaces A: Physicochemical and Eng. Aspects, 539 (2018) 335 − 346.

[63] R. Ellahi, S. U. Rahman, S. Nadeem and N. S. Akbar, Blood flow of nanofluid through an artery with composite stenosis and permeable walls, App. Nanosci., 4 (2014) 919 − 926.

[64] T. Hayat, M. I. Khan, M. Farooq, T. Yasmeen and A. Alsaedi, Water-carbon nanofluid flow with variable heat flux by a thin needle, J. Molecular Liqs., 224 (2016) 786 − 791.

[65] M. A. Meraj, S. A. Shehzad, T. Hayat, F. M. Abbasi and A. Alsaedi, Darcy-Forchheimer flow of variable conductivity Jeffrey liquid with Cattaneo-Christov heat flux theory, App. Maths. Mechs., 201738 (2017) $557 - 566$.

[66] M. I. Khan, M. Waqas, T. Hayat, M. I. Khan and A. Alsaedi, Behavior of stratification phenomenon in flow of Maxwell nanomaterial with motile gyrotactic microorganisms in the presence of magnetic field, Int. J. Mech. Sci., 132 (2017) $426 - 434$.

[67] R. Ellahi, R. Riaz and S. Nadeem, A theoretical study of Prandtl nanofluid in a rectangular duct through peristaltic transport, App. Nanoscience, 4 (2014) $753 - 760$.

[68] M. I. Khan, T. Hayat, M. Waqas, M. I. Khan and A. Alsaedi, Impact of heat generation/absorption and homogeneous-heterogeneous reactions on flow of Maxwell fluid, J. Molecular Liqs., 233 (2017) $465 - 470$.

[69] R. Ellahi, M. Hassan, A. Zeeshan and A. A. Khan, The shape effects of nanoparticles suspended in HFE-7100 over wedge with entropy generation and mixed convection, App. Nanoscience, 6 (2016) $641 - 651$.

[70] M. I. Khan, M. I. Khan, M. Waqas and T. Hayat, A Alsaedi, Chemically reactive flow of Maxwell liquid due to variable thicked surface, Int. Commun. Heat and Mass Trans., 86 (2017) $231 - 238$.

[71] S. Z.Alamri, R. Ellahi, N. Shehzad and A. Zeeshan, Convective radiative plane Poiseuille flow of nanofluid through porous medium with slip: An application of Stefan blowing, J. Molecular Liqs., 273 (2019) $292 - 304$.

[72] T. Hayat, M. I. Khan, M. Waqas and A .Alsaedi, Effectiveness of magnetic nanoparticles in radiative flow of Eyring-Powell fluid, J. Mol. Liq., 231 (2017) $126 - 133$.

[73] M. Akbarzadeh, S. Rashidi, N. Karimi and R. Ellahi, Convection of heat and thermodynamic irreversibilities in two-phase, turbulent nanofluid flows in solar heaters by corrugated absorber plates, Adv. Powder Tech., 29 (2018) $2243 - 2254$.

[74] T. Hayat, M. Waqas, M. I. Khan, A. Alsaedi and S. A. Shehzad, Magnetohydrodynamic flow of Burgers fluid with heat source and power law heat flux, Chinese J. Phys., 55 (2017) 318 – 330.

[75] T. Hayat, M. I. Khan, M. Waqas and A. Alsaedi, Newtonian heating effect in nanofluid flow by a permeable cylinder, Results Phys., 7 (2017) 256 – 262.

[76] M. Hassan, M. Marin, A. Alsharif and R. Ellahi, Convection heat transfer flow of nanofluid in a porous medium over wavy surface, Phys Letter A, 382 (2018) 2749 – 2753.

[77] M. I. Khan, T. Yasmeen, M. I. Khan, M. Farooq and M. Wakeel, Research progress in the development of natural gas as fuel for road vehicles: A bibliographic review (1991 – 2016), Renewable and Sustainable Energy Reviews, 66 (2016) 702 – 741.

[78] T. Hayat, M. I. Khan, M. Waqas and A. Alsaedi, On Cattaneo–Christov heat flux in the flow of variable thermal conductivity Eyring–Powell fluid, Results Phys., 7 (2017) 446 – 450.

[79] S. Rashidi, S. Akar, M. Bovand and R. Ellahi, Volume of fluid model to simulate the nanofluid flow and entropy generation in a single slope solar still, Renewable Energy, 115 (2018) 400 – 410.

[80] N. B. Khan, Z. Ibrahim, M. I. Khan, T. Hayat and M. F. Javed, VIV study of an elastically mounted cylinder having low mass-damping ratio using RANS model, Int. J. Heat Mass Transf., 121 (2018) 309 – 314.

[81] T. Hayat, M. W. A. Khan, A. Alsaedi and M. I. Khan, Corrigendum to Squeezing flow of second grade liquid subject to non-Fourier heat flux and heat generation/absorption, Colloid and Polymer Sci., 295 (2017) 2439 – 2439.

[82] M. W. A. Khan, M. I. Khan, T. Hayat and A. Alsaedi, Entropy generation minimization (EGM) of nanofluid flow by a thin moving needle with nonlinear thermal radiation, Physica B: Condensed Matter, 534 (2018) 113 – 119.

[83] M. Tamoor, M. Waqas, M. I. Khan, A. Alsaedi and T. Hayat, Magnetohydrodynamic flow of Casson fluid over a stretching cylinder, Results Phys., 7 (2017) 498 – 502.

[84] M. Waqas, M. I. Khan, T. Hayat, A. Alsaedi, Nonlinear thermal radiation in flow induced by a slendering surface accounting thermophoresis and Brownian diffusion, European Physical J. Plus, 132 (2017) 132 : 280.

[85] T. Hayat, M.I. Khan, S. Qayyum, A. Alsaedi and M. I. Khan, New thermodynamics of entropy generation minimization with nonlinear thermal radiation and nanomaterials, Phys. Letter A, 382 (2018) 749 – 760.

[86] M. I. Khan, M. Waqas, T. Hayat, A. Alsaedi and M. I. Khan, Significance of nonlinear radiation in mixed convection flow of magneto Walter-B nanoliquid, Int. J. Hydrogen Energy, 42 (2017) 26408 – 26416.

[87] A. R. Bestman, Natural convection boundary layer with suction and mass transfer in a porous medium, Int. J. Energy Res., 14 (1990) 389 – 396.

[88] O. D. Makinde, P. O. Olanrewaju and W. M. Charles, Unsteady convection with chemical reaction and radiative heat transfer past a flat porous plate moving through a binary mixture, Africka Matematika, 22 (2011) 65 – 78.

[89] K. A. Maleque, Effects of exothermic/endothermic chemical reactions with Arrhenius activation energy on MHD free convection and mass transfer flow in presence of thermal radiation, J. Thermodyn., 2013 (2013) 692516 11.

[90] F. G. Awad, S. Motsa and M. Khumalo, Heat and mass transfer in unsteady rotating fluid flow with binary chemical reaction and activation energy, PLOS ONE, 9 (2014) e107622.

[91] Z. Abbas, M. Sheikh and S. S. Motsa, Numerical solution of binary chemical reaction on stagnation point flow of Casson fluid over a stretching/shrinking sheet with thermal radiation, Energy, 95 (2016) 12 – 20.

[92] M. I. Khan, S. Qayyum, T. Hayat, M. Waqas, M. I. Khan and A. Alsaedi, Entropy generation minimization and binary chemical reaction with Arrhenius activation energy in MHD radiative flow of nanomaterial, J. Mol. Liq., 259 (2018) 274 – 283.

[93] Z. Shafique, M. Mustafa and A. Mushtaq, Boundary layer flow of Maxwell fluid in rotating frame with binary chemical reaction and activation energy, Results Phys., 6 (2016) 627 – 633.

[94] M. I. Khan, T. Hayat, M. I. Khan and A. Alsaedi, Activation energy impact in nonlinear radiative stagnation point flow of Cross nanofluid, Int. Commun. Heat Mass Transf., 91 (2018) 216 – 224.

[95] M. Mustafa, J. A. Khan, T. Hayat and A. Alsaedi, Buoyancy effects on the MHD nanofluid flow past a vertical surface with chemical reaction and activation energy, Int. J. Heat Mass Transf., 108 (2017) 1340 – 1346.

[96] M. I. Khan, T. Hayat, A. Alsaedi, S. Qayyum, M. Taimoor, Entropy optimization and quartic autocatalysis in MHD chemically reactive stagnation point flow of Sisko nanomaterial, Int. J. Heat Mass Transf., 127 (2018) 829 – 837.

[97] M. I. Khan, S. Qayyum, T. Hayat, M. Waqas and A. Alsaedi, Entropy generation minimization and binary chemical reaction with Arrhenius activation energy in MHD radiative flow of nanomaterial, J. Mol. Liq., 259 (2018) 274 – 283

[98] M. Dhlamini, P. K. Kameswaran, P. Sibanda, S. Motsa, and H. Mondal, Activation energy and binary chemical reaction effects in mixed convective nanofluid flow with convective boundary conditions, J. Comp. Design and Eng., (2018) (in press).

[99] M. I. Khan, T. Hayat, M. I. Khan, and A. Alsaedi, Activation energy impact in nonlinear radiative stagnation point flow of Cross nanofluid, Int. Commun. Heat Mass Transf., 91 (2018) 216 – 224.

[100] M. A. Chaudhary, J. H. Merkin , A simple isothermal model for homogeneous-heterogeneous reactions in boundary-layer flow. II Different diffusivities for reactant and autocatalyst, Fluid Dyn. Res., 16 (1995) 335 – 359.

[101] N. Bachok, A. Ishak, I. Pop, On the stagnation-point flow towards a stretching sheet with homogeneousheterogeneous reactions effects, Commun. Nonlinear Sci. Numer. Simul., 16 (2011) 4296 – 4302.

[102] P. K. Kameswaran, S. Shaw, P. Sibanda, P. V. S. N. Murthy, Homogeneous-heterogeneous reactions in a nanofluid flow due to porous stretching sheet, Int. J. Heat Mass Transfer., 57 (2013) 465 – 472.

[103] T. Hayat, Z. Hussain, A. Alsaedi, B. Ahmad, Heterogeneous-homogeneous reactions and melting heat transfer effects in flow with carbon nanotubes, J. Mol. Liq., 220 (2016) 200 – 207.

[104] M. Imtiaz, T. Hayat, A. Alsaedi, A. Hobiny, Homogeneous-heterogeneous reactions in MHD flow due to an unsteady curved stretching surface, J. Mol. Liq., 221 (2016) 245–253.

[105] T. Hayat, S. Qayyum, M. Imtiaz, A. Alsaedi, Impact of Cattaneo-Christov heat flux in Jeffery fluid flow with homogeneous-heterogeneous reactions, PLOS ONE., 11 (2016)e 0148662.

[106] T. Hayat, Z. Hussain, T. Muhammad, A. Alsaedi, Effects of homogeneous and heterogeneous reactions in flow of nanofluids over a nonlinear stretching surface with variable surface thickness, J. Mol. Liq., 221 (2016) 1121 – 1127.

[107] M. Sajid, S. A. Iqbal, M. Naveed, Z. Abbas, Effect of homogeneous-heterogeneous reactions and magnetohydrodynamics on Fe3O4 nanofluid for the Blasius flow with thermal radiations, J. Mol. Liq., 233 (2017) 115 – 121.

[108] A. Tanveer, T. Hayat, A. Alsaedi, B. Ahmad, Mixed convective peristaltic flow of Sisko fluid in curved channel with homogeneous-heterogeneous reaction effects, J. Mol. Liq., 233 (2017) 131 – 138.

[109] T. Hayat, Z. Hussain, A. Alsaedi, M. Mustafa, Nanofluid flow through a porous space with convective conditions and heterogeneous- homogeneous reactions, J. Taiwan Inst. Chem. Eng., 70 (2017) 119 – 126..

[110] S. J. Liao, Beyond Perturbation: Introduction to Homotopy Analysis Method, Chapman and Hall, CRC Press, Boca Raton (2003).

Turnitin Originality Report

Nonlinear Mathematical Models with Chemical Reaction by Sadia Rashid .

turnitin

From DRSM (DRSM L)

- Processed on 21-Dec-2020 09:36 PKT
- ID: 1479920633
- Word Count: 22082

Similarity Index
14%
Similarity by Source

Internet Sources:
8%
Publications:
5%
Student Papers:
6%

Focal Person (Turnitin)
Quaid-i-Azam University
Islamabad

sources:

1 1% match (student papers from 14-May-2018)
Submitted to Higher Education Commission Pakistan on 2018-05-14

2 1% match (student papers from 03-Aug-2018)
Submitted to Higher Education Commission Pakistan on 2018-08-03

3 1% match (publications)
International Journal of Numerical Methods for Heat & Fluid Flow, Volume 24, Issue 2 (2014-03-28)

4 1% match (student papers from 02-Aug-2018)
Submitted to Higher Education Commission Pakistan on 2018-08-02

5 < 1% match (Internet from 16-Feb-2020)
https://suche.thulb.uni-jena.de/Summon/Search?dfApplied=1&lookfor=%22Ijaz%2C+M%22&page=2&type=Author

6 < 1% match (Internet from 07-Oct-2020)
https://www.britannica.com/science/homogeneous-reaction

7 < 1% match (publications)
M. Ijaz Khan, Sumaira Qayyum, T. Hayat, M. Imran Khan, A. Alsaedi. "Entropy optimization in flow of Williamson nanofluid in the presence of chemical reaction and Joule heating", International Journal of Heat and Mass Transfer, 2019

8 < 1% match (Internet from 05-Oct-2017)
http://prr.hec.gov.pk/Thesis/2927S.pdf